UNIVERSITY OF SOUTHAMPTON

Direct write printed flexible electronic devices on fabrics

By

Yi Li

A thesis submitted in partial fulfilment for the

degree of Doctor of Philosophy

in the

Faculty of Physical and Applied Science

Department of Electronics and Computer Science

18 February, 2014

Abstract

By *Yi Li*

This thesis describes direct write printing methods to achieve flexible electronic devices on fabrics by investigating, low temperature process; and functional conductor, insulator and semiconductor inks. The objective is to print flexible electronic devices onto fabrics solely by inkjet printing or pneumatic dispenser printing. Antennas and capacitors, as intermediate inkjet printed electronic devices, are addressed before transistor fabrication. There are many publications that report inkjet printed flexible electronic devices. However, none of the reported methods use fabrics as the target substrate or are processed under a sufficiently low temperature (≤150 ^{o}C) to enable fabrics to survive. The target substrate in this research, standard 65/35 polyester cotton fabric, has a maximum thermal curing condition of 180 ^{o}C for 15 minutes and 150 ^{o}C for 45 minutes. Therefore the total effective curing time is best below 150 ^{o}C within 30 minutes to minimise any potential degradation of the fabric substrate.

This thesis reports on an inkjet printed flexible half wavelength fabric dipole antenna, an inkjet printed fabric patch antenna, an all inkjet printed SU-8 capacitor, an all inkjet printed fabric capacitor and an inkjet printed transistor on a silicon dioxide coated silicon wafer. The measured fabric dipole antenna peak operating frequency is 1.897 GHz with 74.1 % efficiency and 3.6 dBi gain. The measured fabric patch antenna peak operating frequency is around 2.48 GHz with efficiency up to 57 % and 5.09 dBi gain. The measured capacitance of the printed capacitor is 48.5 pF (2.47 pF/mm^2) at 100 Hz using the inkjet printed SU-8. The capacitance of an all inkjet printed flexible fabric capacitor is 163 pF (23.1 pF/mm^2) at 100Hz with the UV curable PVP dielectric ink developed as part of this work; thus the equivalent relative permittivity (ε_r) is 11.7. The inkjet printed PTAA transistor has an on/off ratio > 10^3 and carrier mobility of 0.669 cm^2/V s. These inkjet printed electronic devices have advanced that reported by other publications in fabrication, material and performance. Pneumatic dispenser printed flexible capacitors were fabricated to evaluate the dispenser printer capabilities with inkjet printable inks and screen printable pastes. This fabrication method will provide a significant step towards the realisation of low cost, fast printed electronics using a much broader range of rheological properties for the functional materials.

Table of Contents

List of Figures

List of Tables

List of Acronyms

AIJP	All inkjet printing
AM	Additive manufacturing
BJT	Bipolar junction transistor
CNTs	Carbon nanotubes
DOD	Drop-on-demand
F8T2	Poly[(9,9-dioctylfluorenyl-2.7-diyl)-co-bithiophene]
Standard Fabric	Standard 65/35 polyester cotton fabric
FET	Field-effect transistor
HOMO	Highest occupied molecular orbital
ICP	Intrinsically conductive polymer
IF fabric	Interface coated standard polyester cotton fabric
IJP	Inkjet printing
LUMO	Lowest unoccupied molecular orbital
MOSFET	Metal-oxide-semiconductor field-effect transistor
OFET	Organic field-effect transistor
OSC	Organic semiconductor
PEDOT/PSS	Poly (3,4-ethylenedioxythiophene) – Poly (styrenesulfonate)
PET	Polyethylene terephthalate
PEN	Polyethylene naphthalate
PU Fabric	Polyurethane coated stretchable fabric
S/D	Source and drain
TCO	Transparent conductive oxides
TFT	Thin film transistor
P3HT	Poly(3-hexylthiophene)
PTAA	Poly(triaryl amine) or Poly[bis(4-phenyl)(2,4,6-trimethylphenyl)amine]
PVA	Poly(vinyl alcohol)
PVP	Poly(4-vinyl phenol)

List of Symbols

$\boldsymbol{Re}$	Reynolds number
$\boldsymbol{\rho}$	Density of the ink
$\boldsymbol{D}$	The droplet diameter
$\boldsymbol{V}$	The in-flight velocity
$\boldsymbol{\eta}$	The viscosity of the ink
$\boldsymbol{\sigma}$	The surface tension of the ink
$\boldsymbol{\pi}$	The mathematical constant – 3.1415926
$\boldsymbol{\lambda}$	The electromagnetic wavelength
ε_r	The relative permittivity
ε_0	The vacuum permittivity
$\boldsymbol{Pa\ s}$	Pascal second
$\boldsymbol{P_{top}}$	The pressure applied on top surface of the ink which is set by the pneumatic dispenser controller
$\boldsymbol{P_{bottom}}$	The pressure applied to the bottom surface of the ink which is also equal to the atmosphere pressure
$\boldsymbol{P_{\Delta}}$	The differential pressure applied to force the liquid extruded from the dispensing nozzles or needles
$\boldsymbol{L}$	The length of the dispensing needle
$\boldsymbol{g}$	The gravitational force
$\boldsymbol{R}$	The inner diameter of the dispensing needles
$\boldsymbol{\mu}$	The viscosity of the ink or paste measured
$\boldsymbol{V_G}$	Gate voltage applied on the transistor gate terminal
$\boldsymbol{V_D}$	Drain voltage applied on the transistor drain terminal
$\boldsymbol{I_D}$	Drain current passing through the drain terminal
$\boldsymbol{I_G}$	Gate current passing through the gate terminal
$\boldsymbol{C_i}$	Geometric capacitance

This page intentionally left blank

Acknowledgements

During the period of my Ph.D., I have had cause to be grateful for the advice, support and understanding of many people. I would like to sincerely thank my supervisor Prof. Steve Beeby for directing me to this great research field since I was a master student at the University of Southampton. In particular I would like to express my sincere appreciation and gratitude to my supervisors Dr John Tudor and Dr Russel Torah for their continuous moral and technical support. I would like to thank Prof. Peter Ashburn for his valuable advices on my experiments. This work has also benefited greatly from much advice, and many useful discussions with Dr Kai Sun, Dr Kai Yang, Dr Neil Grabham and Dr Dibin Zhu.

I would like to thank every member who was and is in the smart fabrics group and Bay 5 for their helps, discussions and kindness over the past 4 year, including Stephen, Somphop, Ivo, Noreha, Kiwi, Ghaithaa, Gordon, Joseph, Yi, Ahmed, Yang, Komolafe, Zhuo, Huihui, Zihao, Zhao, Sheng, Junjie, Nurs, Huma, Marc and Zeeshan, who made my Ph.D. life a wonderful experience.

Last but not least, I would like to thank my parents, who are far away in China. I can never forget their understandings, endless love, supports and encouragements for my student life in England. Without their love, I could never go this far, pursue this degree or gain a broader view of the world. I really appreciate it from bottom of my heart. This thesis is dedicated to my parents.

This page intentionally left blank

Chapter 1

1 Introduction

1.1 Introduction

Fabric represents material made by weaving, knitting, crocheting or bonding, which may be used in further production of various fabric products. ‘Fabric’ is an all-encompassing term, referring to material made of interlacing fibres, including yarn, yarn products and anything related to fibres. In this research field, the terms ‘fabric’ and ‘textile’ are used interchangeably. Smart fabrics are traditional fabrics with integrated active functionality, that can sense and react to external stimuli, such as mechanical force, temperature, gases and magnetic fields [1]. Smart fabrics have attracted a growing interest in the last decade in many different applications. Examples include in audio entertainment control, monitoring of physiological conditions for health, fashion, advertising, sports training and for intelligent interiors in architecture [2]. Wearable smart fabric applications are one area of smart fabrics, providing extra functionality to everyday consumer fabric products: for example, electrocardiogram (ECG) clothing [3], luminescent fabric [4] and antennas on garments [5]. Generally, conventional microelectronics manufacturing techniques cannot be processed on fabrics, because conventional microelectronic processing methods require a smooth, flat and rigid surface, for example, silicon wafer. Fabrication techniques for achieving smart fabrics include attaching electronic components, active yarns constructed smart fabrics or printing active materials onto the standard fabric. Currently screen printing is the most widely used printing technique for depositing electronically functional and coloured inks onto fabrics because it is a single-step additive deposition which does not damage the fabric substrates. However, screen printing needs a pre-defined screen to achieve the printed pattern. Therefore, direct write techniques which deposit functional inks onto an arbitrary substrate with the desired pattern in three dimensions without a screen are attractive. This research work concerns the direct write printing of electronically functional materials to create flexible electronic devices on fabric surfaces. In addition, it compares the two direct write technologies, inkjet and pneumatic dispenser printing.

1.2 Objectives

The main objective of this research work is to realise flexible electronic devices on fabrics by using direct write fabrication techniques. There are two direct write techniques considered in this research: inkjet printing and pneumatic dispenser printing. This research work has been broken down into the following 6 objectives based on the topic of all direct write printed flexible electronic devices on fabric substrate.

(1) Evaluate different flexible substrates with final objective of the standard 65% polyester 35% cotton fabric substrate.
(2) Investigate low temperature processed electronically functional inks to apply on fabric.
(3) Achieve and analyse inkjet printed fabric half wavelength dipole antennas at 2.4 GHz.
(4) Achieve and analyse inkjet printed fabric parallel plate capacitors at 10 pF/mm^2.
(5) Achieve and analyse pneumatic dispensed flexible capacitors for its fabrication capability.
(6) Achieve and analyse inkjet printed transistors on a silicon dioxide coated silicon wafer to evaluate the deposition of inkjet printable semiconductor ink in ambient environment for smart fabric applications.

In this study, functional materials are deposited with three types of electronically functional inks (insulator, conductor and semiconductor inks) by direct write printing techniques on selected substrates. :

(1) Glass slide
(2) Polyimide film (Kapton)
(3) Standard polyester cotton fabric (Standard fabric)
(4) Commercial polyurethane (PU) coated stretchable fabric (PU fabric)
(5) Interface (Fabink-IF-UV4) coated standard 65/35 polyester cotton fabric (IF fabric)

Two intermediate electronic devices are investigated before the stage of transistor development:

(1) Antennas consisting of only one conductive ink
(2) Capacitors consisting of both conductive and dielectric inks

The last inkjet printable electronic device is a transistor consisting of three electronically functional inks, namely, conductive, insulator and semiconductor inks. Both antenna and capacitor are considered as separate electronic devices and also part of the components in

building a transistor. Fabricating antenna will gain the experience of using conductive ink and depositing conductive electrodes. Fabricating capacitor will gain the experience of printing multilayers device, alignment, parallel structure device and different inks' interactions. In addition, the low temperature processable insulator ink is investigated for final objective of inkjet printed transistor. Then the transistor stage will only focus on the investigation of low temperature processable inkjet printable semiconductor inks and their interactions with other sequential layers. Therefore, the challenges in all inkjet printed transistor will be spilt down to several learning stages with different novelties.

1.3 Statement of novelty

The novelties arising from this research have been briefly summarised into five key areas:

(1) The first inkjet printed half wavelength dipole antenna on fabric is achieved
(2) The first inkjet printed microstrip patch antenna on fabric is achieved
(3) The first all inkjet printed SU-8 capacitor on Kapton is achieved
(4) The first all inkjet printed flexible capacitor on fabric is achieved
(5) New inkjet printable poly(4-vinylphenol) (PVP) based dielectric ink formulation for inkjet printed thin film on fabric is achieved

Making electronic devices by direct write printing is a new research area, especially in regard to realising flexible electronics on fabric substrates. In previous related publications, the majority of direct write printed electronic devices have involved other deposition methods besides purely inkjet or pneumatic dispenser printing. In addition, none of the publications has reported electronic devices inkjet printed on flexible fabric substrates. In this report, the aim is to achieve a fabrication method that only uses all inkjet printing or alternately, all pneumatic dispenser printing to create flexible electronic devices on fabric substrate. The electronic devices include antennas, capacitors and transistors. Novelty is achieved by all inkjet printing for the first time two types of flexible fabric antenna (dipole and patch antennas), flexible SU-8 capacitor and flexible PVP capacitors on fabric. To achieve these objectives, the low temperature processed conductor, insulator and semiconductor inks are essentially required. Finally, a new inkjet printable UV curable dielectric ink is a further novelty arising from this research. It achieves the low temperature processable inkjet printable dielectric thin layer as

currently no other reported solvent based inks can be inkjet printed and UV cured to form thin dielectric layer in the order magnitudes of 1 μm.

Further, the following new knowledge has been created in this research:

(1) New inkjet printed smart fabrics: specifically an antenna and a capacitor on a fabric substrate for wearable application is new knowledge created in the field of inkjet printed electronics research.
(2) Applying the interface layer onto fabric to support subsequent inkjet printed functional layers on a fabric substrate is new knowledge created in inkjet printed electronics research.
(3) The UV curable inkjet printable insulator ink based on solvent is new knowledge created in inkjet printed electronics research.

1.4 Publications arising from this research

1. Y. Li, R. Torah, S. Beeby, J. Tudor, *An all-inkjet printed flexible capacitor for wearable applications*, Symposium on Design, Test, Integration & Packaging of MEMS/MOEMS, France, 2012.
2. Y. Li, R. Torah, S. Beeby, J. Tudor, *Inkjet printed flexible antenna on textile for wearable applications*, The 88th Textile Institute World Conference, Malaysia, 2012.
3. Y. Li, R. Torah, S. Beeby, J. Tudor, *An all-inkjet printed flexible capacitor on a textile using a new poly(4-vinylphenol) dielectric ink for wearable applications*, IEEE Sensors 2012, Taipei.
4. A. Chauraya, W. G. Whittow, J, C. Vardaxoglou, Fellow IET, (Loughborough University), Y. Li, R. Torah, K. Yang, S. Beeby, J. Tudor, (University of Southampton), *Inkjet Printed Dipole Antennas on Textiles for Wearable Communications*, IET Microwave, Antennas & Propagation, Vol. 7, Iss. 9, 18 June 2013, pp. 760-767.
5. K. Liang, M. Gong, (Sichuan University), Y. Li, R. Torah, S. Beeby J. Tudor, (Southampton University), *Spectroscopy Analysis of the Prophase Invalidation Mechanism of Inkjet Printed Organic Transistors*, The Journal of Light Scattering (China), Vol. 25, Iss. 3, 2013, pp. 316-321.
6. A. Chauraya, W. G. Whittow, J, C. Vardaxoglou, Fellow IET, (Loughborough University), Y. Li, R. Torah, K. Yang, S. Beeby, J. Tudor, (University of Southampton), *Inkjet Printed*

Microstrip Patch Antennas for Wearable Applications, IEEE Antennas and Wireless Propagation Letters, Vol. 13, 2013, pp. 71-74.

7. A. Chauraya, W. G. Whittow, J, C. Vardaxoglou, Fellow IET, (Loughborough University), Y. Li, R. Torah, K. Yang, S. Beeby, J. Tudor, (University of Southampton), *Printed Frequency Selective Surfaces on Textiles*, IET Electronic Letters, 2014 (In preparation).

1.5 Structure of the thesis

Chapter 1 introduces the underlying motivation of this research and outlines the areas of focus. An introduction to the research work is also given, emphasising the critical features of the direct write systems and the novelty achieved in realising all direct write printed flexible electronic devices onto fabrics.

Chapter 2 mainly describes two key direct write techniques, inkjet and pneumatic dispenser printings, emphasising their physical limitations in material processing and fabrication capability. This provides a full understanding of the two fabrication techniques for further practical research work. The second half of the chapter also discusses and summarises the other direct write techniques available. In addition, the advantages and disadvantages of direct write techniques are discussed in the summary section.

Chapter 3 outlines the possible direct write printable materials, catalogued in sections on organic and inorganic materials. In the organic section, materials are divided into insulator, conductor, semiconductor and other functional groups. In the inorganic section, materials are divided into metallic nanoparticles, metal oxides material, conventional semiconductor silicon and germanium, as they are the more widely used inorganic solution processed materials. Moreover, commercial printable electronically functional materials are summarised with a focus, for the purposes of this research, low processing temperature inks. Formulas, processing requirements and features of the different materials are described in subsections.

Chapter 4 summarises the literature review to explain the state-of-the-art of smart fabrics and direct write printed electronics devices. The main part of this chapter presents an intensive review of existing inkjet printed electronic devices relevant to this thesis in order of device complexity: conductor (antenna), capacitor and transistor. Then, dispenser printed electronic

devices are briefly reviewed. In addition, the possibility of realising direct write printing for smart fabrics has been reviewed and discussed.

Chapter 5 presents the inkjet printed fabric dipole and patch antennas. The chapter begins with the theory and design of the two types of potentially inkjet printable fabric antennas. Next the fabrication process for the antenna is described. Firstly, substrate selection is considered since the antennas are inkjet printed onto various substrates to evaluate the different substrates and processes. The substrate selection section discusses in detail the different substrates used in this research work; these same substrates will be used for the fabrication of the capacitor and transistor. This is followed by discussion of the antenna fabrication. The next section presents the device testing and evaluation of the antenna. Finally an overall discussion and conclusions are presented. Chapter 6 and 7 follows the same chapter structure as Chapter 5 in sections of theory, design, architecture, fabrication and device testing.

Chapter 8 summarises the research work done to achieve the objectives and novelties. In addition, this last section lists possible future work towards improving the final objective of the research, namely, direct write printed flexible electronic devices on fabrics.

Chapter 2

2 Literature review: direct write printing technologies

2.1 Introduction

Recently, there has been a significant growth of interest in direct write processed electronic devices, as the electronics industry sector aims towards low cost fabrication, rapid manufacturing and shorter time to market, as well as reduced environmental impact. Direct write processing technology is the core element of this research work. This chapter reviews the state-of-the-art of direct write technology with a key focus on inkjet and pneumatic dispenser printing techniques. The capabilities, properties and limitations of inkjet and pneumatic dispenser printing are discussed in detail. Moreover, other existing direct write processing techniques are briefly introduced to further explore the concept of direct write technology. In addition, the advantages and disadvantages of direct write technology are summarised at the end of this chapter.

2.2 Background of direct write printing

Many definitions of direct write have been offered by different research groups [6, 7, 8]. For the purposes of this study, direct write is defined as an additive technique enabling the deposition of electronic components, functional or structural patterns from different kinds of functional materials. The printing directly follows a pre-designed layout without utilising masks or subsequent etching processes. After the deposition of each layer onto the substrate is completed, a further curing treatment process, such as thermally or UV curing, is often needed for the deposited material to achieve its full functional performance before deposition of the next functional layer. Direct write printing has been demonstrated to be a fast, flexible prototyping tool with the ability to pattern a wide range of materials to create diverse two- or three-dimensional shapes and devices [9]. In comparison to subtractive microfabrication and screen printing techniques, which utilise masked pattern and subtractive processes such as

lithography and etching, the number of process steps, energy demanded and waste chemicals generated is significantly lower by direct write printing, as illustrated in figure 1.

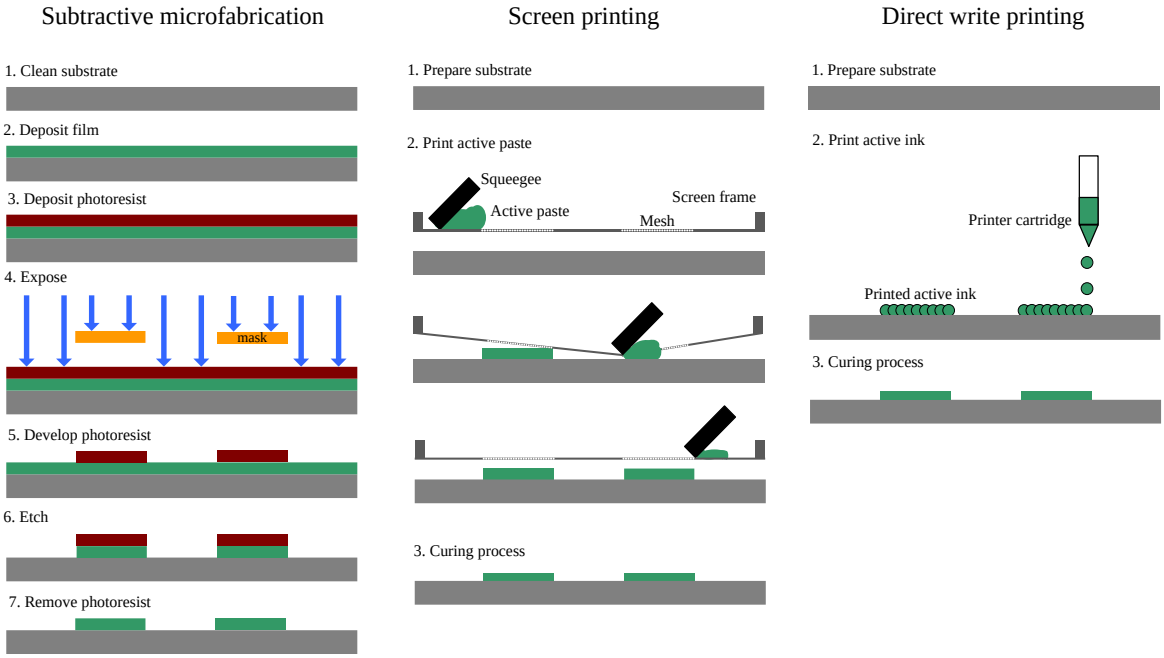

Figure 1. A comparison of the processing steps involved in subtractive microfabrication (left), screen printing process (middle) and additive direct write printing (right).

A variety of direct write techniques have been developed in recent years. However, most of the existing direct write techniques can be classified within one of the following three categories:

1) Droplet based direct writing: the typical example is inkjet printing technology such as the Dimatix inkjet printer [10] described in more detail in section 2.2.1.

2) Filament based direct writing: this is sometimes referred to as a continuous approach or flow-based technique. Typical examples are the commercially available products MicroPen [11] and nScrypt [12] as shown in figure 2. The technique used in this thesis is the pneumatic dispenser which can perform both the filament based dispensing and the droplet based modes. This technique is described in section 2.2.2.

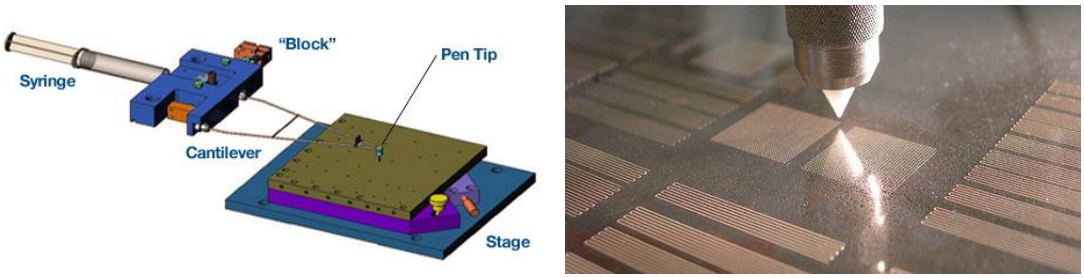

(a) (b)

Figure 2. (a) MicroPen operation principle diagram, (b) nScrypt micro dispensing pump.

3) Tip-based direct writing: the typical example is thermal dip pen nanolithography (DPN) which is useful in nanoscale applications. Commercially available dispenser and tip-based direct write printing are described in section 2.2.3.

2.2.1 Inkjet printing

The first desktop inkjet printer, the ThinkJet, was released by Hewlett-Packard in the early 1980s and used thermal evaporation technology to generate the pressure impulses. From that time up to the present, the inkjet printer has played a major role as a full colour printing device. However, they can also deposit active functional inks for printed electronic devices. The most important feature of the inkjet printing technique is that it is a digital fabrication process. This means it can apply each droplet at a given location. To do this, the pattern is digitised into a droplet bitmap. Therefore, the printed layer may not be exactly identical to the designed pattern in the scale of droplet diameter due to artefacts. A printed pattern can suffer from the artefact of the converted file from the drawing package, because the inkjet needs to convert the pattern into the bitmap format. According to the boundary of each pattern, if the width of a pattern can be divided by the printing resolution, the artefact can be reduced to the minimum of each droplet resolution. If not, the pattern width tends to be one droplet shorter. It is recommended to use the bitmap editor to locate each droplet landing location. Especially, the small featured inkjet printed layer in the scale of the droplet diameter 60 μm can be affected significantly by the pixilation effect. This artefact does not change the percentage dimension much in the large patterned layout which the droplet diameter can be negligible in layout dimension.

Inkjet printing is based on the droplet jetting mode. In inkjet printing, an inkjet printable ink is ejected from nozzles onto a substrate. Normally the inkjet printers operate either in continuous or drop-on-demand (DOD) printing mode. In continuous mode inkjet printing, the ink is pumped through a nozzle to form a continuous liquid jet. Continuous mode inkjet printing is typically used in high speed graphical applications, e.g. fabrics printing and labelling. Drop-on-demand (DOD) mode offers a smaller drop size and higher placement accuracy by means of a pressure pulse ejecting ink droplets from a reservoir through a nozzle. The pulse can be generated either thermally or piezoelectrically. Thermal bubble systems launch inks onto substrates by rapid heating; piezoelectric system applies electrical signals onto a piezoelectric membrane to eject small droplets of ink onto a substrate as shown in figure 3.

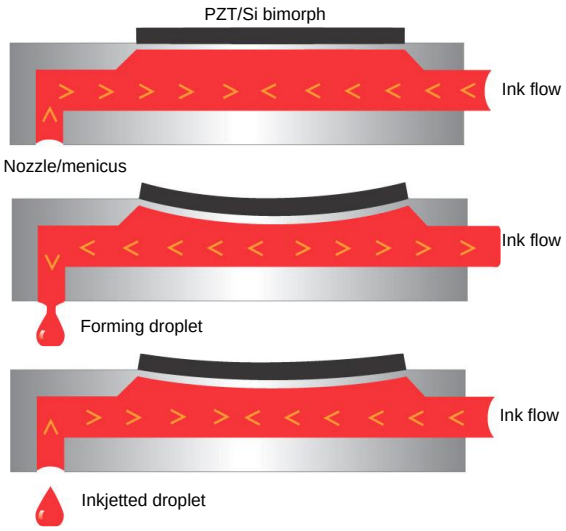

Figure 3. Cross sectional view of the droplet formation flow diagram of a DMP 2831 inkjet printer's piezoelectric nozzle head.

At the beginning of the inkjetting pulse, the voltage applied to the bimorph is zero volts to bring the PZT/Si bimorph back to a relaxed position with the chamber at its maximum volume. At this stage the ink is pulled into the chamber through the cartridge, whist the bimorph also pulls the meniscus at the nozzle as shown in the first stage in figure 3. The second stage is the droplet ejection stage. The chamber is compressed and a sufficient pressure is generated to eject the droplet by increasing the voltage applied to the PZT/Si bimorph. The final stage is the recovery stage where the piezo voltage is set back down to its bias level. The chamber decompresses at first only partially and then refilled for the next pulse. In addition, this stage also pulls back on the ejected droplet.

For inkjet printed electronic devices, the piezoelectric nozzle is currently the only option, as the instant thermal bubble system could change the functional ink's electrical properties. The functional materials can be prematurely cured by the instantaneous high temperature generated by the thermal bubble nozzle system.

In inkjet printed device fabrication, the effective working principle is the droplet's formation, in-flight and landing. The droplet diameter is the most important parameter after it lands on the substrate. It controls the printing resolution significantly; the smaller the droplet the higher the ultimate printing resolution that can be reached. Typically the droplet diameter size after landing is about 60 µm (from 50 µm to 70 µm depending on the ink's surface tension and other physical properties). 60 µm droplet diameter corresponds to a drop volume of around 10 pL [6].

Inkjet printable inks have a very narrow acceptable range of rheological properties within which they can be inkjetted properly. DMP 2831, made by Dimatix Fujifilm, is the inkjet printer used in this thesis. There are six important liquid formulation guidelines for inks to be suitable for working with the DMP 2831 inkjet printer: liquid evaporation, viscosity, surface tension, suspensions, filtering and degassing [13].

1) Liquid evaporation rate: the jetting liquid system must not dry at the nozzle and air interface. Therefore, the liquid must have a low evaporation rate. Liquids usually perform better with the addition of a humectant such as a glycol to assist in lower evaporation. Solvent systems should be formulated using low evaporation and high boiling point solvents.

2) Viscosity: it ideally should be between 10 to 12 mPa s (cP) at operating temperature. The printer head can be heated up to 70 ℃ to allow inkjet printable inks viscosity up to 30 mPa s to be jetted. However, the optimum jetting performance may not be achieved for some applications. Lower viscosity liquids can be jetted, but the operating performance is typically limited.

3) Surface tension: it should be between 0.028 to 0.033 N/m (28 and 33 dynes/cm). Typically a surfactant is added to water based liquid to achieve this surface tension range, because water has a much higher surface tension, 0.072 N/m. Typical organic solvents have lower values, for example, isopropanol 0.022 N/m and acetone 0.024 N/m. High surface tension liquid (up to 0.06 N/m) may be jetted with limited jetting performance. Because the pressure generated by piezoelectric printer head cannot break the surface tension force, droplet formation can be problematic.

4) Suspensions: particles must not settle or agglomerate rapidly. It is suggested that a suitable stabiliser (dispersant) be added to the suspension to avoid rapid settling. For examples, polyesters of hydroxystearic acid based dispersant from solsperse range is used in the formula of inkjet printable ceramic ink [14]. A functional material dissolved in a solvent does not have this problem.

5) Filtering: liquids are recommended to be filtered through a 0.2 μm filter to remove large aggregates or particles. In general, the particles in the liquid should be less than 1/100 the size of the inkjet nozzle. The actual diameter of the 10 pL nozzle is 21.5 μm; therefore any particle, polymer or aggregate should be less than 0.2 μm.

6) Degassing: removal of dissolved air bubbles improves the jetting and printing characteristics of most liquid. Air bubbles can pause the jetting temporarily, causing missing dots and lines. The liquid is advised to be degassed in a vacuum chamber before being loaded onto the printer. The degassing process does not change the properties of the inks but it improves jetting performance. Typically, the degassing process only takes 5 to 10 minutes.

Table 1 summarised DMP 2831 inkjet printer's specification for printing [15].

Dimatix DMP 2831 Inkjet Printer	
Maximum substrate thickness	25 mm
Repeatability	±25 μm
Operating environment	15-40 °C
Drop volume	1 pL and 10 pL
Drop spacing	5 to 254 μm
Liquid temperature control	Up to 70 °C
Substrate temperature control	Up to 60 °C
Cartridge capacity	1.5 mL
Ideal viscosity	10 to 12 mPa s
Acceptable viscosity	2 to 30 mPa s
Surface tension	0.028 to 0.033 N/m
Maximum surface tension	0.060 N/m
Maximum particles size	0.2 μm

Table 1. DMP 2831 inkjet printer and required inks rheological specification.

2.2.2 Dispenser printing

Dispenser printing can be used in a droplets based mode or a filament based mode. Dispenser printing is a simple and versatile method for additively depositing a variety of materials, including slurries, solutions and suspensions, generally referred to as 'inks'. This is a filament based method of direct write patterning, with the ability to deposit inks at room temperature and under ambient conditions, all the while generating negligible materials waste as inkjet printing. The dispenser controller system used in this research work is based on the Musashi ML-808FXcom-CE, a pneumatic type of direct write dispenser.

This section mainly explains the operational principle of the custom-built pneumatic dispenser system based on the principle of the basic pneumatic dispenser. The dispenser printer used in this research work is a custom designed but was not built as part of this project. Other dispensing valves [16] joint with pneumatic dispenser are not discussed in detail in this section, they are including diaphragm valve, high pressure valve, positive displacement valve, needle mini valve, poppet valve, cartridge valve, spray valve and pinch tube valve.

To deposit a designed pattern with a pneumatic dispenser, the ink inside the dispenser barrel is pushed out by a pre-programmed dispensing pressure and time setting through a hollow needle of predetermined dimensions and deposited onto a substrate via a succession of dots or extruded lines.

When the pneumatic dispenser dispenses individual dots of liquid from an orifice, the end result is very similar to that of a commercial inkjet printer. The pneumatic dispenser operates by air pressure impact causing it to respond to the request for a dot as PZT bimorph displacement is used to generate a dot in inkjet printing. The dispenser vacuum level allows the pressure inside the barrel to hold the ink at the meniscus point at the end of the dispensing tip as the inkjet printer meniscus setting does. Liquid degassed by the vacuum chamber fills the barrel. This action displaces liquid and causes a dot of liquid to be ejected out of a nozzle. There are two fundamental statements to observe in pneumatic dispensing:

1) Air is compressible and liquid is not compressible. This first dispensing principle explains why a liquid can be dispensed; if the liquid were compressible, accurate dispensing could never be achieved. The principle also explains why there is a delay in liquid flow when using an air pulse to the air must first be compressed before impacting on the liquid. Then the air pressure remains at the desired pressure level.

2) Dispenser printing liquid is related to three key parameters: 1. Air pressure, 2. Time, 3. Nozzle dimension. Any one of these parameters will alter the dispensing result. Volumetric flow rate equation and simulation will be presented in Chapter 6.

Besides the two fundamental statements, in droplet mode dispensing, a dispenser printed dot volume is equal to one half volume of a droplet [17]. This principle will calculate the reservoir supply and liquid usage based on the volume of each droplet [17]. The droplet size is determined by the needle's dimension, ink rheology, applied pressure and dispensing time. The resulting printed film morphology depends on the dimensions of the extruded droplets as well as on the stage moving distance, speed and time between each shot.

The three axis stages (X, Y and Z) on which the syringe and substrate are mounted and the pressure applied from a pneumatic controller generates the dimensions and shapes of the deposited films. Regarding the dispenser built in this research work, the three stage motors are supplied by the Sigma Koki Company, as they make high precision stepper motors with precise

movement down to sub-micron per pulse. The three stage motors are the same product with product code of SGSP-26-50 from Sigma Koki.

According to the manufacturer's specification, the Sigma Koki SGSP-26-50 stage (X, Y and Z) motors are set at 1 µm per pulse resolution with repeatability of ± 5 µm. A maximum moving speed of 9 mm/s can be reached with automatic control. Needles and nozzles with 0.1 µm to 2.4 mm inner diameter sizes are available from various commercial suppliers with standard lure lock fitting. With an assortment of needle sizes (0.1 µm to 2 mm), precise dispensing time (0.01 sec to 999.9 sec) and a broad range of pneumatic pressures (20 to 800 kPa) that can be applied, the dispenser printer is able to print a variety of inks into a range of printed feature sizes. All the equipment is controlled and automated through customised LabView interface software. A schematic diagram of the droplets mode dispenser printing is shown in figure 4 (a). It shows the droplets in coalesced mode to form a printed film.

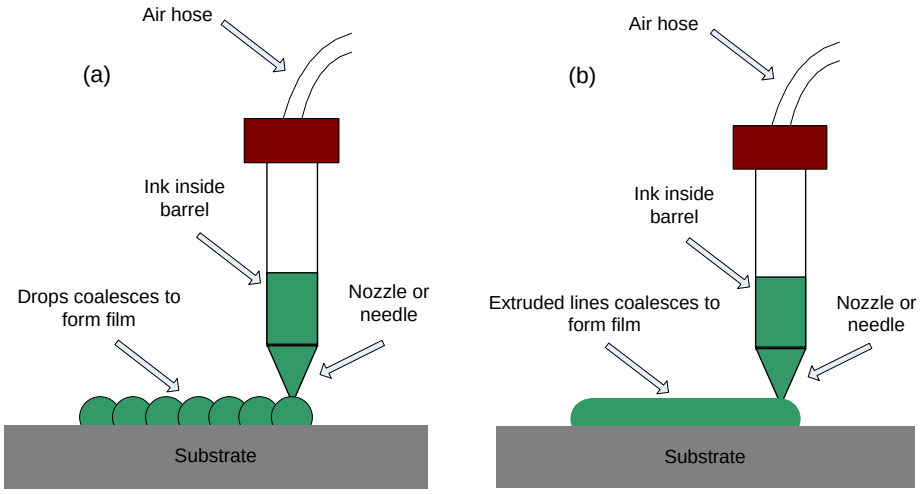

(a) (b)

Figure 4. Schematic of direct write dispenser printing under droplet based mode and filament based mode.

Figure 4 (b) shows the filament based line coalesced mode to form the film. For the droplet mode dispensing, both X and Y axes resolutions have to be set based on optimisation of each active ink. For fine line dispensing applications, only the line gap has to be set. In both dispensing modes, the dispenser requires an accurately controlled dispensing gap which is distance between the tip and the substrate. If the dispense gap is too large, the liquid bead will not properly wet the substrate. This will result in a poor resolution defined pattern. On the other hand, if the dispense gap is too small, the flow of liquid will spread, also resulting in a poor resolution pattern. The maximum needle dispensing speed is constrained by the rate of material wetting to the substrate. The ink's wettability, representing the interaction between ink and

substrate, defines the pattern resolution before the curing stage. If the material has not wetted substrate sufficiently, it will stay attached to the needle rather than to the substrate and then resulting in an incomplete dispensed pattern.

In summary, the basic requirements for pneumatic dispensing ink include almost the same parameters as inkjet printing but with a much wider acceptable range. The following requirements could restrict functional materials selection, but each of the requirement has very wide range as illustrated:

1) Liquid evaporation: the dispensing system must not dry quickly at the nozzle/air interface.
2) Viscosity: the pneumatic dispenser accepts a very wide range of the liquid up to 1000 Pa s.
3) Surface tension: due to the operating principle of the pneumatic dispenser, surface tension has less impact on actual dispensing compared to the applied air pressure. In theory the gravity and the substrate surface energy force are higher than the ink surface tension force at the dispensing tip, thus enabling the dispensing to be performed. Otherwise the ink will stick to the dispensing tip during dispensing and move afterwards.
4) Suspensions: particles must not settle rapidly or agglomerate, dispersant is recommended. As this is customised dispensing system, a magnetic stirrer can be added into the barrel while dispensing with an alternating magnetic field around the barrel.
5) Filtering: in general, a filter is used to remove any large aggregates or particles which could potentially block the nozzles. However, different nozzle diameter sizes can be used.
6) Degassing: removal of dissolved gas improves dispensing characteristics of most liquids and helps to prevent dispensing failure as air bubbles can break a printed conductive line.

Table 2 summarised pneumatic dispenser printer and inks rheological specification for printing.

Pneumatic dispenser printer specification	
Maximum substrate thickness	No limit
Repeatability	± 5 μm
Increment distance (X,Y,Z)	1 μm
Minimum drop spacing	1 μm
Substrate temperature control	Up to 250 °C (Peltier)
Barrel capacity	0.1 to 10 mL
Acceptable viscosity	1 to 1,000,000 mPa s

Table 2. Pneumatic dispenser printer and inks rheological specification.

2.2.3 Other direct write techniques

2.2.3.1 Aerosol Jet

The Aerosol Jet system [18] made by Optomec is composed of two key components, the atomiser and the deposition head, as shown in figure 5.

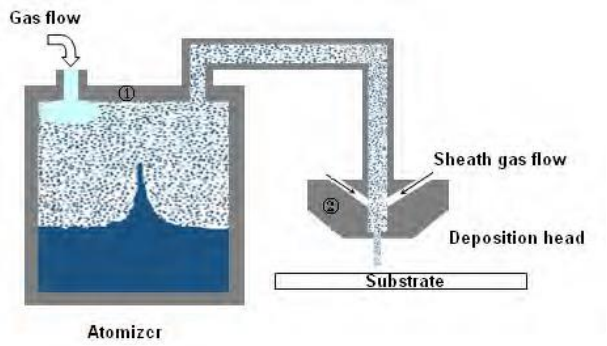

Figure 5. Illustration of the Optomec Aerosol Jet [18].

The raw material to be deposited must be in liquid form and is first placed into either an ultrasonic or a pneumatic atomiser, which is used to generate a dense vapour of material droplets between 1-5 microns in size in a process known as 'mist generation'. Then the generated mist or aerosol, is transferred into a tightly confined jet by a gas flow running through the atomiser and out into the deposition head. The aerosol stream brought into the deposition head is further focused by a second gas flow introduced into the jet. The aerosol stream and the newly introduced sheath gas interact with each other to form a co-axial annular flow, which then leaves the deposition head through a nozzle and lands on the substrate. The Aerosol Jet system can create lines as fine as 10 μm with a minimum pitch of 20 μm. The material handling ability in terms of viscosity falls into a wide range of 0.001 and 2.5 Pa s, which enables deposition of a wide range of materials. [18] [19]

2.2.3.2 nScrypt

A typical filament based direct writing technique is the nScrypt dispensing technique, where a direct write dispensing tool is integrated with nScrypt's novel pump called Smart Pump TM, which is illustrated in figure 6.

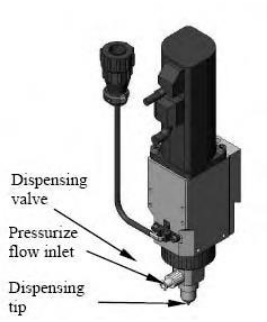

Figure 6. The nScrypt Smart Pump [18].

The integrated smart pump is able to dispense materials with a viscosity of up to 1,000 Pa s with accurately controlled air pressure, valve opening and dispensing height [13]. When dispensing is initiated, a valve opens so as to allow the material to be dispensed to flow through the dispensing tip onto the substrate. Once dispensing stops, the valve closes to block material from leaking. One advantage of the smart pump is that it includes a sucking-back movement of materials into the dispensing nozzle when deposition is terminated. A negative pressure is maintained in the dispensing tip chamber to induce material sucking back when deposition is ceased. This feature allows the orifice to be left clean and clear without -any agglomeration of- material or the possibility of nozzle clogging, and delivers a consistent start every time dispensing commences. Consequently filament based mode printing can be precisely controlled and the width of the dispensed material can be maintained consistent without bulges at the ends. [18]

2.2.3.3 Dip-pen nanolithography

The dip-pen nanolithography (DPN) technique utilises an atomic force microscope (AFM) tip to deliver molecules from the dispensing AFM tip onto substrates, which is especially useful in nanoscale applications. Due to the capillary effect, the AFM tip is capable of dispensing ink adhering to it from previous dipping onto substrates which have an affinity for the ink, in a similar way to a dip pen writing on a piece of paper, as shown in figure 7.

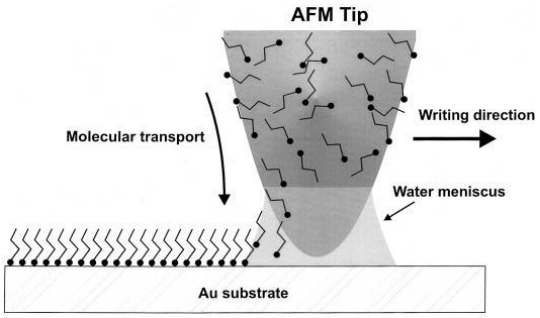

Figure 7. The dip pen nanolithography technique operating principle [18].

The finest feature researchers have achieved with tDPN is close to 75 nm wide. Researchers has also successfully demonstrated writing indium metal onto a substrate and the potential operating temperature is claimed to be much higher than the melting point of indium, as high as 1000 ℃. One key feature of tDPN lies in that it enables ink to be deposited with such abundant thermal energy as to organize into monolayers prior to its solidification. [20]

2.3 Conclusions

The definition of direct write technology has been introduced to explain the operational principle of inkjet and pneumatic dispensing. In addition, other commercially available direct write deposition methods have been introduced to enhance the reader's understanding of the ideas involved in direct write deposition. Physical and chemical limitations of the inkjet printers are explained to highlight the key constraints and objectives in formulating inkjet printable functional inks which will be presented in the chapter 3 with examples. Especially, the inkjet printer has narrow acceptance in selecting the inks on viscosity and surface tension. The dispenser can overcome the inkjet printer's barriers to realising higher capability of printable electronically functional inks. The dispenser can cover a much wider range of solutions' rheological properties than the inkjet printer. In this research, inkjet printing is used as the main direct write fabrication technique as it is the most widely used direct write technique. Then pneumatic dispenser will be tested and evaluated in later chapter as a new direct write technique to compare with the inkjet printing method.

Chapter 3

3 Literature review: electronic materials for direct write

3.1 Introduction

Solution processable active materials are the main driving force in printed electronics research. Organic active materials are is the most straightforward material used in printed electronics and can be easily made into a solution for printed electronics. This chapter starts with reviewing the organic materials used in direct write printed electronics. Organic printable electronic materials can be grouped into three categories,

(1) Insulator
(2) Conductor
(3) Semiconductor

In addition, there is a growing interest in exploring solution processable inorganic materials, because conventional electronics based on inorganic materials has reached a very high level in microfabrication and electronic performance, for example, fine feature size in nanometre scale and high integrated circuit operating frequency. Currently, direct write printable inorganic electronic materials are not as widely used or investigated as the organic materials, but have been noted for their performance, reliability and potential printability. Therefore this chapter will also review the printable inorganic electronic functional materials, following the section on organic materials. Three categories of widely used printable inorganic materials are summarised,

(1) Metallic conductor materials
(2) Transparent metal oxides materials
(3) Silicon and germanium materials

The next key stage in realising the direct write printed electronic devices on fabrics is to investigate the low temperature processed solution-based electronic functional inks. In the last

section of this chapter, the state-of-the-art of low temperature processed functional inks is surveyed, on the basis of commercially available products and published literature.

3.2 Organic materials for printed electronics

Organic electronics is an emerging scientific field of potentially huge technological and commercial relevance. Globally it is an increasingly ubiquitous research activity. Organic electronics, including organic field effect transistors (OFET) and organic light emitting diodes (OLED), can potentially be employed in applications such as RFID tags and the lighting industry. In order to be commercially competitive, these devices must be printed by a low-cost, high throughput process. Additive solution based printing techniques such as inkjet and dispenser printings are attractive processing options. To satisfy the printing process requirements, the functional material should be formulated into inks with appropriate rheological properties for the targeted printing process. In this section, organic materials will be summarised in the following order: organic insulator, organic conductor, organic semiconductor and other functional materials.

Most organic materials are insulators for two reasons. Firstly, the highest occupied molecular orbital (HOMO) of most molecules is completely filled and there is a significant energy difference from the lowest unoccupied molecular orbital (LUMO). Secondly, the solids are usually molecules, not possessing a system of covalent bonds extending over macroscopic distances. To obtain a higher conductivity and hence semiconducting behaviour, the HOMO to LUMO gap needs to be reduced; this can be achieved with extensive π bonding, or by including heteroatoms with lone pair electrons, for example, polyacetylene, polyaniline or polyaromatics. This reduced band gap allows electrons to jump more easily between conduction and valence bands and gives rise to the semiconductor properties towards to conductive grade [21]. For example, the extensive benzene based π-bonding can reduce the energy gap due to the resonance of its own benzene ring shown in figure 8.

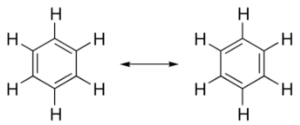

Figure 8. Benzene ring resonance of the π-bonding.

There are a few possible routes by which to realise the inkjet printable inks, as shown in figure 9.

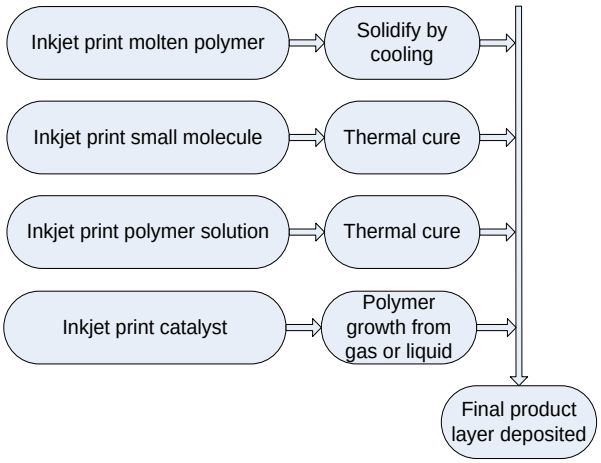

Figure 9. Possible routes for depositing final organic materials product by inkjet printing.

The first route is only applied to organic materials which can be heated to form ready to print molten ink. This route is not suitable for the DMP 2831 used in this research, because it does not support cavity heating for melting the polymer inside. The second and third routes are designed for small molecule and polymer solutions by inkjet printing followed by the curing process. These two methods are commonly used to deposit organic materials at room temperature. The last route consists of inkjet printing a catalyst, normally followed by gas phase treatment for further chemical transition.

3.2.1 Organic insulator materials

Insulator and dielectrics are used to describe a material whose internal electric charges do not flow freely. Dielectrics are insulators, but insulators may not be dielectrics. Dielectric materials can be polarised, where insulators cannot. Therefore, dielectric materials are used in making printed capacitor and insulator materials are used in making printed transistor in this research work. Many organic insulator materials existing which can be used as insulator layer in printed organic electronic devices, for examples, SU-8 (photoresist) and poly(methyl-methacrylate) (PMMA). Most polymer insulators can completely dissolve into organic solvent to form a stable solvent based solution, thus avoiding possible clogging or aggregation of the deposition tools. Polymer insulators benefit from solution processable feature, which can be simply and typically applied by spin coating. In OFET applications, the insulator material is the key material with which to separate the semiconductor layer and the conductive gate

terminal. The electrons pass through the semiconductor layer on the interface boundary with the insulator layer. Therefore the homogeneity and insulating property of the insulator layer is becoming critical for OFET performance.

Figure 10 shows the typical organic insulator materials widely used in direct write deposition and they are catalogued based on their curing methods.

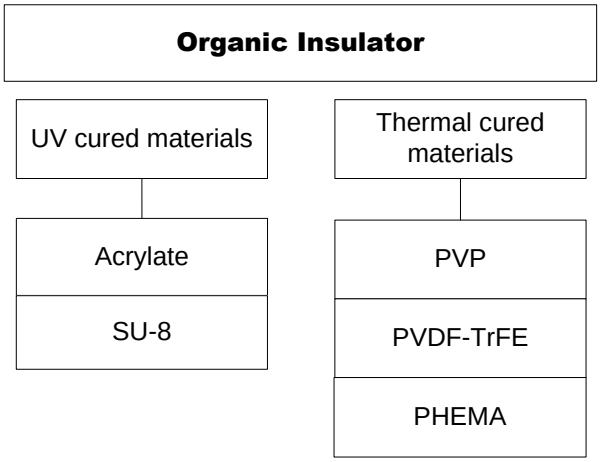

Figure 10 Organic insulator sub-catalogues based on their curing methods.

In general, organic insulator materials can be catalogued into two groups based on their curing condition after direct write deposition:

(1) UV curable organic insulator materials.
(2) Thermally curable organic insulator materials.

3.2.2 Organic conductor materials

A conductor is defined as a material that allows the flow of electric charge to pass through it in any direction in a range of conductivity (10^2 to 10^8 S/cm). Conductivity is the inverse value of resistivity. Resistivity (ρ) equation 1 [22] is based on the conductor's thickness, area (length ×width) and resistance:

$$\rho = R\frac{A}{l} \tag{1}$$

Where

ρ is the resistivity of the conductor in Ω·m,

R is the resistance of the conductor along its length in Ω,

A is the area of the cross section in m^2,

l is the length of the conductor in m.

Therefore the conductivity, which is the inverse value of resistivity, can be obtained as equation 2:

$$\sigma = \frac{1}{\rho} \tag{2}$$

where

σ is the conductivity of a conductor in S/m

ρ is the resistivity of the conductor in Ω·m.

Polymers, either natural or synthetic, are large molecules (macromolecules) comprised of small building blocks or repeating units connected to each other by covalent bonds. In 1954, perylene and bromine complex are invented as the first man-made organic conductive complex of polycyclic aromatic compounds and halogens [23]. This complex has conductivity of 0.1 S/m but very poor stability. This invention led to a new research area in organic compounds. In 1973, the first organic 'metal' tetrathiofulvalene tetracyanoquinodimethan (TTF) (TCNQ) was found to have high conductivity (10^5 S/m) at room temperature [24] [25]. Since 2000, organic conductive materials began to migrate from the research lab to commercial industry. Over the years, polythiophene and poly (3,4-ethylenedioxythiophene) (PEDOT) in particular, have attracted considerable attention because of their high conductivity among organic materials, good environmental stability and potential application in light-emitting diodes (LEDs) [26], organic photovoltaic (OPV) [27], EMI shielding [15], heat generation and chemical sensors [28]. There are two main types of organic conductors, as shown in figure 11:

(1) The conjugated polymer conductor or intrinsically conductive polymer (ICP).
(2) The organic/inorganic composite conductor or extrinsically conductive polymer.

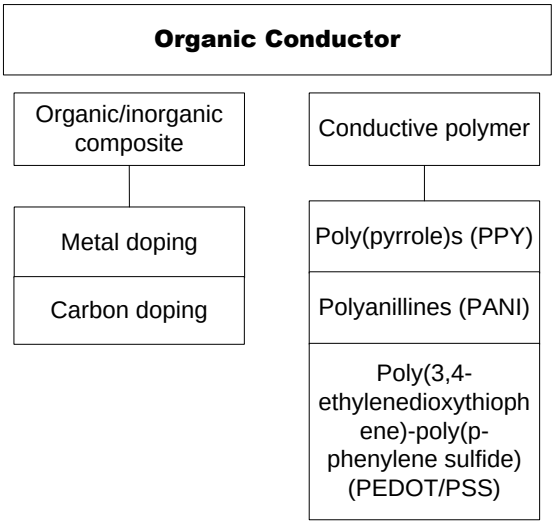

Figure 11. Organic conductor sub-categories based on intrinsic or doping materials.

Conjugated polymers, also known as synthetic metals, can conduct electricity because of the presence of the overlapping of π-orbitals along the molecule [29]. Due to their electron transport characteristics, conjugated polymers are regarded as semiconductors or even sometimes as conductors. Conductive polymers can also be produced by physical blending of conductive materials such as carbon nanotubes (CNTs), carbon black, conjugated polymers, or metallic fillers with inherently insulating thermoplastic polymers. These organic/inorganic composites are known as extrinsically conductive polymers or conductive polymer composites. The conjugated polymer is used as intrinsic polymer material but typically poor conductivity, whereas conductive polymer composites are used to achieve higher conductivity but may not be transparent or recognised as organic devices.

Many conductive organic materials have low ambient stability as well as difficulties in solution processing, therefore commercialisation has not been possible. Thus, many attempts have been made to establish new ICPs with good conductivity, long term stability and better processability so that they can be more easily commercialised. Among the wide range of conjugated polymers already developed, PEDOT also known under the trade names Clevios is one of the most promising conducting polymer to date. PEDOT has provided a good solution of printable intrinsic organic conductive material for printed electronic devices and optoelectronics applications. However, like other organic conductors, PEDOT also has a stiff conjugated aromatic backbone structure, which makes it insoluble and infusible in most organic solvents. Bayer resolved this problem by introducing polystyrene sulfonic acid (PSS), a water-soluble polyanion, during the polymerisation of PEDOT as a charge balancing dopant. This water-soluble PEDOT/PSS complex, known commercially as Clevios, has electrical and film

forming properties that allow fairly stable, transparent conductive polymer coatings on a variety of substrates. However, PSS itself is a non-conducting material, which limits the conductivity of the PEDOT/PSS complex to the 100 to 1000 S/m range [30].

The organic conductors have very poor conductivity compared to metal and doped metal semiconductor, therefore commercial PEDOT/PSS was inkjet printed as a resistor ink as well as reported in a publication of all polymer inkjet printed RC filter in 2003 [31]. Microfab and DuPont in close collaboration developed a conductive polyimide resistive inkjet printable ink [32]. In inkjet printing resistor ink, the conductive polyimide ink is the only inkjet printable resistor ink which has been found in the literature.

3.2.3 Organic semiconductor materials

Organic semiconductors typically are catalogued by the carrier types into p-type and n-type organic semiconductor materials. The design and synthesis of p type organic semiconductor is an area of intense chemical research. Since Koezuka et al [33] claimed to the world's first organic field effect transistor in 1987, the performance of organic p type semiconductor has been investigated thoroughly and steadily improved. The n type organic semiconductor is as important as the p type, due to the need for the fabrication of organic bipolar transistor and complementary logic circuits. However, most of the literature to date places emphasis on the p type materials. Synthesising n type organic semiconductor still presents a serious challenge because of the inherent instability of organic anions that are susceptible to atmospheric oxidants such as water and oxygen. Fullerenes (C60 and C60/C70) and their derivatives are the first groups and most promising group of n type organic semiconductors studied; for example, C60 reaches 0.56 cm^2/V s mobility under high vacuum condition by molecular beam deposition. Therefore in this section, p type semiconductor materials are summarised within the two groups of organic small molecule and polymer semiconductors, as shown in figure 12.

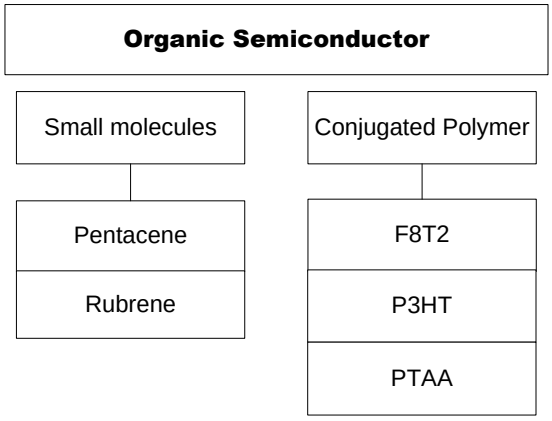

Figure 12. Organic semiconductor sub-categories based on the size of the organic materials.

3.2.3.1 Organic small molecule semiconductors

Small molecule organic semiconductors are currently among the most widely studied organic semiconductors. Particular attention is on the linear aromatic hydrocarbons composed of laterally fused benzene rings, called linear acenes or oligoacenes. Pentacene is the most widely used small molecular p-type organic semiconductor with a linear acene consisting of five linearly fused benzene rings. In this chemically structured acene, the band gap depends on the number of benzene rings in a line, the more benzene rings in it, the lower the band gap. Pentacene is the best organic semiconductor so far in the organic transistor field. Because it is a small molecule organic semiconductor, it does not require a high curing temperature. Air dried inkjet printed Pentacene precursor ink has been reported after [34] [35]. However, a vacuum or nitrogen curing condition is recommended to avoid its semiconductor oxidation, enhance its field effect mobility by creating denser structure and optimise the electrical properties [36].

3.2.3.2 Polymer semiconductors

Polymer semiconductors have high solubility in aromatic solvent and good film forming abilities in solution processing techniques compared with organic small molecule semiconductors in. There are two main groups of polymer semiconductors: amorphous and microcrystalline polymers. The amorphous polymers generally have poor electrical performance compared with microcrystalline material. However, Polytriarylamine (PTAA) and its derivatives are exceptions, offering good electrical behaviour and stability [37]. PTAA is the most widely used amorphous polymer semiconductor because of its outstanding

performance in the group. A typical microcrystalline polymer is Poly[(9,9-dioctylfluorenyl-2.7-diyl)-co-bithiophene] (F8T2), constructed from two polythiophene derivatives. The difference between F8T2 and other general polymer semiconductors, e.g. P3HT and PTAA, lies in the repeating unit of F8T2 which contains two different polythiophenes.

F8T2 is a rigid rod conjugated main chain liquid crystalline copolymer which is normally used in organic electronics as an organic semiconductor, especially in OFET and OPV devices. Under room temperature, it has a shiny bright yellow colour at stable solid form. It will enter the liquid crystalline phase only above 265 ^{o}C after printing [38]. Another advantage of F8T2 over P3HT is its relatively high stability against chemical doping by environmental oxygen or other impurities, e.g. mobile sulphuric acid (PSS) in the conductive PEDOT/PSS ink. It is a widely used p-type organic semiconductor with solution processing capability. F8T2 can be dissolved into various aromatic solvents, for example, xylene, dichlorobenzene and toluene. The solutions are relatively stable in ambient conditions of air and light. To date, due to its crystalline structure, F8T2 based OFET fabrication has required a high curing temperature between 150 ^{o}C and 280 ^{o}C [36]. This ink is of limited use in fabric applications because of its high curing temperature which is higher than the desired 150 ^{o}C maximum processing temperature of standard polyester cotton fabric.

Polytriarylamines (PTAA) has the properties of air stable, solution processable. Their performance has been shown to be inert to ambient air and humidity, which, for long term operation, provides sustained and consistent currents, enabling them to outperform most of the less stable semiconductors. A high temperature annealing is not required to obtain optimal performance, which contributes a great interest in low temperature processing applications. Therefore this amorphous polymer semiconductor is a promising candidate for realising inkjet printed flexible transistors on fabric substrates.

3.2.4 Other organic materials

A further group of materials concerns the use of organic materials for sensors. The operating principle of organic functional sensing material is derived from its conjugated polymer chemical structure, which has been briefly explained earlier in this section. Organic sensing materials can be catalogued into four groups based on their sensing methods:

(1) Resistance changes

(2) Electrochemical potential changes
(3) Photovoltaic changes
(4) Fluorescence alternation changes

The first three sensing methods are more likely to use the conductive conjugated polymers; for example, PEDOT/PSS, polyacethylene, polyaniline, polythiophene and polypyrrole have been used in sensing humidity, metal vapour, gas and other compounds. The fourth sensing method typically uses poly(phenylenevinylene) (PPV), polyparaphenylene (PPP), polyfluorene (PF) and poly(pheny leneethynylene) (PPE) to realise photoluminescence property. Organic sensing materials have three advantages over inorganic or metal oxides sensing materials:

(1) They can be solution processed in the printed electronics industry.
(2) They offer wide scope for synthesis with which to form novel functional properties through change in their chemical structure.
(3) They can fill in the blank area where the inorganic sensing material cannot sense, because synthetic chemical can be made upon requested sensing objectives.

3.3 Inorganic materials for printed electronics

Inorganic materials have always been the most important role as functional materials in the electronics manufacturing industry. Since direct write printing technology has been developing rapidly over the past decade, more and more inorganic materials have been investigated and synthesised to adapt to the various printed electronics disposition methods. Because inorganic electronics have existed for over half a century, the functionality and reliability of inorganic materials are much higher than those of organic materials in electronic performance. Therefore, the research interest of inorganic materials applied in direct write printing research has been growing significantly in the last few years. There are a few challenges to realisation of direct write printable inorganic materials to form a solution or a stable dispersion. In this section, three widely used inorganic materials in the literature are summarised to explain the ability to apply inorganic materials in direct write electronics.

This section starts with metallic materials which are the most widely investigated inks to be used in printed electronics. Then transparent metal oxides are summarised, focusing on ZnO.

Lastly, conventional semiconductor materials silicon and germanium are summarised based on the reported methods of realising the inkjet printable inks.

3.3.1 Metallic conductor materials

Metallic materials can only be inkjet printed if they are in solution or dispersion form. Figure 13 shows the current possible routes for depositing final metal layers (e.g. silver) using inkjet printing.

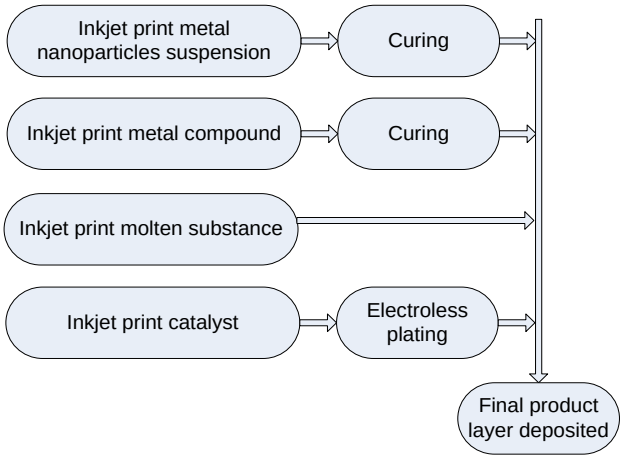

Figure 13. Possible routes for depositing final metal materials product by inkjet printing.

The first route is by metal nanoparticles dispersion, which is the most widely used method for inkjet printed metallic materials. The metal nanoparticles ink have an average diameter of the nanoparticles typically below 200 nm, which is 1/100 of the nozzle size for standard 10 pL nozzles. Nanoparticle size is important as it can affect the dispersion settling time and the curing condition. The larger the nanoparticle size is, the higher settling rate and the higher curing temperature will be. The sintering temperature decreases rapidly as the surface area and volume ratio decrease [39]. To direct write metal nanoparticles, for example silver, is very attractive because of the ability to directly print and cure as electrodes, which results conductive tracks at room temperature. Therefore, this process can be compatible with low temperature processed direct write printed flexible electronics on temperature sensitive substrate, for example, polyethylene terephthalate (PET) and polyester cotton fabric.

The second route is the next most widely used method for inkjet printed metallic materials. It inkjet prints metal salt solutions, for example silver neodecanoate in xylene and copper hexanoate in either isopropanol or chloroform to form a stable solution. This method can completely avoid clogging or aggregating of nanoparticles in the dispersion. Use of metal salts

which decompose under the application of heat or light have been widely reported. For example, More recent studies have shown that the silver neodecanoate conversion temperature can be reduced if the ink is printed directly onto a pre-heated substrate at 130 ^{o}C, which gives resistivity eight times that of bulk silver [40]. Silver nanoparticles can be cured at lower temperature, although the conductivity can only typically reach about 10 % of the bulk metal [41]. Most direct write printable inks are based on metal nanoparticles rather than metal salt solutions. The main reason is the conductivity of the printed conductive tracks is higher with nanoparticles ink than metal salt inks. It is difficult to produce conductive tracks with metal salt inks that are thick or a continuous conductive path, due to the low density of metal atoms in the metal salt ink. However, the metal nanoparticle ink has much higher metal atoms solid content, presenting challenges to the formation of a stable conductive dispersion ink.

The third route, to inkjet print molten metal onto the target substrate, is the simplest and most straightforward deposition method. This method is normally used to solder droplets onto a circuit board. The final route is to inkjet print a catalyst layer, followed by submersion in an electroless plating bath [42].

Considering the four routes, inkjet printing metal compound is a potential option, but it requires several deposits to avoid discontinuous conductive tracks due to the low metal content in the ink. Inkjet printing molten metal is not possible as the inkjet printer used in this research does not have the function of high cavity temperature to melt the raw metal materials. Inkjet printing metal nanoparticles dispersion is the most straightforward method of defining the electrodes in this research work and also widely used method in inkjet printed electronics.

3.3.2 Transparent metal oxides materials

Transparent metal oxides materials benefit from high mobility, high transparency, and good environmental stability. They can behave like a semiconductor in their intrinsic form. They can also behave as a conductor by doping; widely used transparent conductive indium tin oxides (ITO) is an example. Therefore transparent metal oxides materials are another important material group related to the applications of displays, photovoltaics and integrated circuits. Metal oxides semiconductors are much less expensive than organic semiconductors. They belong to the ceramic materials group. For example, zinc oxides are the most widely investigated metal oxides material used in direct write printed electronics. Zinc oxides (ZnO) is a nontoxic inorganic semiconductor substance, the nanoparticles of which can be dispersed

into water or other solvent dispersions, such as, Buhler AG made ZnO dispersion in water [43]. The ZnO field effect transistor's mobility 27 cm^2/V s [44] is much better than that of organic FETs typically under 1 cm^2/V s. However, its flexibility is not as great as that of organic semiconductor layers. The reason metal oxides semiconductor solutions are introduced before the conventional semiconductor materials is its optical transparency; at the same time, research carried out and commercial products available on inkjet printable conventional semiconductor material are very limited. In this section, ZnO is used as an example to explain the two methods of inkjet printing metal oxides materials, as shown in figure 14.

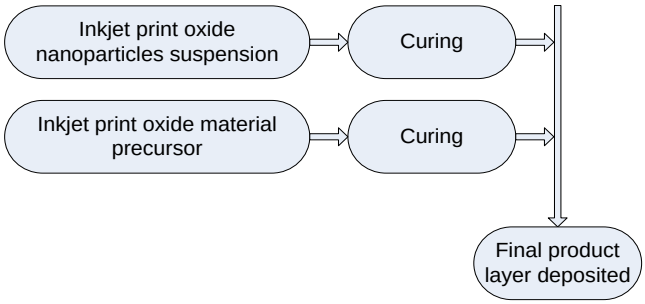

Figure 14. Possible routes for depositing final oxides materials product by inkjet printing

The first route is the same as in the previous method, with metal nanoparticles used to deposit metal oxides materials (e.g. zinc oxides nanoparticles dispersion). However, metal oxides materials tend to have a higher melting point than pure metal (e.g. silver), so the required thermal curing temperature is relatively high and of longer duration. Other sintering methods could be evaluated to avoid flexible substrate damage. For example, a high pulse light can be another option with which to avoid substrate damage. For inkjet printed ZnO dispersion specifically, this method also needs a curing temperature at 200 ^oC for an hour to achieve ZnO film [45] [46]. The standard fabric processing temperature is about 150 ^oC and the maximum temperature is 180 ^oC. Therefore, photonic curing can be the only option for curing the inkjet printed ZnO layer to avoid high temperature curing which could damage the fabric substrate.

The second route is to deposit the metal oxides material precursor, followed by thermally annealing for the chemical transition reaction. An example of zinc acetate dihydrate solution is the ceramic zinc oxides precursor. The most widely used ZnO precursor ink formula is zinc acetate dihydrate with a stabiliser dissolved into methoxyethanol (ethanol or isopropyl alcohol). This method requires a high processing temperature, between 350 ^oC to 450 ^oC [47] [48]. Therefore, this second route cannot applied to smart fabric applications due to high processing temperature.

3.3.2 Silicon and germanium materials

The inorganic semiconductor materials have been involved in the inkjet printed electronics, whereas the inorganic semiconductor materials are typically used in the conventional microfabrication including photolithography and etching. Silicon and germanium are recognised as the most widely used semiconductor material in conventional semiconductor device fabrication. By introducing metal nanoparticles and metal compounds, silicon and its doped product can also be used to achieve an inkjet printed transistor serving as both semiconductor and conductor layers. At present, a direct write processed inorganic semiconductor is relatively rare compared to direct write processed conductor, insulator and organic semiconductor. Particularly in the inkjet printed electronics area, the majority of research studies have focused on printing metal nanoparticle solutions for metallisation and organic semiconductor solutions for the semiconductor layer. In comparison, inkjet printed organic semiconductors can be easily dissolved into aromatic solvents to form a stable solution, while inorganic semiconductors cannot.

There are two companies in the world, Kovio [49] in the US and Intrinsiq Materials [50] in the UK, which are openly developing inorganic semiconductor inkjet printable inks based on a silicon nanoparticles dispersion. Inorganic semiconductors provide the basis for high performance microelectronics devices. They can potentially reach the intrinsic mobility up to 1430 cm^2/V s, lifetimes of over 50 years and switching speeds beyond 1GHz in bulk scale. Unfortunately, the pure inorganic semiconductors are not intrinsically soluble in any type of solvent and do not offer structural variability as a mechanism for altering their solubility. There are only two possible methods by which to direct write inorganic semiconductors as an active ink.

1) Make nanoparticle sized inorganic semiconductor powder and then mix it with dispersant and solvent into nanoparticle sized inorganic semiconductor dispersion. The dispersion is ready to direct write within the required range of rheological properties to meet the specific printing equipment requirements.
2) Direct write inorganic semiconductor precursor solutions, then treat them with post thermally or photonic treatment to chemical transition to form a thin film inorganic semiconductor layer.

The Kovio Company has successfully made an inkjet printed silicon transistor claiming a mobility of 80 $cm^2/V\ s$ [51]. The functional electronics silicon inks can be intrinsic silicon ink or doped silicon ink. This approach requires a very high temperature to cure the silicon nanoparticles following inkjet printing, because the melting point of silicon nanoparticles of 5 nm average diameter is 727 ^oC [52]. However, like the conductive silver and metal oxides inks, the silicon nanoparticle ink can be cured photonically using high energy pulsed light at room temperature. The second approach is similar to that used for earlier inorganic functional materials which can be made by precursor solution. This method can be easily formulated and printed, but the curing conditions are very complicated. Silane based liquid precursor was reported as realising solution processed silicon thin films and transistors with high precision control of different high temperature stages (above 300 ^oC) and different gases input at the different curing stage [53].

3.4 Direct write printable electronic functional materials

3.4.1 Commercial inkjet printable inks

There are a limited number of companies which have commercially available inkjet printable electronically functional inks. Conductive inks, in particular conductive silver ink, are the most common commercially available inkjet printable inks. Inkjet printable conductive inks are the most widely commercialised functional inks, because most other functional inks are still used in the lab. Inkjet printable insulator inks are available commercially, as most of them consist of organic insulator materials dissolved in solvents or acrylate based. Semiconductor materials are much less commercialised than the other functional materials, since they mainly rely on chemical innovation. Table 3 presents a summary of the most promising commercially available inkjet printable electronic functional inks categorised according to the three important functions in this research: conductor, insulator and semiconductor,

Company names	Conductor				Insulator inks		Semiconductor	
	PEDOT/PSS	Silver	Copper	Gold	Thermally	UV	Organic	Si
ABC Nano	-	✓	-	-	-	-	-	-
ANP	-	✓	-	-	-	-	-	-
Agfa	✓	-	-	-	-	-	-	-
Chisso	-	-	-	-	✓	-	-	-
Cima Nano	-	✓	-	-	-	-	-	-
Collins	-	-	-	-	-	✓	-	-
Heraeus	✓	-	-	-	-	-	-	-
Hexion Chemical	-	-	-	-	-	✓	-	-
Hisense	-	✓	-	-	✓	-	✓	-
Intrinsiq Material	-	-	✓	-	-	-	-	✓
Johnson Matthey	-	-	-	✓	-	-	-	-
Kovio	-	-	-	-	-	-	-	✓
Merck	-	-	-	-	-	-	✓	-
Methode Electronics	-	✓	-	-	-	-	-	-
MicroChem	-	-	-	-	-	✓	-	-
NanoMass	-	✓	-	✓	-	-	-	-
Novacentrix	-	✓	✓	-	-	-	-	-
Polyera	-	-	-	-	✓	-	✓	-
SmartKem	-	-	-	-	-	-	✓	
SunChemical	-	✓	-	-	-	✓	-	-
Xennia	✓	✓	-	-	-	✓	-	-

Table 3. Summary table of current commercialised inkjet printable electronically functional inks.

3.4.2 Pneumatic dispensing inks

Various liquids, including adhesives and electronic functional inks, have been deposited using pneumatic dispensers. Pneumatic dispensable inks have a very wide acceptable range of rheological properties. Most pneumatic dispensers are designed to operate with liquid viscosity up to 1,000 Pa s, which covers the majority of liquid materials, as shown in table 4. Therefore, in practice the pneumatic dispenser does not have a specific and strict ink requirement.

Liquid material types	Detailed possible liquid products in the same group
Various adhesives	UV setting adhesives, cyanide based adhesives (super glue), anaerobic adhesives, rubber family adhesives, one-part epoxies, two parts epoxies, hot melt adhesive and pressure-sensitive adhesives.
Solvent/volatile materials	Alcohol, methyl ethyl ketone, ammonia, toluene, trichloroethylene, acetone, Freon.
Semiconductor and PC board component mounting related liquids	Solder, flux, conductive adhesive (silver paste), urethane adhesive, junction coating epoxy resin, junction coating resin and resist.
Various lubrication agents	Silicone oil, silicone grease, industrial oil, industrial silicone grease, engine oil, motor oil and precision equipment oil.
Various resins	UV resins, epoxy resin with filler, paraffin (heated), wax, hot melt resin and emulsion resin for fibres.
Various paints	Inks, dyes, solvent based paints, water-soluble paints, fluorescent paints, lacquers and enamels.
Others	Various brazing pastes (gold, silver, copper), sealing agents, sealing silicone liquids, one-part Room Temperature Vulcanising (RTV) rubber and two-part RTV rubber.

Table 4. Summary table for pneumatic dispenser printing including most widely used material.

3.4.3 Discussion

Flexible electronics fabrication is one of the main applications for direct write printing technology. Most flexible substrates suffer as a result of high processing temperatures (>150 ^{o}C); for example, polyethylene film and fabrics. Therefore, to realise direct write printed flexible electronics on fabric, low temperature processed functional inks must be investigated thoroughly. Low temperature processed functional inks are discussed within three categories: conductor, insulator and semiconductor inks. The full range of inkjet printable inks, including all screen printable pastes, can potentially be pneumatically dispensed. Therefore, only the low temperature processed inkjet printable inks will be reviewed in this section. In addition, all metal related inks including nanoparticles dispersion and compound solution can be potentially photonically cured with high energy pulsed light. However, this technique is unavailable at the University of Southampton. Standard mercury bulb UV curing and thermal curing methods are discussed in relation to the low temperature processed inkjet printable inks.

Low temperature processed conductive materials used in direct write printing are typically the inorganic silver nanoparticles dispersions and the organic PEDOT/PSS ink for inkjet printing. Inorganic silver nanoparticles dispersion ink curing temperature varies from 120 ^{o}C to above

200 ºC depending on curing time and the size of the silver nanoparticles. In addition, there is compromise between the curing temperature and the conductivity under the same curing time and conditions. Ideally, the higher the curing temperature for silver nanoparticles formed film, the better in respect of the layer's uniformity and conductivity. Different curing processes for PEDOT/PSS are suggested by the Heraeus Clevois company. Curing effectiveness starts at 80 ºC, as the higher the temperature, the shorter the curing time. Typically the curing temperature is set within the range of 80 ºC to 120 ºC, with the specific time depending on the temperature, coating thickness and curing conditions. The minimum curing time is limited by the evaporation rate of the water from the PEDOT/PSS ink, which is about 30 to 60 s in a thermal oven [54].

Low temperature processed insulator materials, either organic or inorganic, used in direct write printing are not widely reported. Inkjet printable inorganic solution based insulator materials are not common and require a high curing temperature at or above 200 ºC [55] [56]. Typically, researchers tend to use dip coating and spin coating organic insulator inks to create a uniform thin insulator layer on top of which further layers are deposited sequentially. In addition, the spin coated solvent based insulator film is typically followed by thermal curing with the temperature at or above 200 ºC, which is not compatible with most flexible substrates. Most inkjet printable UV curable insulator inks benefits from room temperature processing are typically acrylate materials. However, Liu et al [31] reported that the inkjet printed poly(biphenyltetracarboxylic dianhydride-co-phenylenediamine) (PBPDA-PD) can be thermally cured into insoluble stable polyimide at 50 ºC. Choi et al [57] reported a spin coating formulation of poly(4 vinylphenol) (PVP) insulator solution that can be cross linked at 70 ºC. PVP is the most widely used inkjet printable organic insulator ink in inkjet printed electronics research, because of its high insulator performance while interacting with inkjet printed organic semiconductors and conductors. Therefore, investigation of low temperature processed inkjet printable PVP ink will be one of the tasks and novelties in this research work.

Low temperature processed inkjet printable semiconductor inks are limited to organic semiconductor materials. They mainly fall within the groups of amorphous organic polymer semiconductor which does not require a specific curing stage except a drying stage to fully evaporate the solvent. In addition, the small molecule organic semiconductor materials, which typically are transformed from the chemical precursors under thermal curing, can be transformed by their chemical precursor solution for inkjet printing; for example, TIPS-

pentacene can be cured at 80 ºC for an hour in a nitrogen environment which increases the difficulty and complexity of the process.

3.5 Substrates for printed smart fabrics

This research is primarily targeting fabrics which are suitable for everyday clothing, since there is a significant number of applications in this area. In these applications, the most widely used fabrics are cotton, polyester, and polyester cotton blends. An important consideration when printing smart fabrics is the curing temperature required for the printing inks/pastes. This must be lower than the maximum temperature that the substrate can survive without observable degradation. Of the three widely used fabrics. Polyester cotton has both cotton and polyester in, therefore, whichever has a lower limit in processing temperature and chemical resistant properties will limit the process condition. In our experiment, polyester cotton can survive at 150 ºC for 45 minutes without observable degradation. Longer time and higher temperature lead to discolouration. The higher the temperature increases, the shorter the survival time. Therefore, the target is to develop a suitable printing capability with a low enough process temperature for polyester cotton: this technology can therefore migrate to polyester and cotton fabric as they can survive higher temperatures.

In the polyester cotton fabric, polyester fibres have a melting temperature of 250 to 300 ºC. [58] At these temperatures, the polyester will melt into tiny beads, which become absorded on the cotton matrix. The cotton does not melt but decolourises approximately 175 ºC and pyrolyzes into a gas at approximately 427 ºC. The cotton fibres are still solid as the polyester fibres melt and therefore the cotton fibers become a scaffold for the polyester beads of the liquid melt which occurs around 254 ºC. [59]

There are other commercially available fabrics which have higher survival temperature above 200 ºC, for example, Kermel and Kevlar. Kermel is a specialist fabrics target to personal protetive equipment applications, e.g. firefighters' uniforms. Kevlar also finds applications in personal protective equipment, such as special military uniforms. However, these are not as widely used fabric as the 65/35 polyester cotton and are not used in everyday clothing.

3.6 Conclusions

This chapter introduced the widely used materials for direct write processes on inkjet and pneumatic dispenser printings. The discussion is mainly emphasised on inkjet printable inks as dispenser could have very wide tolerance in material selecting. The potential materials from organic and inorganic groups for this research work are noted, along with their physical, chemical and rheological properties for achieving the final objectives. The ink requirements are explained in detail for inkjet ink and pneumatic dispensable ink groups respectively. To realise the direct write printed flexible fabric electronic devices, the low temperature processed inkjet printable materials are reviewed in the last section of this chapter and potential materials for this research work have been indicated for further practical works. Inorganic silver nanoparticles dispersion (SunChemical) and organic PEDOT/PSS (Clevios) can be potential candidates to realise low temperature processing of direct write printed conductive patterns. PVP insulator material is chosen to further investigate on low temperature processed inkjet printable PVP ink this research. Organic amorphous polymer semiconductor is the potential material to realise inkjet printed transistors. In addition, the potential challenges in investigating new materials have been pointed.

Chapter 4

4 Literature review: inkjet and dispenser printed antennas, capacitors and transistors

4.1 Introduction

Inkjet printing is the most widely investigated direct write printing technique. Researchers first started to use inkjet printing as a patterning tool in 1997 in electronics fabrication [60]. Since then there is a significant growing interest in inkjet printed electronics after the first inkjet printed transistor was made in 2000 [38]. In this chapter, inkjet printed electronic devices will be reviewed in this order: antenna, capacitor and transistor followed by a brief review of pneumatic dispenser printed electronic devices. The ultimate aim of this research work is to apply direct write printing to fabric substrate to realise smart fabrics. Therefore, opportunities for applying direct write technology to smart fabrics and key applications are discussed in the last section of this chapter.

4.2 Inkjet printed conductor and antenna

4.2.1 Stretchable conductive pattern

An inkjet printed stretchable conductive pattern has never been reported in the literature and it presents a significant challenge compared with traditional metal or non-metal conductors as they are not stretchable. Stretchable electronics can be achieved in two conceptually different, but complementary, ways.

(1) One method develops new stretchable materials in conventional layouts.

However, only a few stretchable conductive materials have been realised: Stretchable CNTs conductor made of CNTs mixed with ionic liquid [61] [62] and stretchable metal conductor made by a molecular self-assembly process called Electrostatic Self-Assembly (ESA) [63].

(2) The other method relies on the use of new structural layouts with conventional not stretchable materials

There are three approaches based on changing the structure layout:.

(I) The first approach exploits an elementary result in mechanics: any material in sufficiently thin form which is flexible does not have to be stretchable. By virtue of bending strains decrease linearly with the decreasing thickness as shown in figure 15. A silicon wafer is brittle and rigid, but ribbons, wires or membranes of silicon in nanometre scale are flexible [64].

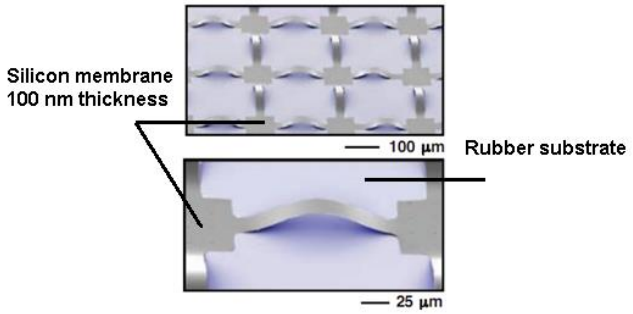

Figure 15. Silicon membrane (100 nm thickness) patterned into a mesh geometry and bonded to a rubber substrate only at square pads located between arc sharped bridge structures, presented in moderate (top) and high (bottom) magnification scanning electron microscope (SEM) images. [64]

(II) The second approach is making the thin evaporated metal layer into wavy shapes as shown in figure 16 [65] and bonding them into elastomeric substrates yields stretchable systems.

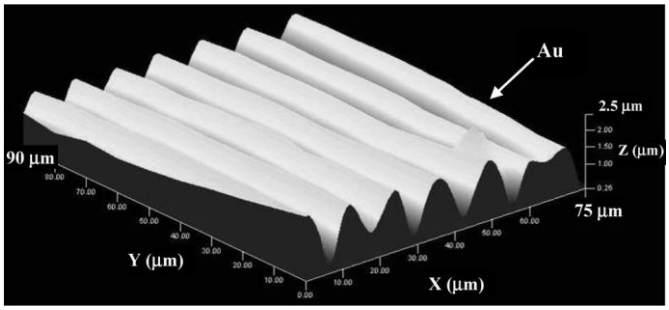

Figure 16. Three dimensional profile of a gold surface wavy film after released 15 % pre-stretch

This method has also been used to pattern stretchable organic PEDOT/PSS conductive film [66]. This pre-stretched printing pattern method combines the special wavy structure and the flexible thin film properties, achieving a stretchable and compressible film.

(III) The third approach is the horseshoe shaped structure, shown in figure 17, which was developed as part of the SWEET [67] and STELLA [68] European Union projects.

Figure 17. Plan view of a horseshoe shaped structure layout

This method does not use the thin film bending advantage but achieves the stretchability by reducing the strain on the conductive track in the horseshoe shape pattern while being stretched.

Using this horseshoe shape fabrication method, a stretchable dipole antenna can also be inkjet printed to realise a frequency tuneable antenna by changing its effective transcieving length. Previous works have been done [69] [70] [71] to achieve a stretchable antenna: Arriola et al [69] uses a meander shaped conductive pattern on stretchable polyurethane and silicone substrates to realise a stretchable dipole antenna, Kubo et al [70] realised a stretchable dipole antenna based on microfluidic conductive liquid with stretchable polydimethylsiloxane (PDMS) and Liu et al [71] achieved a stretchable dipole antenna and planar inverted-F antenna (PIFA) on PDMS substrate.

No publication on stretchable antennas has covered either inkjet printing or fabric substrates. Therefore, an inkjet printed stretchable antenna on fabric would provide an advance on the current state of the art.

4.2.2 Inkjet printed antenna

The inkjet printed conductor is the most basic electronic component in inkjet printed electronics. An inkjet printed basic antenna structure, for example, a planar dipole antenna, requires only one conductive inkjet printable ink for the conductive radiating layer planar antenna. The most promising antenna geometries for direct write printing are planar monopole [72], planar dipole [73], loop antenna [74], patch antenna [75] and inverted-F antenna [76]. The majority of publications of inkjet printed antennas are inkjet printed RFID antennas, which are typically loop antennas or planar dipole antennas. There are a variety of antennas which can be applied to RFID applications including dipole antenna, loop antenna, crossed dipole antenna and patch antenna. Planar loop and dipole antennas, applied in RFID applications, are the most widely investigated antennas in inkjet printed RFID antennas.

However, there are no publications or commercial products realising an inkjet printed antenna on a fabric substrate. The substrates reported in the publications are mainly flexible substrates including paper [72], Kapton [74] [76] and PET [75]. Inkjet printed conductors can be potentially used to make an inkjet printed antenna on fabric. There are no publications or research work relating to inkjet printed fabric antenna. Therefore, the following section will summarise the achievement of wearable fabric antennas, pointing towards realising inkjet printed wearable fabric antennas in a chapter 5.

4.2.3 Wearable fabric antenna approaches

A wearable fabric antenna is defined as an antenna that is composed of conventional or industrial fabrics [77]. Typically, fabric antennas are made from conductive fibres with the antenna being part of the fabric. Several types of antennas can be realised in wearable implementations as they have relatively small profile planar structures, which can be unobtrusive in everyday clothes. A wearable fabric antenna is flexible in two dimensions and can simultaneously bend along two planes and potentially stretch. It is optimised to perform in close proximity to the human body and conforms to the surface on which it is attached (e.g. the human body) [78]. Wearable fabric antennas are needed to achieve wireless communication between the wearable system and the outside world as it is a desirable requirement for many smart fabric applications. This technology is aimed at various wearable fabric applications including medical, sports training, military and 'first responders' garments. For example, a wearable electrocardiogram system can send the signal wirelessly from the patient thus improving patient comfort; soldiers can communicate together by means of fabric antenna integrated in their uniforms. In addition, RFID tagging on clothes is another important area as it allows stock checking and security measures.

There are three main approaches to the manufacture of wearable antennas. The first approach is to attach conventional antennas onto fabric, a system defined as wearable electronics rather than smart fabrics. It merely involves conventional components being contained or attached to clothing. The first commercial wearable antenna in 2007 [5] and a similar commercial product in 2009 [78] fit within this category, as they use fabric to envelop a conventional flexible antenna. Also in 2007, a rigid solid tactical vest antenna [79] was released using two unspecified commercial wearable antennas. The wearable antennas were either flexible [78] or rigid [79].

The second approach to wearable antennas is a yarn based method, using weaving or knitting conductive yarn within a conventional fabric to realise a conductive fabric acting as a radiation element or ground plane. The first knitted copper yarn based fabric antenna was made in 2003 [80]. The entire antenna was constructed in fabric with a fleece substrate, while the radiation element and ground plane were made of knitted copper. Development of a woven fabric antenna was presented in 2003 [81]. The material of the antenna patch and the ground plane were made of woven conductive fabric and then sewn into clothing.

The third approach to wearable antennas is to deposit a conductive layer onto a fabric acting as the radiation element or the ground plane. With this approach, the vast majority of published studies achieve a fabric antenna by depositing a conductive layer using the metal plating method (2004) [82] [83] or metallised adhesive tape (2004) [84] to form a conductive layer on top of the fabric substrate. Massey et al [82] is considered to be the world's first fabric antenna made in 2001; its radiation element and ground plane were made of copper plated nylon.

Printing is another method within the third approach to deposit a conductive layer onto fabric. Several printing methods have been used to realise wearable fabric antennas. Screen printing is the most widely used deposition technique for printed fabric antennas, as it can easily pattern conductive paste onto fabric to form a flexible, strong and suitably thick functional layer [85] [86]. Direct write printing has been firstly used to develop wearable fabric antennas in 2007 [87] [88]. Patra et al [87] [88] the first direct write printed patch antenna on 100 % cotton mercerised twill fabric substrate using a technique called micro drop deposition. The micro drop deposition is one of the direct write printing, which can be considered as dispenser printing. Figure 18 (a) shows the direct write printed fabric patch antenna.

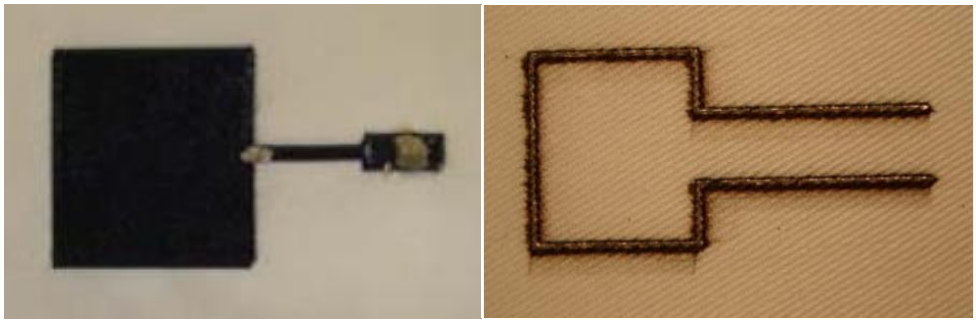

(a) (b)

Figure 18. Plan view images of (a) micro droplet deposition printed patch antenna by PEDOT/PSS and (b) inkjet printed silver lines on the top of the PEDOT/PSS polymer line as an interface layer.

Figure 18 (b) shows the printed silver nitride line directly onto the inkjet printed PEDOT/PSS line as the interface layer on fabric. The fabric used in the figure 18 has higher cost, higher level of lustrous appearance and less widely used in everyday life rather than the widely used standard 65/35 polyester cotton fabric. The reason of choosing the 100 % cotton mercerised twill fabric may be that, it is easy for printing and low roughness surface. Reference [87] [88] are the only two publications related to direct write printed fabric antenna until the author reported the first inkjet printed dipole antenna on the standard 65/35 polyester cotton fabric substrate in 2012 [89].

4.3 Inkjet printed capacitor

An inkjet printed capacitor is one of the fundamental passive electronic components in future inkjet printed smart fabric electronic circuits. A basic inkjet printed capacitor structure requires two functional materials: a conductor and an insulator. The structure can be either a parallel plate structure or an interdigital structure [90] as shown in figure 19.

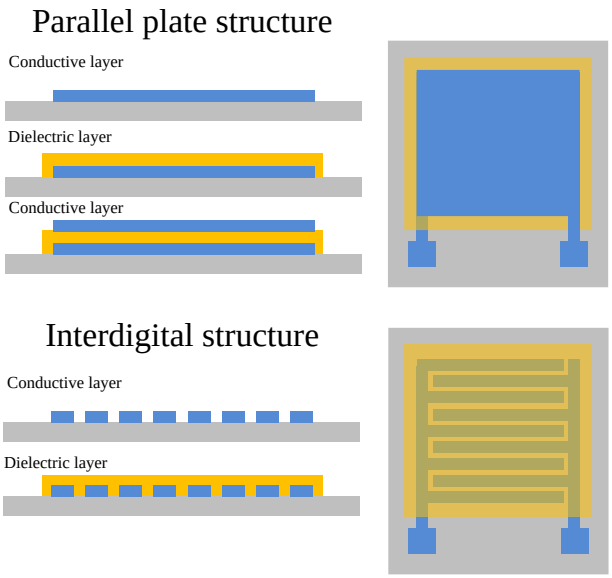

Figure 19. The cross sectional view and planar view of both parallel plate structure capacitor fabrication steps and interdigital structure capacitor fabrication steps.

When fabricating a capacitor, the area and thickness of the dielectric layer in parallel plate structure, while the gap and length of the interdigital in interdigital structure could be varied to achieve a range of target capacitance values.

Comparing the two capacitor structures, it can be seen that three layers are required for the parallel plate structure and only two for the interdigital structure. For fabrication, it is much easier to inkjet print the interdigital structured capacitor. However, the final objective of this research work is ultimately to realise a flexible transistor. The capacitor is an intermediate development stage with which to investigate the capable inkjet printable low temperature processed dielectric ink as a preparation for the more complex electronic device fabrication. The interactions between three layers in a capacitor and dielectric properties can all be studied using the parallel plate structure format capacitor. In addition, problems of alignment between inkjet printed layers can be identified and improved using this structure. Therefore, in this research work the parallel plate structured capacitor is selected in later practical work.

For printing on fabric, it is preferred to use inks with low curing temperatures (<150 ℃). In an all-inkjet printed capacitor, the thickness, smoothness and dielectric properties of the printed dielectric will significantly affect its performance. Typically, two deposits of the dielectric ink for one layer are required to avoid or minimise the pinholes in the dielectric film by overlapping the two deposits. The pinholes will cause short circuits or reduce the performance of the dielectric. A thicker inkjet printed layer will decrease the capacitance of the capacitor. In addition, a thick insulator layer also precludes the use of the dielectric layer in other all inkjet printed applications such as printed transistors. A thick insulator layer in a printed transistor will require high operating gate voltage to turn on the device. Solvent based inkjet printable dielectric inks can produce a thin dielectric layer, but these typically require higher curing temperatures, e.g. a thermally curable inkjet PVP layer requires 200 ^{o}C [91]. Therefore, an inkjet printable UV curable dielectric ink for thin film deposition by inkjet printing at room temperature is of significant interest.

There have been a number of approaches to capacitor fabrication using inkjet printing. Some use additional fabrication methods other than inkjet printing to realise the capacitor [92], others are based on rigid substrates [31, 93] or require temperatures at 280 ℃ [93] which are too high for the majority of fabrics. All inkjet printed (all organic [31] and all inorganic [94]) structured capacitors have been reported. Sriprachuabwong et al [92] describes a capacitor in which the conductive plates are inkjet printed using a PEDOT/PSS conductive polymer ink on two flexible PET substrates. An ethyl-2-cyanoacrylate adhesive was used to stick the two PEDOT/PSS coated PET substrates together and act as the dielectric of the capacitor. Liu et al [31] describes an all polymer capacitor fabricated on a rigid substrate by all-inkjet printing

using PEDOT/PSS ink and a polyimide (amic acid solution) dielectric ink. In 2011, an all inkjet printed capacitor was fabricated on a rigid alumina substrate using a silver conductor ink cured at 370 ℃ and a $BaTiO_3$ dielectric ink cured at 280 ℃ [93].

Based on the literature review, there is no all inkjet printed capacitors on fabric or flexible substrate with processing temperature less than 150 ^oC. The author reported the first inkjet printed SU-8 capacitor on flexible Kapton film [95] and a smart fabric capacitor standard 65/35 polyester cotton fabric substrate [96] in 2012.

4.4 Inkjet printed transistor

A transistor is the key active electronic device in integrated circuits. The inkjet printed transistor with an organic semiconductor as the channel material, has had a major impact on the direct inkjet printing of polymer OFETs. Researchers at the University of Cambridge made the first high resolution channel length all polymer TFTs in 2000 with a combination of inkjet printing and spin coating, using an organic semiconductor material F8T2 [38]. However, the general electronic mobility of inkjet printed organic semiconductor materials are still very poor in the range of 10^{-2} cm^2/V s to 1 cm^2/V s compared to the intrinsic silicon mobility up to 1430 cm^2/V s. Spin coated organic semiconductor layer may produce a mobility value a few times higher than the inkjet printed same material, as it results in a smoother surface layer than inkjet printing.

The inkjet printed transistor is not well defined in the literature. A transistor has been defined as inkjet printed even if only one of the four functional layers in the transistor (gate electrode, insulator, source/drain electrodes and semiconductor layers) is printed. The term ‘all inkjet printed’ transistor is introduced, referring to one which is fabricated by all inkjet printing the four layers without any other deposition method. Typically, researchers tend to inkjet print the source/drain/gate electrodes only and spin coat the other semiconductor and insulator layers. There are six publications including a patent which describe an all inkjet printed transistor, all of them claimed to have fabricated the all inkjet printed polymer transistor [6, 7, 34, 97, 98, 99, 100, 101, 102]. However, none of the methods could apply to this research work, for the reasons of processing temperature, equipment limitation or unknown ink formulations.

(1) The first publication of an all inkjet printed transistor on glass substrate [6] used etch-mask definition before inkjet printing inks in 2004 by Palo Alto Research Center.

(2) In the same year, Berkeley research group reported the world's first true all inkjet printed transistor on PET that was made of gold conductor, PVP insulator with a pentacene precursor as the organic semiconductor [97]. The curing temperature of the PVP insulator is not stated in the publication.

(3) In 2007, an all inkjet printed transistor technology was registered as a patent; it was made by silver conductor, UV ink insulator and TIPS-PVP as the organic semiconductor [99]. UV curable polymer insulator is used. Patent file does not include the polymer insulator name.

(4) In 2008, Palo Alto Research Center reported an all inkjet printed transistor on polyethylene naphthalate (PEN) with silver electrodes, PVP insulator and PQT-12 semiconductor layers [98]. PVP insulator formulation and curing condition are not included in the publication.

(5) In 2009, Berkeley research group that made the world's first all inkjet printed transistor [97] reported another all inkjet printed transistor process, but with surface energy modification [100]. The PVP insulator is thermally cured at 200 ^{o}C in the printed transistor.

(6) In 2009, a further all inkjet printed transistor on polyethylenesulfone (PES) was made with silver conductor, sol-gel insulator and pentacene TIPS precursor as organic semiconductor [7]. Synthesized organic/inorganic hybrid insulator precursor solution requires inkjet printer head nozzle size of 50 μm.

(7) In 2010, Ricoh reported an all printed organic TFT. A surface energy control method is used for the desired pattern [100].

(8) In 2011, the most recent publication of a fully inkjet printed transistor was reported [34] [102]. However 200 ^{o}C curing temperature is required for the thermally curable PVP insulator ink.

The claimed all inkjet printed transistors are summarised in table 5.

No.	Year	All inkjet printed (AIJP)	Conductor	Insulator	Semiconductor	Substrate	Flexibility
1	2004	AIJP with etching process	Gold	Si_3N_4/SiO_2	PQT-12	Glass	-
2	2004	Fully inkjet printed	Gold	PVP	Pentacene	PET	✓
3	2007	Fully inkjet printed	Silver	UV ink	Pentacene	-	-
4	2008	Fully inkjet printed	Silver	PVP	PQT-12	PEN	✓
5	2009	AIJP on modified surface	Silver	Sol-gel	Pentacene	Si wafer	-
6	2009	Fully inkjet printed	Silver	Sol-gel	Pentacene	PES	✓
7	2010	AIJP on modified surface	Silver	Polyimide	Small molecule	Kapton	✓
8	2011	Fully inkjet printed	Silver	PVP	Pentacene	Glass	-

Table 5. A summary table of the claimed all inkjet printed transistor publications.

The reasons for spin coating the semiconductor and insulator layer not using the inkjet printing are:

(1) Spin coating can provide a 'large area' transistor array fabrication in a very short time, e.g. a whole wafer sized substrate rather than a few transistors in a millimetre squared area.
(2) Semiconductor and insulator layer thicknesses need fine control for a high performance transistor; a 15 to 30 nm thickness is needed for the semiconductor layer as part of a flexible transistor, as well as submicron thickness for insulator layers [38]. Inkjet printing does not give good thickness control. Inkjet printing cannot achieve as inkjet printed layer is digitised into pixel droplets resulting in a pixilation effect. In addition, inkjet printing typically accumulates a thick ink layer, which results in an uneven cured surface in thickness.
(4) Pin holes tend to appear randomly in the inkjet printed film due to nozzles clogging or cured uneven layer thickness. This can cause device failure, especially in sandwich structure devices fabricated by inkjet printing.

Researchers generally follow two themes in inkjet printed flexible transistor research:

(1) In inkjet printed transistor research, achieving higher resolution of inkjet printed channel length with different additional assisting equipment or processes are one research theme in literature review. The semiconductor and insulator layers are generally spin coated. The channel length is defined by the distance between source and drain electrodes. Publications report different methods with combination of other additional equipment and inkjet printing to achieve new processes. Examples of other assisting equipment are including surface modification, nanoprinting and laser sintering.

(2) In inkjet printed transistor research, inventing new semiconductor chemicals for the semiconductor layer will significantly increase transistor performance in terms of the materials' intrinsic properties; for example: carrier mobility and air stability.

4.5 Dispenser printed electronic devices

Dispenser deposition in manufacturing is a more mature technology than inkjet printing and has been widely used in the electronics manufacturing industry, for example, dispensing sealant, adhesive in bonding electronic devices and packaging. However, the materials being dispensed

are not electronically functional materials. Since 2000, research interest in dispenser printed electronics has been growing slowly compared to inkjet printing electronics. Researchers use the dispenser to make complicated structures, such as, direct write printed 3D silk/hydroxylapatite scaffolds [103] for the medical industrial and direct write printed ITO microelectrodes [104] for electronics manufacturing. A pneumatic dispenser printed zinc microbattery [105] [106] was a milestone in dispenser printed electronics in 2008. Since that time, the thermoelectric energy harvester [107] and the proof mass of MEMS vibration energy harvester [108] have been made by dispenser printing. The dispenser printed electronic devices are still very limited. There are only limited research groups in the world involved in this research field, whereas Lewis Research Group [109] and Berkeley Manufacturing Institute [110] are the two leading research groups in dispenser printed electronics.

4.6 Direct write printing in smart fabrics

Direct write printed electronics has rarely been applied to smart fabrics except there are two US National Textile Center annual project reports reported dispenser printed antenna directly onto fabric substrate [87][88]. These two publications were previously discussed in section 4.2.3. Inkjet printing has more strict requirements in selecting materials than dispenser and other direct write printing techniques and dispenser can deposit all inkjet printable inks. Therefore, in this section inkjet printing is discussed without emphasising pneumatic dispenser printing.

Inkjet printable inks have a very high solvent content (> 85 %) compared to other direct write printing inks. Therefore, to inkjet print electronics directly onto standard fabrics poses a formidable challenge, as the fabric materials can absorb the inks immediately when it lands. Therefore, the screen printed interface (Fabink-IF-UV4) has been pre-screen printed on standard fabric for further direct write printing. Screen printed interface layer on fabric has never been achieved outside the University of Southampton. The interface layer acts as the supporting layer for the subsequent printed layers. The functionality of screen printed interface layer will be described in details in later chapter. Hence, all electronic devices including passive and active devices in this research work can potentially be inkjet printed on to fabric using the interface coated fabric substrate.

4.7 Conclusions

This chapter has summarised the following inkjet printed devices: antennas, capacitors and transistors. In the inkjet printable antenna section, the state-of-the-art of inkjet printed antennas has been reviewed. Wearable fabric antennas have been discussed and compared to the printed approach, highlighting their limitations such as traditional flexible antenna enveloped by fabric and deposited conductive layer onto fabric without interface. This antenna review has shown that there are a number of potential planar antenna structures that may be suitable for direct write printing on fabric.

Inkjet printed capacitors have been reviewed with a comparison of the two different structures (parallel plate and interdigital). The review has highlighted the limitations of current dielectric materials used in flexible capacitors such as, high curing temperature and thick dielectric layer. Therefore, alternative materials need to be identified.

Inkjet printed transistors have been reviewed chronologically by distinguishing the inkjet printed transistor and the all inkjet printed transistor. In addition, the challenges of realising an all inkjet printed transistor on fabric have been highlighted for further investigation.

Finally, dispenser printed electronic devices have been introduced with examples. The literature has shown the possibility of applying direct write printing on to fabric to create smart fabric materials which would have greater design freedom. This solution could be easier to manufacture and produce less waste than conventional smart fabric manufacturing.

Chapter 5

5 Inkjet printed smart fabric antenna

5.1 Introduction

This chapter discusses the fabrication and performance of inkjet printed smart fabric antennas. Two types of antenna have been inkjet printed onto a standard fabric substrate. These are a half wavelength dipole antenna and a patch antenna, both designed to operate at the 2.4 GHz communications frequency except aeronautical devices, as agreed by the European Commission Radio Spectrum Decision [111] and International Telecommunication Union (ITU) [112]. This chapter begins with the theory, design and architecture of the two selected antenna types, followed by their fabrication. Flexible substrates are evaluated by inkjet printing conductive layers on the selected substrate surfaces. Conductive inks are tested and selected based on an evaluation of their printability, flexibility and conductivity.

The theory and fabrication sections are followed by a device testing section. In the device testing section, the performance of the inkjet printed smart fabric dipole antenna and patch antenna are examined and discussed. The inkjet printed antennas work is a collaboration between the University of Southampton and Loughborough University. The University of Southampton realised all the fabrication part of the work and Loughborough University carried out all radio frequency measurement based on the printed antenna samples.

5.2 Theory, design and architecture of printed antennas

An antenna (or aerial) is a signal transducer that can transmit or receive radio frequency electromagnetic waves. There is a slightly fundamental difference between transmitting and receiving antennas. Therefore, the same antenna is often used for both tasks, such as antennas in radar and ID card transceiver systems. In future, the increasing interest in RFID devices in the ‘internet of things’ [113] could require one transceiving antenna for each object in the world. In the previous chapter, antennas were evaluated in terms of their potential to be direct write

printed. Figure 20 divides the antennas types into five main groups: wire antennas, microstrip antennas, reflector antennas, travelling wave antennas and aperture antennas.

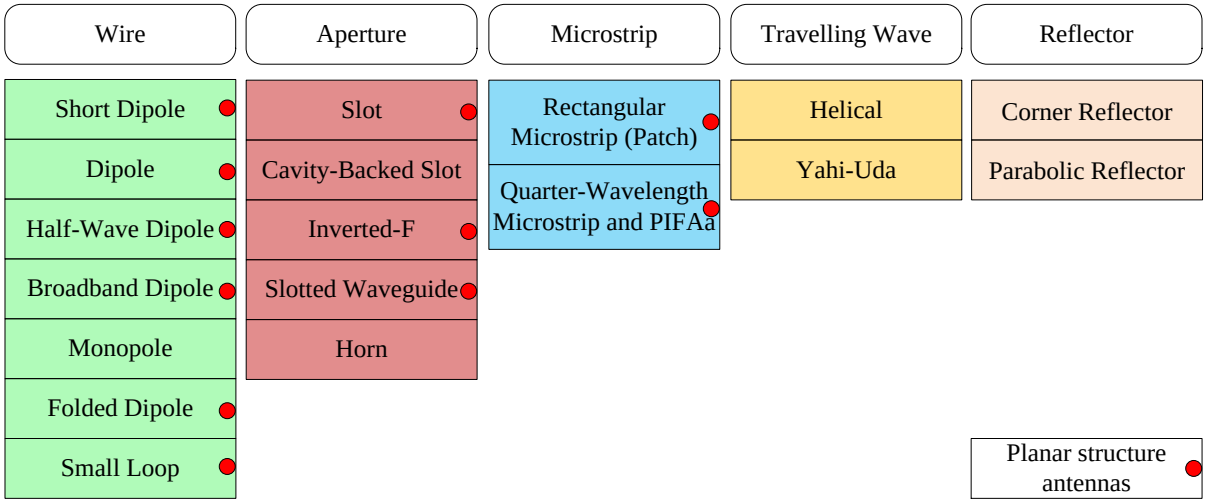

Figure 20. Categories of antenna types with markers on potential inkjet printable options.

Different antenna types marked with a red dot represent the planar structure antenna type, which can be potentially inkjet printed. Inkjet printing is limited to the fabrication of planar structured electronic devices as stated in the previous literature review, section 4.2.2. Consequently, only planar layered antennas are considered in this study. The planar antenna designs are the short dipole antenna, the dipole antenna, the half wave dipole antenna, the small loop antenna, the microstrip patch antenna and the inverted-F antenna. The half wavelength dipole antenna and the microstrip patch antenna are selected to be the two antenna devices in this research work. This is because these selected antennas are relatively small and simple compared to the other possible planar structured antennas, for example, the dipole antenna is two times longer than the half wavelength dipole antenna.

5.2.1 Dipole antenna

In this research, a half wavelength dipole antenna was designed for the 2.4 GHz communications frequency. Using equation 3 with a 2.4 GHz frequency, at a half wavelength, the dipole length of one side of the dipole should be 31.25 mm as shown in figure 21.

$$\lambda = \frac{c}{f} \tag{3}$$

where

λ is the wavelength in m,

c is the speed of light in m/s,

f is the antenna working frequency in Hz.

Figure 21. Plan view of a half wavelength antenna design.

However, equation 3 assumes free space operation of the dipole antenna. In practice, the substrate material will affect the antenna performance in terms of the electrical permittivity of the substrate material. The permittivity can be measured and simulated before the final antenna design is made to adapt the final design. The simulation presented in section 5.4 take into account of the substrate permittivity. Equation 4 modified the equation 3 take into account of the substrate permittivity. It shows the relationship between the effective propagation speed and the actual dipole length.

$$L = \frac{\lambda_d}{2} = \frac{k \cdot \lambda_0}{2} = \frac{k \cdot c}{2 \cdot f} \quad (4)$$

Where

L is the half wavelength dipole length in m,

λ_d is the actual dipole wavelength transcieving on the dipole antenna in m,

k is the adjustment factor compensating the propagation speed less than light,

λ_0 is the wavelength calculated by free space equation (3) in m,

c is the speed of the light, 3×10^8 m/s,

5.2.2 Patch antenna

In this research, a patch antenna is also selected as an inkjet printed fabric antenna design for 2.4 GHz communication frequency. This antenna type is also relatively small and simple, and is more widely used than the other planar antenna structures. The radiating patch element is a single rectangular conductive layer. In designing a patch antenna for this research, 2.4 GHz is the target operating frequency, the same as the half wavelength fabric dipole antenna. The

length of the patch varies the resonant frequency as shown in equation 5 [114], the patch antenna length calculation equation.

$$L = \frac{c}{2 \cdot f \cdot \sqrt{\varepsilon_r}} = \frac{1}{2 \cdot f \cdot \sqrt{\varepsilon_0 . \varepsilon_r \cdot \mu_0}} \quad (5)$$

Where

c is the speed of light in m/s,
f is the antenna working frequency in Hz,
L is the length of the radiating patch plane in m,
ε_r is the relative permittivity of the insulator layer,
ε_0 is the vacuum permittivity as a constant of 8.854×10^{-12} in F/m,
μ_0 is the vacuum permeability as a constant of 1.257×10^{-6} in H/m.

The width of the patch antenna can be calculated from the target resonant frequency and required patch length. In addition, there is a delta patch length (L_Δ) which can affect the resonant frequency. However it can be ignored in this calculation as it is only a few micrometres at a frequency of 2.4 GHz, compared to the tens of millimetres for the patch dimensions. The width of the patch antenna can be calculated using equation 6 [115], the patch antenna width calculation equation.

$$W = \frac{c}{2 \cdot f \cdot \sqrt{\frac{\varepsilon_r + 1}{2}}} = \frac{1}{2 \cdot f \cdot \sqrt{\mu_0 \cdot \varepsilon_0}} \cdot \sqrt{\frac{2}{\varepsilon_r + 1}} \quad (6)$$

Where

c is the speed of light in m/s,
f is the antenna working frequency in Hz,
W is the width of the radiating patch plane in m,
ε_r is the relative permittivity of the insulator layer,
ε_0 is the vacuum permittivity as a constant of 8.854×10^{-12} in F/m,
μ_0 is the vacuum permeability as a constant of 1.257×10^{-6} in H/m.

Figure 22 shows the one patch dimension provided by Loughborough University to achieve the 2.4 GHz desired operating frequency.

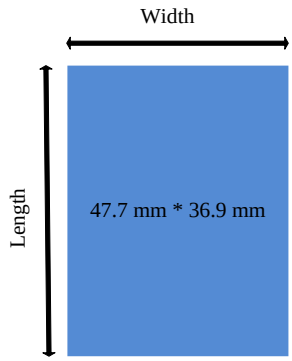

Figure 22. Plan view of a radiating patch plane dimensions of a patch antennas.

Loughborough University specialises in simulating, designing and measuring the RF properties of different antennas, as this research work is a collaboration project. University of Southampton is on the fabrication part of the work.

5.3 Fabrication

5.3.1 Substrate evaluation

Five different substrates are examined in this section in the sequence of glass slide, Kapton film, commercial polyurethane (PU) coated fabric (PU fabric), standard polyester cotton fabric (Standard fabric) and screen printed interface coated fabric (IF fabric). These were chosen to examine the fabrication method on substrates with different physical and chemical properties. The glass slide is used as a rigid substrate because it is hard, smooth, flat and used regularly in the literature for inkjet printed devices. Kapton film is smooth, flat and flexible. Commercial PU coated fabric is used as an example of a smooth, stretchable fabric made from combined nylon and lycra weave. Standard 65 % polyester and 35 % cotton fabric is the final substrate used and has a non-uniform surface and high flexibility. Then the additional interface layer is provided on the standard fabric as a pre-treatment to improve its surface smoothness. A detailed explanation of the five different substrates follows.

5.3.1.1 Glass slide

The glass slide used is from Corning (Corning 2948) [116] with dimensions of 75 mm × 25 mm × 1 mm. A glass slide is used as a substrate for the initial evaluation stage because of its rigid, flat surface. There are several ways to clean the substrate before use. In this work the glass slide is placed into an ultrasonic bath for 5 minutes using deionised (DI) water. This cleaning cycle can ensure the surface energy homogenous across the slide. Antennas are not inkjet printed on to glass slides in this work. The glass slide is used only to evaluate the initial assessment of the inkjet printing process, for example, adjusting the jetting waveform, droplet analysis, thermal curing condition and optimising the printing resolution.

5.3.1.2 Kapton film

Kapton film is a polyimide film developed by DuPont which has very good flexibility over a wide temperature range (normally from -273 ^{o}C to +400 ^{o}C) and is resistant to many chemical solvents [117]. Because of its chemical and physical properties, Kapton film is widely used in flexible electronics as a substrate or an insulating layer. Kapton with a thickness of 100 µm (Figure 23 (a)) was selected for high flexibility. Huerta et al [118] reported the surface roughness of Kapton film is in a range of 1.1 to 2.9 nm. However in this research, the absolute Kapton roughness cannot be achieved due to the cleanroom class 1000 grade. Figure 23 (b) shows the plan view of the Kapton used in this research, there are a few uneven dents and bulges (< 5 µm) visible in a micrograph with 2000 magnified area.

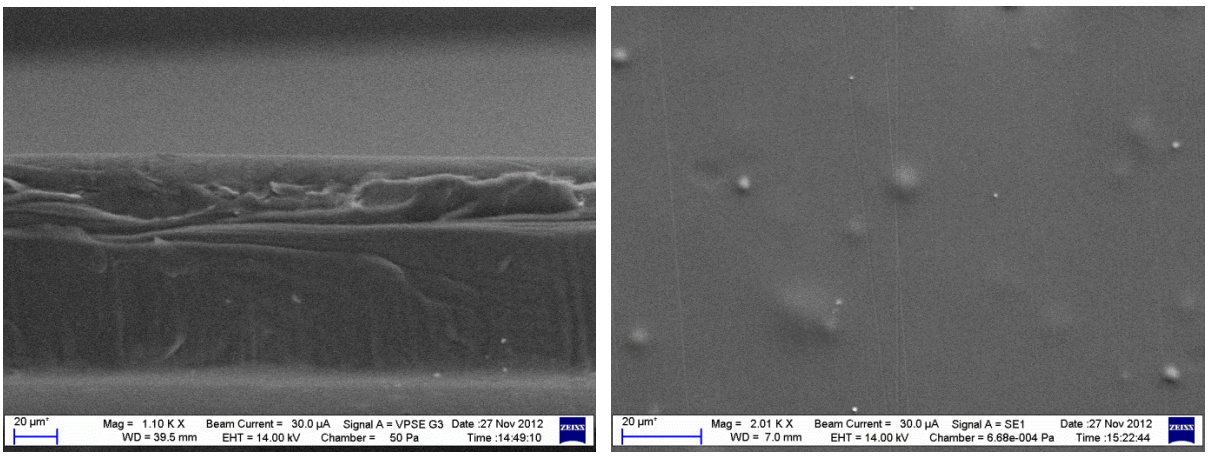

(a) (b)

Figure 23. (a) Cross sectional view SEM image of 100 µm thick Kapton film, (b) Plan view SEM image of 100 µm thick Kapton film.

5.3.1.3 Polyurethane coated stretchable fabric

A commercial polyurethane coated stretchable fabric (PU Fabric) is supplied from Plastibert Ltd [119]. This polyester cotton and lycra based fabric is typically used in the medical sector for applications such as mattress protectors. This PU coated fabric substrate was chosen as the third stage substrate because it provides an intermediate step between the smooth Kapton film and the rough fabric. Figure 24 (a) shows the transfer coated polyurethane layer transforming the rough fabric surface to a relatively flat continuous surface, more suitable for printing processes. However, the transfer coated polyurethane layer on top of the stretchable fabric is not as smooth as the Kapton film as shown in the micrograph in figure 24 (b) at 500 magnification and 2000 magnification respectively.

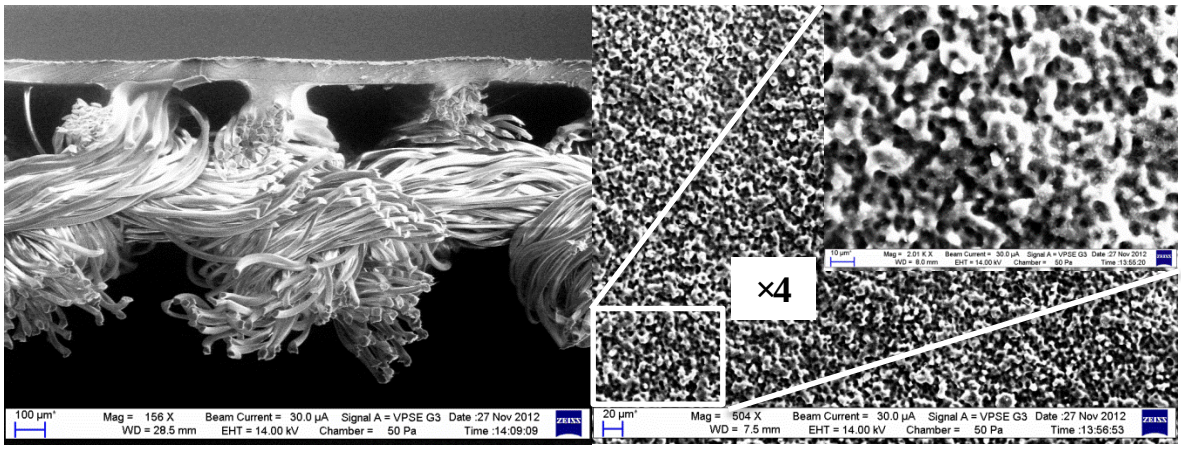

(a) (b)

Figure 24. (a) Cross sectional view SEM image of PU fabric, (b) Plan view SEM images (×500 and ×2000 magnified areas) of PU fabric.

Its surface deviation is around 10 µm to 20 µm across the whole transfer coated PU layer. The manufacturer's datasheet states that the maximum temperature it can sustain continuously is 80 ^{o}C. Therefore, before printing, the fabric was subjected to heating at 150 ^{o}C for 10 minutes, to test the curing condition of the silver ink. However, experiment showed no significant visible damage to the fabric after thermal curing.

5.3.1.4 Polyester cotton fabric

The target fabric used in this research work is a standard 65/35 polyester cotton fabric (Standard fabric) which is a blend of the two most common fabric yarns. The 65/35 polyester cotton fabric is the most commonly used fabric for standard clothing in everyday life. This fabric has a woven structure consisting of interlacing warp and weft yarns. Figure 25 shows this woven

structure in cross sectional and plan views and illustrates the impact this has on the surface profile of the material.

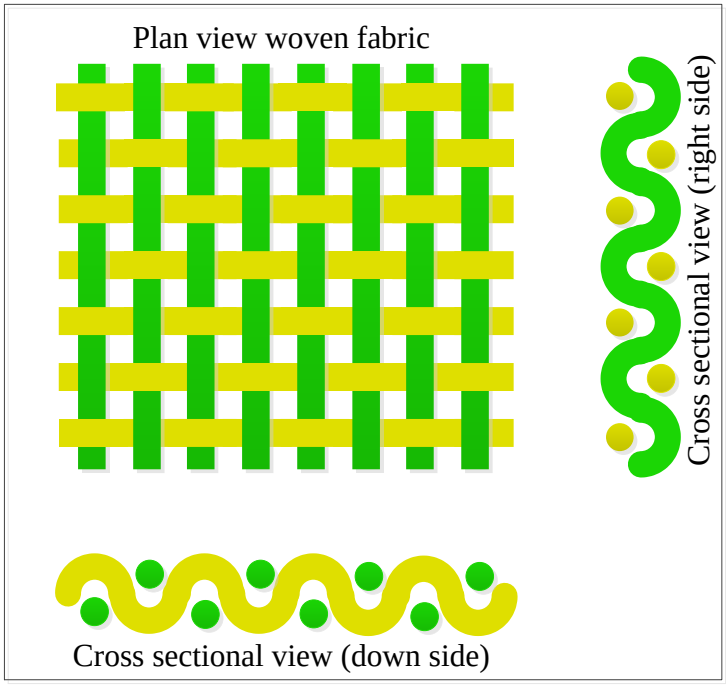

Figure 25. Plan and cross sectional view of standard woven fabric structure.

This specific fabric has a number of physical properties that make inkjet printing based deposition difficult. The maximum temperature that it can withstand is low, meaning low-temperature curing inks is required. The standard fabric was supplied by Klopman International [120] and their characterization data shows that the fabric can be heated at 150 ºC for 45 minutes, 175 ºC for 15 minutes, 200 ºC for 10 minutes or 225 ºC for 3 minutes without noticeable colour change or degradation [121]. Therefore, a 150 ºC curing temperature provides a suitable compromise between conductivity and compatibility with fabrics for an inkjet printed conductive track. Furthermore, its surface roughness is much higher than the other substrates selected, as shown by comparing the cross sectional view of the three SEM images, figure 23 (a), figure 24 (a) and figure 26 (a). Manufacturer's datasheet reports its average the surface roughness is 143.3 µm [3]. Figure 26 (b) shows the rough top surface of the standard fabric in SEM plan view image at 100 magnification.

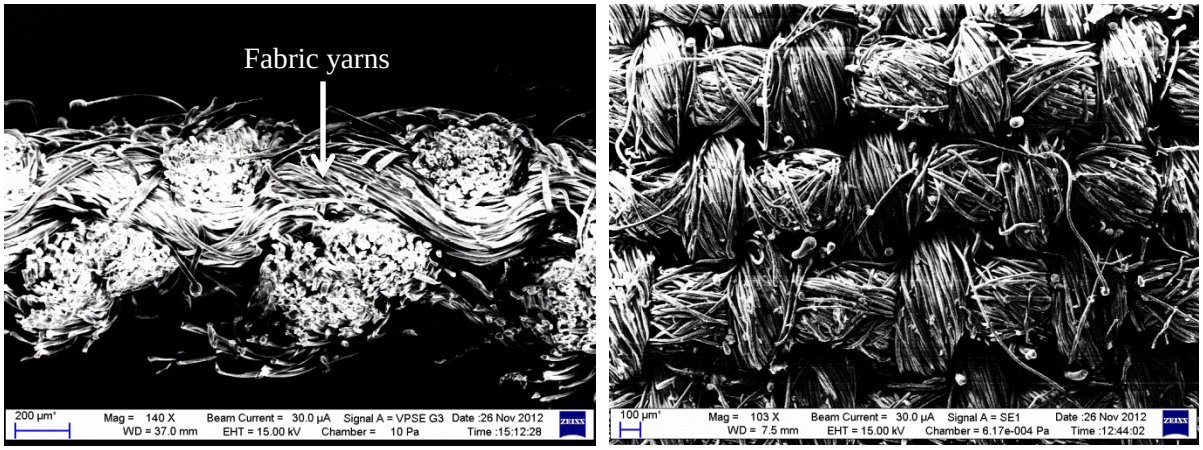

(a) (b)

Figure 26. (a) Cross sectional view SEM image of standard 65/35 polyester cotton fabric, (b) Plan view SEM image of standard 65/35 polyester cotton fabric.

Parameter Limitation	Values
Curing temperature	150 ºC, 45 minutes maximum
Maximum working temperature	175 ºC, 15 minutes maximum
Contact angle	Too hydrophilic
Degradation temperature	290 ºC
Reaction to organic solvents	Resistant to most common industrial and household solvents

Table 6. Standard polyester cotton physical properties [121].

5.3.1.5 Pre-treated standard fabric

The target fabric substrate used in this research work is a standard fabric with a screen printed interface layer. An interface layer is a layer on top of fabric performing an intermediary role to reduce the high roughness surface and fill the weave of the fabric to create a smooth surface for subsequent processes. The interface layer is screen printed directly onto polyester cotton as a supporting layer for subsequent inkjet printed silver layer in this research as shown in figure 27.

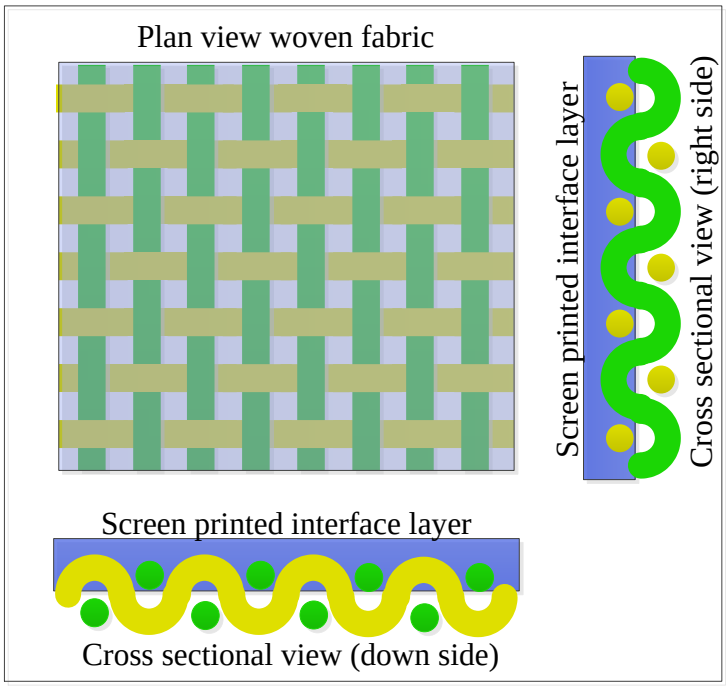

Figure 27. Plan and cross sectional view of standard woven fabric structure with screen printed interface layer.

To reduce the roughness of the standard fabric, the fabric is pre-treated using a screen printed interface layer (Fabink-IF-UV4) from Smart Fabric Inks Ltd. [122]) before further inkjet printing. This paste is UV curable so does not require a heating process which reduces the risk of potentially harmful volatile organic compounds being released. The interface layer has a surface free energy of 35 mN/m as measured with a Kruss DSA30B tensiometer. This value confirms that the surface promotes wettability of the majority of solvent based inkjet printable electronic inks which have a lower surface tension, typically around 30 mN/m. The ink's wettability, representing the physical interaction between ink and substrate, defines the level of the pattern definition before the curing stage. The interface layer has good thermal resistance and can withstand 150 ^{o}C for 30 minutes in a conventional thermal oven, without degradation, which may be required for subsequently printed inks. In addition, the interface has good chemical resistance properties and shows no obvious damage when exposed to widely used organic solvents such as ethanol, isopropanol and 1-hexanol. It is also advantageous as a technique to reduce surface roughness as the screen printed interface layer is only applied in the area surrounding the subsequent inkjet printed design so that, unlike the commercial coated fabric, the properties of the fabric such as breathability and flexibility are maintained. Figure 6(a) shows that the screen printed interface layer has a thickness of 200 µm from the top printed surface to the yarn level. It also provides better flatness and smoothness compared to the

commercial polyurethane coated fabric (Figure 24 (b)) or the standard fabric (Figure 26 (b)), as it has maximum 5 μm defects roughness in diameter (Figure 28 (b)).

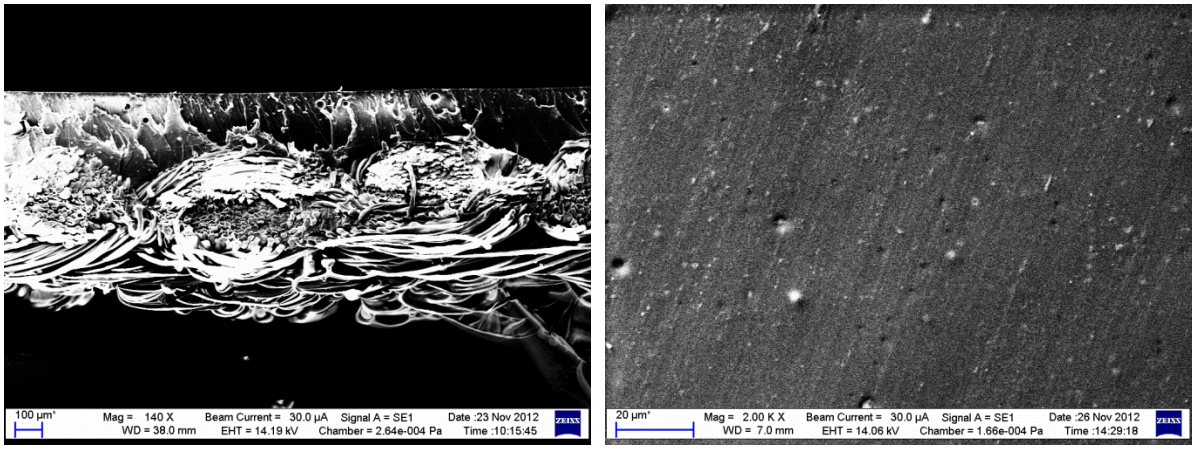

(a) (b)

Figure 28. (a) Cross sectional view SEM image of standard 65/35 polyester cotton fabric with screen printed interface layer, (b) Plan view SEM image of standard 65/35 polyester cotton fabric with screen printed interface layer.

5.3.2 Conductive material for smart fabric antennas

Conductive ink is used for antenna's radiating element as the core functional material. There are two groups of conductive ink, organic conductors and inorganic conductors, as detailed in the introduction in the previous chapter 3. The most frequently used organic conductive ink is PEDOT/PSS which has much lower conductivity (100 S/m) than that of silver ink (1.2×10^7 S/m). This organic conductive ink does not have a high curing temperature, only requiring 80 ^{o}C to perform effective curing resulting in a solid conductive layer. Therefore, it is an appropriate material for low temperature processing fabrication on fabrics. The most frequently used inorganic conductive ink is a silver nanoparticles dispersion ink which gives high conductivity and good flexibility. The curing temperature for commercially available inkjet printable silver nanoparticles dispersions is higher than 200 ^{o}C. However 120-150 ^{o}C curing temperature works adequately for SunChemical U5714 silver ink, therefore providing another candidate inkjet printable conductive ink.

The conductive material's conductivity will affect the antenna efficiency, and later the fabricated capacitor's serial resistance and the ohmic effect in the fabricated transistor. Considering that PEDOT/PSS has lower conductivity than silver ink, and that they can both be cured at fabric compatible temperature, an inkjet printable silver ink is chosen as the conductive ink used in this research work. The inkjet printable conductive silver ink used here is supplied

from SunChemical, SunTronic Jettable Silver U5714. It has 40 wt% silver content, a viscosity of 10 to 13 mPa s and surface tension of 27 to 31 dynes/cm. These values are within the ideal range of the DMP 2831 inkjet printer according to the manufacturer's datasheet.

Figure 29 shows the plan view SEM images of an inkjet printed single silver deposit on Kapton (Figure 29 (a)), two silver deposits on PU fabric (Figure 29 (b)), two silver deposits on pre-treated standard fabric (Figure 29 (c)) and one silver deposit on pre-treated standard fabric (Figure 29 (d)).

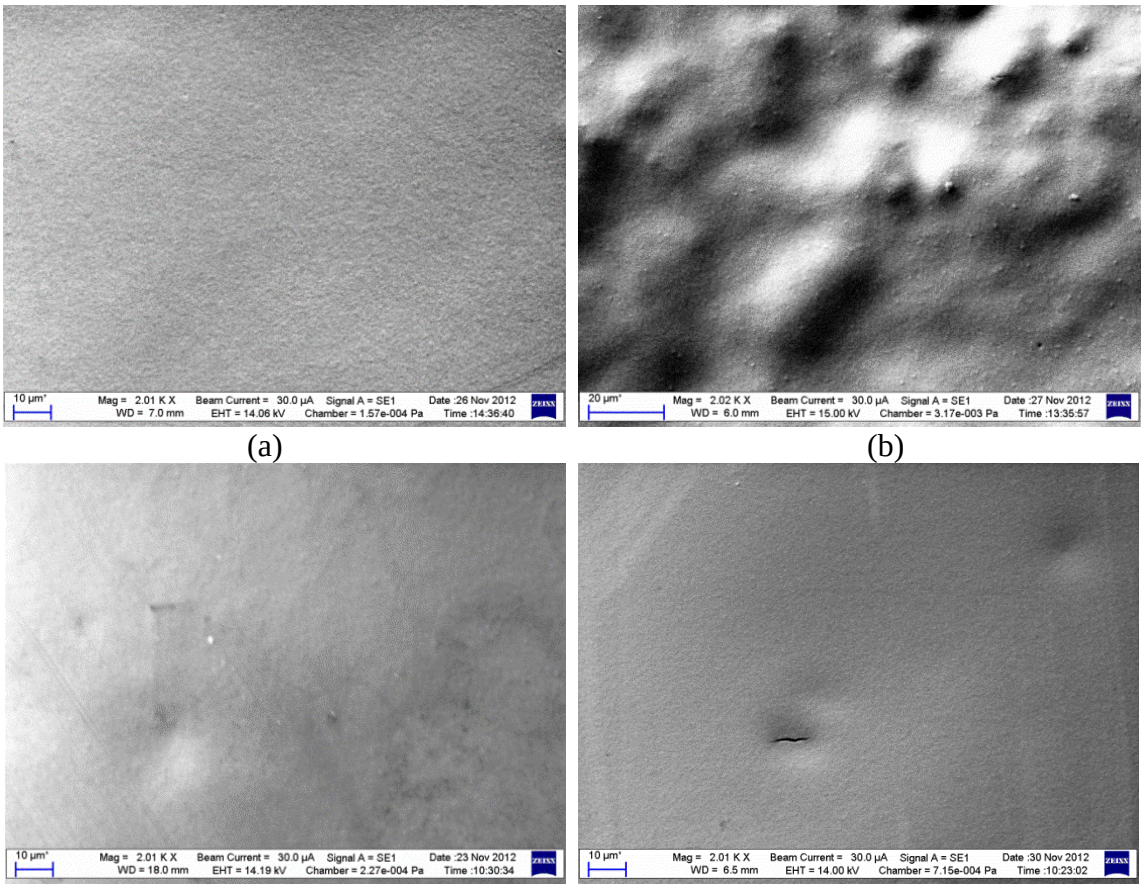

(a) (b)

(c) (d)

Figure 29 Plan view SEM images (a) one deposit conductive silver layer inkjet printed on Kapton film, (b) two deposits conductive silver layer inkjet printed on PU fabric, (c) two deposits conductive silver layer inkjet printed on IF fabric, (d) one deposit conductive silver layer inkjet printed on IF fabric.

These four SEM images are all taken under the same magnification level of ×2000. The printed silver layer in figure 29 (c) on the IF fabric are equally flat and smooth as the conductive silver layer shown in figure 29 (a) on Kapton film. However, a few dents are identified in figure 29 (c). These may be caused by the pinholes or by the slightly uneven printed interface layer on

the fabric. The single deposit inkjet printed silver layer (Figure 29 (d)) gives a relatively uniform conductive layer but with visible pinholes and dents in the magnified area of ×2000. This explains the higher resistance measured with one deposit silver layer compared to two deposits for samples on pre-treated standard fabric. Figure 29 (b) shows the two deposits silver layer inkjet printed on PU fabric. It shows very rough but continuous silver layer on the transfer coated layer compared to figure 29 (a).

In summary, Plastibert fabric substrate will not be used further due to high surface roughness, even after silver layer deposition. Two deposits as one layer conductive silver on IF fabric will be used as the standard process for future inkjet printed conductive tracks on IF fabrics.

5.3.3 Fabrication process

Figure 30 shows the fabrication process in cross sectional view in this research work, comprising two deposition stages for the interface and conductive layer. Both depositions require a curing stage to transform the liquid layers into flexible functional solid layers. A UV curing method is applied to the interface layer and a thermal curing method is applied to the conductive silver layer. Where two deposits silver layer are printed, they are deposited one after another, with the subsequent curing process carried out after both deposits are inkjet printed.

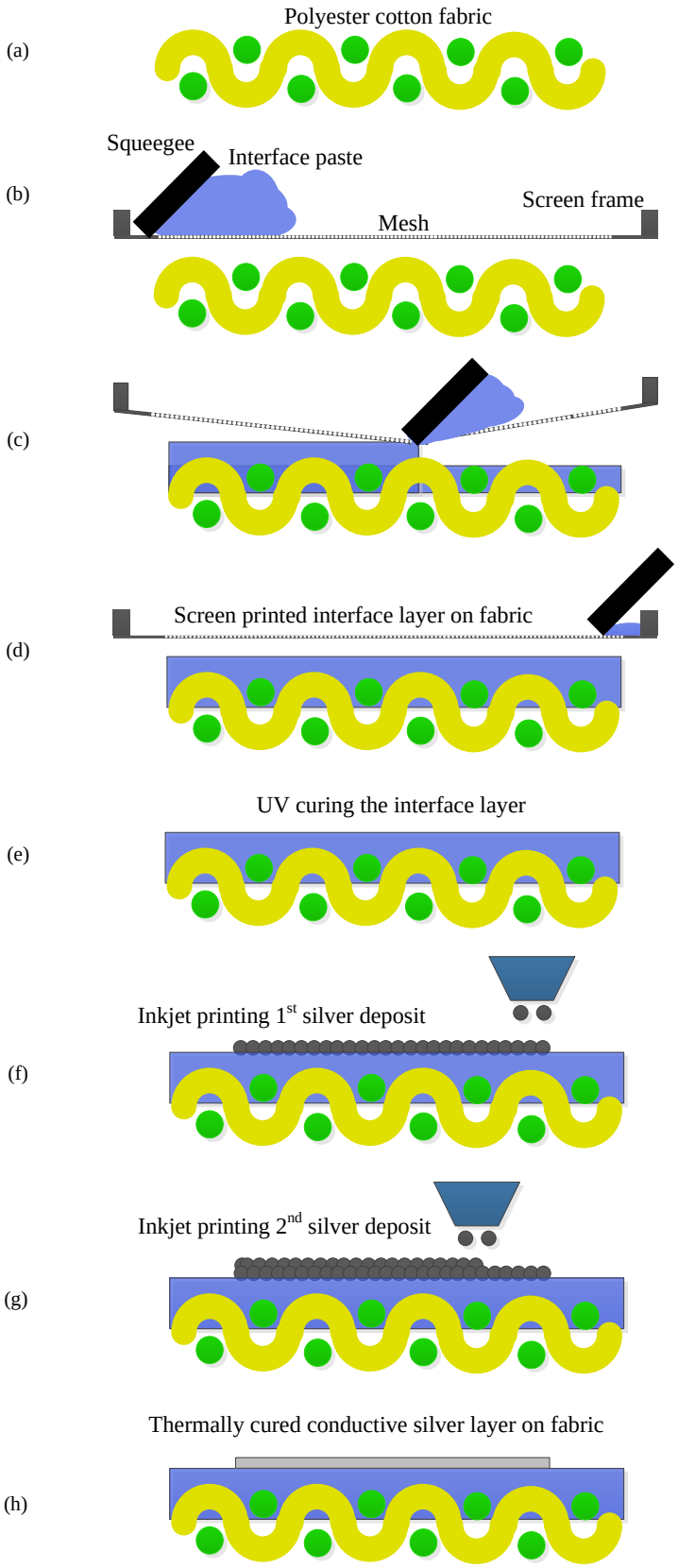

Figure 30. A flow diagram showing the fabrication process for the inkjet printed smart fabric patch antenna.

The interface layer coated fabric (IF fabric) is provided by a colleague at the University of Southampton for this research work. The process details are:

(1) Screen mesh size 250 lines/inch mesh,
(2) Squeegee pressure 6 Kg,
(3) Printing gap 0.8 to 1 mm,
(4) Levelling time 1 minute,
(5) No drying stage required,
(6) Curing schedule, 30 second in UV cabinet (500 to 1500 mJ/cm^2).

The first step is to wipe the interface coated substrate surface with lint free cleanroom wipes dipped in DI water. This step removes potential contamination on the interface substrate surface and ensures a homogenous surface energy across the printing area. This ensures the contact angle for each printed droplet is the same, which results in a better pattern definition. The 10 pL print heads for the DMP 2831 have a nozzle diameter of 21.5 μm which produces a droplet with a 60 μm diameter (Figure 29) when using the U5715 silver ink from a single nozzle with a recommended jetting velocity of 7 to 9 m/s.

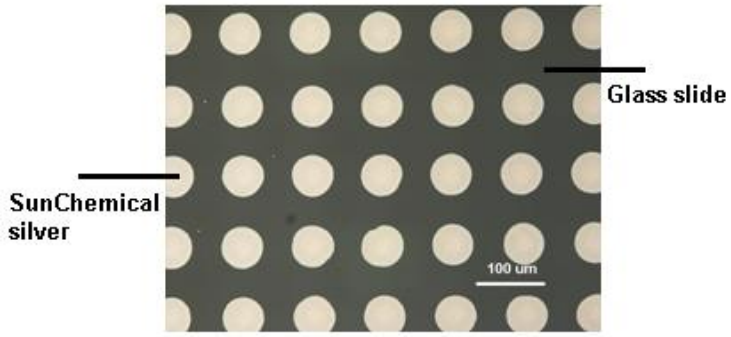

Figure 31**.** Optical image of silver ink droplets on glass substrate showing the diameter of each droplet is around 60 μm.

For a 60 μm droplet, the maximum droplet spacing is 60 μm to achieve a conductive line. However, choosing a droplet spacing equal to the drop diameter results in poor conductivity because the drops do not overlap. Choosing a 30 μm drop spacing improves the conductivity since the drops overlap but results in strongly castellated edges to the lines. A 15 μm drop spacing is selected to provide good conductivity and line edge definition while minimising the ink usage. The ink showed good jetting properties with a droplet velocity of 8 m/s.

The deposition step is to inkjet print the conductive silver ink. After inkjet printing, the conductive pattern is cured for 10 minutes at 150 ^{o}C. PU fabric has comparatively high surface

roughness (10-20 µm) continuously across the whole coated area. Therefore, the inkjet printer is set to print two deposits silver ink with 15 µm drop spacing on the PU fabric. IF fabric was determined to have much better smoothness with less than 5 µm roughness as stated in section 5.3.1. Therefore, one and two deposits of one conductive layer are chosen to inkjet print on to pre-treated standard fabric to test its conductivity. An additional printed layer is required for the IF fabric substrates compared to Kapton to ensure sufficient conductivity and good pattern definition; because the higher surface roughness of the IF fabric could degrade the printed edge definition. Kapton has the smoothest surface among the three selected substrates. Therefore, there is only one silver layer inkjet printed with a 15 µm resolution for Kapton film, as there is not visible pin holes detected under SEM image shown in figure 29. Standard fabric has up to five deposits conductive silver printed to prove it is not capable to be directly printed on with inkjet printable inks due to its high roughness, yarn based structures and ink's high solvent content. Table 7 shows the summary of 4 selected flexible substrate and number of inkjet silver deposits for the printed antenna.

Substrate	Kapton	PU Fabric	Standard Fabric	IF Fabric
Surface Roughness	< 5 µm	10-20 µm	143.3 µm	< 5 µm
No. IJP deposits	1	2	1/2/3/5	1/2

Table 7. Summary table of 4 selected flexible substrate and number of inkjet printed silver deposits for printed antenna.

The final stage of the process is to connect the SMA (SubMiniature version A) connector to the inkjet printed half wavelength dipole antenna using a silver epoxy (Circuitworks CW2400). One terminal connects to the inner contact and the other terminal connects to the outer shielding. The SMA is the standard antenna connection port in communication measurement equipment.

5.4 Device testing

5.4.1 Fabric dipole antennas measurement

2.4 GHz dipole antennas are inkjet printed separately on Kapton (Figure 32), PU fabrics (Figure 33), standard fabric (Figure 34) and IF fabric (Figure 35).

Figure 32. Plan view of three inkjet printed 2.4 GHz dipole antennas on Kapton.

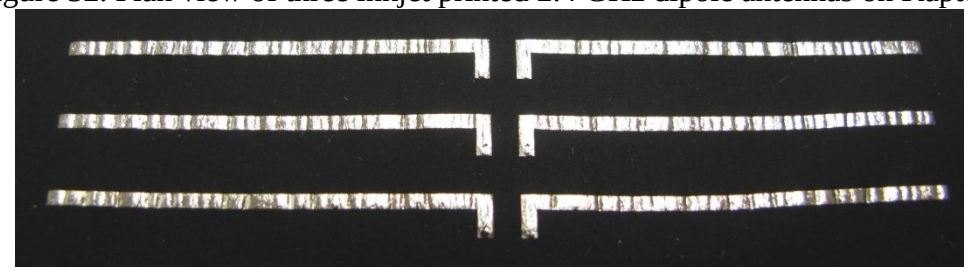

Figure 33. Plan view of three inkjet printed 2.4 GHz dipole antennas on PU fabric.

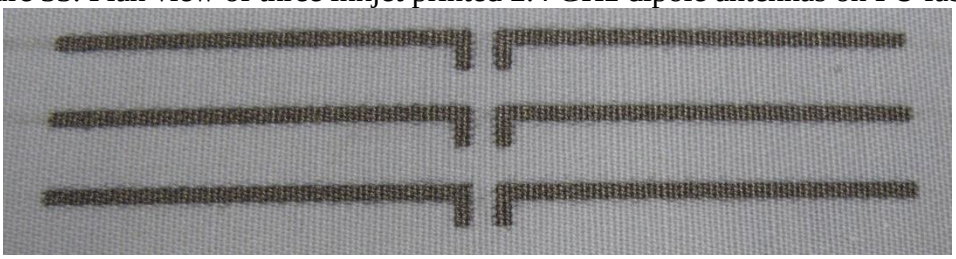

Figure 34 Plan view of three inkjet printed 2.4 GHz dipole antennas on standard fabric.

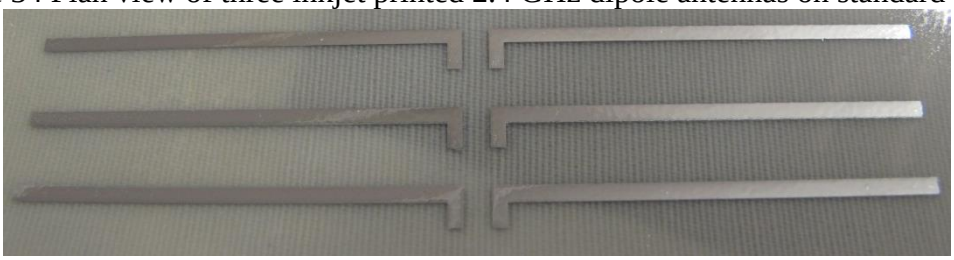

Figure 35. Plan view of three inkjet printed 2.4 GHz dipole antennas on IF fabric.

Three out of four types of substrates yielded antennas working around the designed frequency of 2.4 GHz with impedance around 50 Ω. The detailed results will be given and discussed later in this section. The dipole antenna inkjet printed directly on to untreated fabric (Figure 34) did not operate correctly due to its poor conductivity and poor pattern definition.

Rohde & Schwarz ZVB4 Vector network analyser (VNA) measurements were then taken of reflection coefficient (S11) of the printed dipole antennas. In practise, the most typically quoted parameter in regards to antennas is the S11 plot. The S11 plot represents how much power is reflected from the antenna and hence known as the reflection coefficient or return loss. If S11=0 dB, then all the power is reflected from the antenna and nothing is radiated. If S11=-10 dB, this implies that if 3 dB of power is delivered to the antenna, -7 dB is the reflected power. The remainder of the power was "accepted by" or delivered to the antenna. This accepted power is

either radiated or absorbed as losses within the antenna. Since antennas are typically designed to be low loss, ideally the majority of the power delivered to the antenna is radiated [123]. The key parameter was measured and compared between the antennas on the three different flexible substrates.

Figure 36 shows the impedance and the peak operating frequency measurement results for the half wavelength dipole antenna inkjet printed on Kapton.

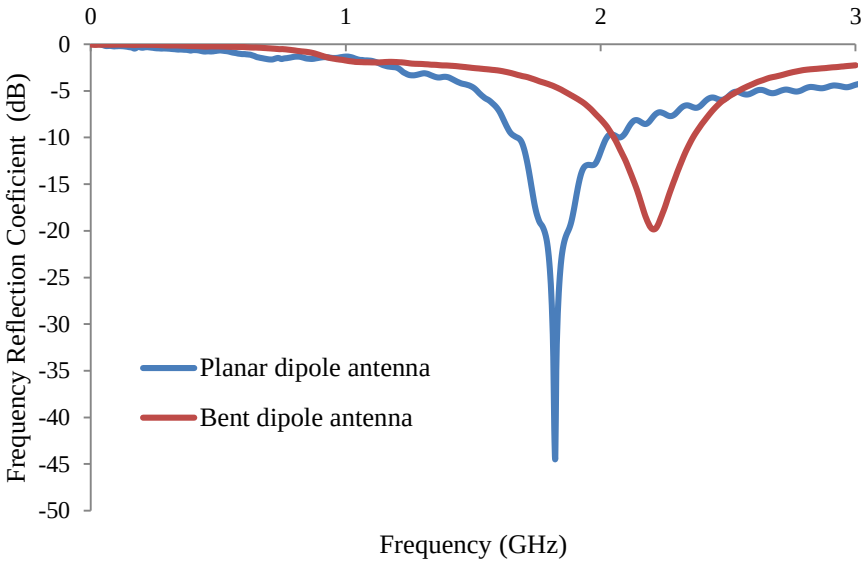

Figure 36. S11 parameter frequency return loss of the inkjet printed 2.4 GHz antenna on Kapton.

The blue line in figure 36 represents the measured peak working frequency of 1.82 GHz. The red line in the S11 plot (Figure 36) represents the frequency shift up to 2.21 GHz, when the flexible antenna's two dipoles are bent perpendicular to the plane of the antenna.

The design aims to provide a peak working frequency of 2.4 GHz. Referring to the meander dipole antenna theory [124], bending the dipole structure results in a shorter effective dipole length and a higher peak frequency. The antenna length is effectively reduced by bending the linear antenna into a spiral or a meander. However the effective dipole length is determined by a complex calculation dependent on its new dipole shape. Figure 37 shows the printed dipole antenna under bending.

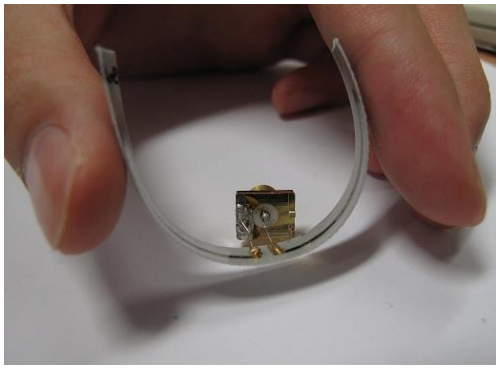

Figure 37. Image of bent inkjet printed half wavelength dipole antenna on IF fabric.

Figure 38 shows the impedance and the peak operating frequency measurement results for the half wavelength dipole antenna inkjet printed on PU coated stretchable fabric. The impedance is 52 Ω and the measured peak frequency is 1.82 GHz (Figure 38, blue line). There is a shift in peak frequency up to 1.91 GHz (Figure 38, red line) when this antenna is bent in the same way applied to the Kapton based antenna.

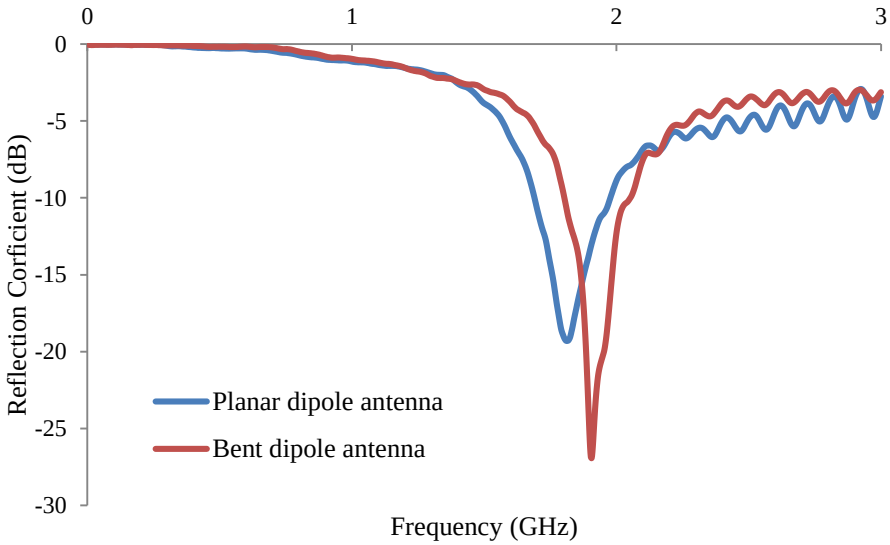

Figure 38. S11 parameter frequency return loss of the inkjet printed 2.4 GHz antenna on PU fabric.

Figure 39 shows the impedance and the peak operating frequency measurements for the half wavelength dipole antenna inkjet printed on IF fabric. The measured impedance is 64 Ω and the measured peak working frequency is 1.76 GHz (Figure 39, blue line). The designed peak working frequency is 2.4 GHz. There is a shift in peak frequency up to 1.86 GHz (Figure 39, red line) when bending the antenna in the same way as the previous two flexible antennas.

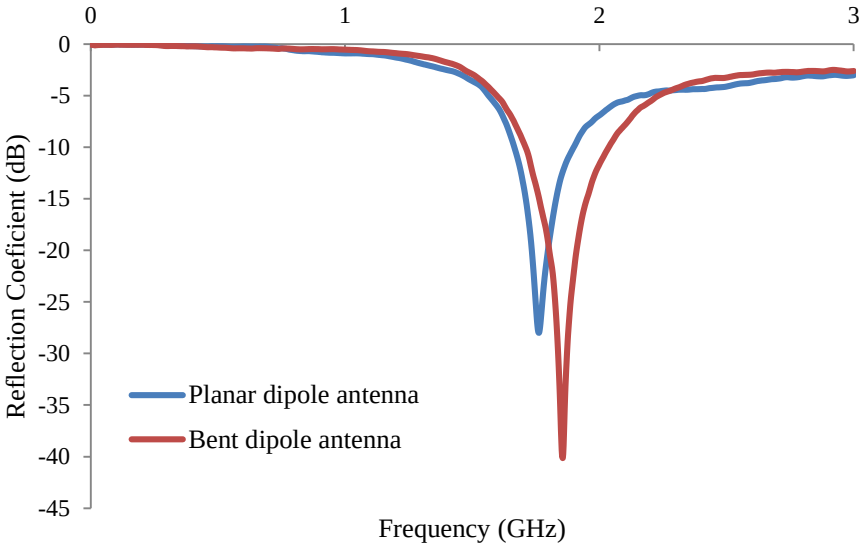

Figure 39. S11 parameter frequency return loss of the inkjet printed 2.4 GHz antenna on IF fabric.

Table 8 summarised the results obtained based on the printed half wavelength dipole antennas' key parameters.

Substrates	Inkjet deposits	Frequency (MHz)	S11 (dB)	Bent dipole frequency (MHz)	Bent dipole S11 (dB)
Kapton	1	1720	46.7	2210	19.8
PU fabric	2	1760	28	1860	40.1
IF fabric	2	1820	19.3	1910	26.8

Table 8. Measured antenna parameters of inkjet printed dipole antenna at resonance frequency.

The measurements described up to this point were performed in the University of Southampton. This work also involved collaboration with Loughborough University for analysis of the inkjet printed fabric dipole antennas and inkjet printed fabric patch antennas. Samples of each antenna were sent to Loughborough University for comprehensive measurements in their anechoic antenna testing chamber to compare with simulated results. The rest of the measurement results in this section were obtained from Loughborough University.

One of the major challenges in the fabrication of fabric antenna prototypes is the manner in which a transmission line or cable connected to the antenna's input terminals ensuring that a match load of 50Ω and a robust connection are achieved. To validate the performance of the inkjet printed dipoles discussed, Loughborough University adopted a simple unbalanced feed.

An unbalanced feed consists of a 50Ω semi rigid cable having the inner and outer parts connected separately to the dipole arms.

To ensure repeatable results, the dipole antennas were physically supported by a 10mm thick Rohacell rectangular board with dimension of 85.5 mm × 41 mm. Rohacell is a trade name of polymethacrylimide (PMI) foam. This platform enabled measurements in an anechoic chamber as shown in figure 40. In this set-up, the antenna under test was placed at distance of 225mm away from the positioner in order to minimise any reflections from the positioner. The cylindrical positioner post has a radius of 36mm as shown in figure 40. The post is made of Acrylonitrile Butadiene Syrene (ABS) plastic and has a relative permittivity and loss tangent (tan δ) of 2.91 and 0.025 respectively. 3D finite difference time domain (FDTD) using EMPIRE XCcel commercial software was used to simulate the half wavelength dipoles. The permittivity of the substrate and the conductivity of the ink were adjusted in this simulation to match the resonant frequencies and efficiencies to the measured results.

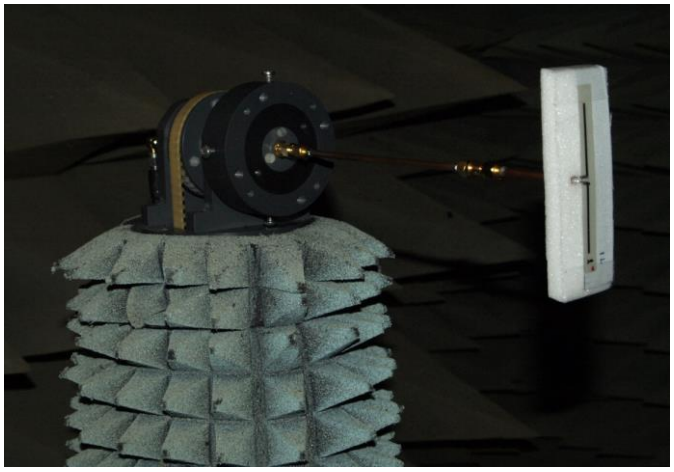

Figure 40. Inkjet printed fabric half wavelength dipole antenna held by a vertical tower in an anechoic antenna testing chamber.

Table 9 shows the measurements of DC resistance of several inkjet printed dipole arms on Kapton film, PU fabric, standard fabric and IF fabric. The mean value is the average of the measured resistance values including both left and right dipole arms: so the mean value is made up of ten measurements.

Substrate material	Deposits	Dipole1(Ω)	Dipole2(Ω)	Dipole3(Ω)	Dipole4(Ω)	Dipole5(Ω)	Mean(Ω)
Standard Fabric	1	864; 1012	910; 955	1251; 1124	970; 920	754; 784	954.4
Standard Fabric	2	126; 101	108; 101	104; 119	152; 105	151; 115	118.2
Standard Fabric	3	55; 42	43; 49	52; 50	64; 59	57; 59	53.0
Standard Fabric	5	23; 14	15; 14	19; 15	15; 15	17; 13	16.0
Kapton	1	3.7; 3.6	3.9; 3.8	3.6; 3.3	3.6; 3.3	3.5; 3.5	3.6
PU Fabric	2	13.5; 15.4	20.1; 11.2	13.5; 20.9	12.5; 13.3	12.1; 14.8	14.7
IF fabric	1	28.5; 18.5	27.2; 20.2	27.6; 29.2	-	-	25.2
IF fabric	2	2.7; 3.5	2.8; 2.8	3.0; 4.0	3.5; 2.8	-	3.1

Table 9 DC Resistance (ohms) of 31.3mm long inkjet printed dipole arms.

Each substrate was trialled using different numbers of inkjet printed silver layers. The DC resistance was measured using a Solartron Schlumberger digital multimeter. Results with multiple samples give an indication as to the repeatability of the fabrication method. These results confirm that it is very difficult to print directly onto fabrics and the resulting DC resistance is very large unless many layers are printed at the expense of time, cost and edge resolution. The IF fabric demonstrates significant improvement in this regard and a 2nd inkjetted silver deposit further reduces the resistance. Although the Kapton film is not fabric, it has been included to allow comparison of the surface roughness of the different fabrics. Further investigation with the SEM and digital microscope revealed micro cracks along the printed dipole tracks on PU fabric. These micro cracks are probably caused by the elasticity of the fabric. Despite the existence of these deformations, this research study has successfully demonstrated conducting ink jet printed circuits on fabrics comparable with the inkjet printed silver on rigid substrate in DC resistances. However, additional deposit of conductive ink tends to distort the edges of the antenna and produce thicker layer which can be easily cracked by bending. Simulated and measured return loss results are shown in figure 41.

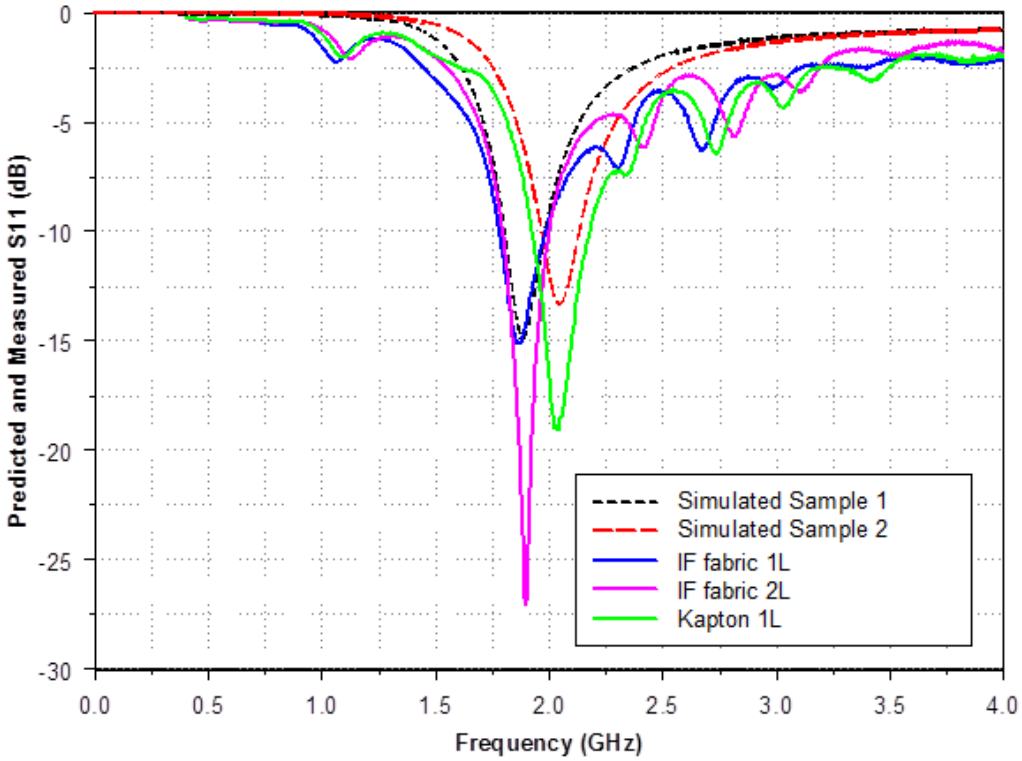

Figure 41. The comparison between simulated and measured return loss of 5 half wavelength dipole antennas.

All the antennas were well matched. The differences in the antennas' resonant frequencies were due to the dielectric loading of the IF fabric and Kapton film. The simulated frequency matched the measured results when the relative permittivity ε_r= 3.5 ('Simulated Sample 1') was used for the IF fabric substrate and ε_r= 1.88 ('Simulated Sample 2') for the Kapton substrate. In addition to the simulated results, the positioner in the measurement system is also included in the simulations. The positioner can affect the gain and increase it above the expected value for a dipole of 2.2dBi. Therefore the efficiency is a more reliable measure of the antenna performance. The performance of the antennas is summarised in table 10.

Substrate	Inkjet deposits	Freq (MHz)	S_{11} (dB)	Gain (dBi)	10dB BW (MHz)	Efficiency (%)
Simulated sample 1	-	1890	14.9	2.64	180	78.1
Simulated sample 2	-	2005	13.3	2.94	168	79.9
Meas: IF fabric	1	1875	15.2	2.24	205	60.2
Meas: IF fabric	2	1897	27.1	3.60	205	74.1
Meas: Kapton	1	2040	19.1	3.16	255	85.1
Meas: PU fabric	2	2128	9.4	0.68	N/A	31.6
Meas: Standard fabric	5	1840	21.1	1.92	283	56.6
Meas: Etched on low loss laminate	-	1778	17.1	3.45	180	77.5

Table 10. Simulated and measured antenna parameters of inkjet printed dipoles at resonance frequency.

The following antenna parameters were measured: frequency is the resonant frequency; S11 is the ratio of the energy delivered and the energy received back; gain measures the ratio in decibels between the signal radiated and the signal radiated from a reference antenna in the same direction and power [125]; efficiency measures the ratio of the total radiated power to the power accepted by the antenna at the input. The simulated antenna efficiency was 92 % with a highly conductive layer ($\sigma = 5.88 \times 10^7$ S/m). To replicate the measured efficiency (~80 %), the conductivity of the simulated uniform metallic tracks was reduced to 5.6×10^6 S/m which gives an indication to the conductivity of the ink tracks. The measured single inkjet printed layer on the IF fabric had an efficiency of 60 % which is sufficient for many applications. This was increased to 74 % with two inkjet printed deposits. The efficiency for the dipole on the stretchable fabric was 31.6 % with two inkjet printed deposits. To demonstrate the effectiveness of the interface layer in increasing the smoothness of the standard fabric, a dipole was fabricated with 5 deposits of inkjet printed silver directly onto the fabric without the interface layer. Significant bleeding occurred during printing results that the dipole arms were not well defined as shown in figure 42.

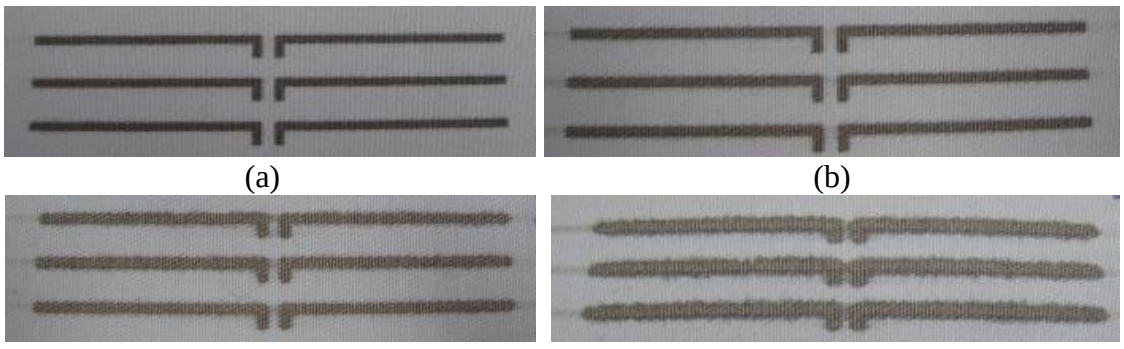

Figure 42. Inkjet printed silver layer on standard fabric, (a) one silver deposit, (b) two silver deposits, (c) three silver deposits and (d) five silver deposits on standard fabric.

The ink bleeding caused the small gap between the two dipole arms to short out. This indicates that inkjet printing conductive inks directly onto fabric is impractical. The dipole with only one inkjet silver deposit on the IF fabric had a better efficiency than that with 5 deposits of silver ink on the standard fabric. Therefore, the interface layer saves time, reduces costs and improves the printing resolution and RF performance.

Figure 43 shows the measured radiation patterns at resonance of the inkjet printed dipoles.

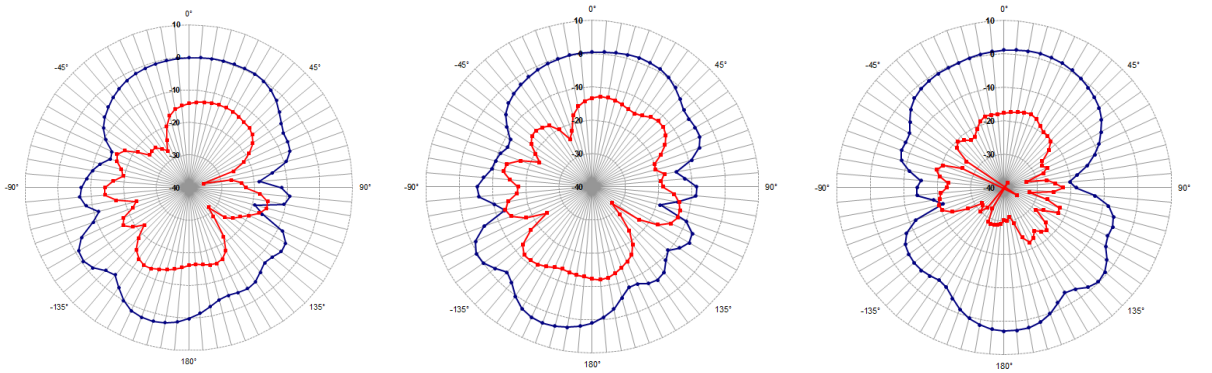

(a) ICS 1L at 1875MHz; Φ = 0°

(b) ICS 2L at 1895.5MHz; Φ = 0°

(c) Kapton at 2040MHz; Φ = 0°

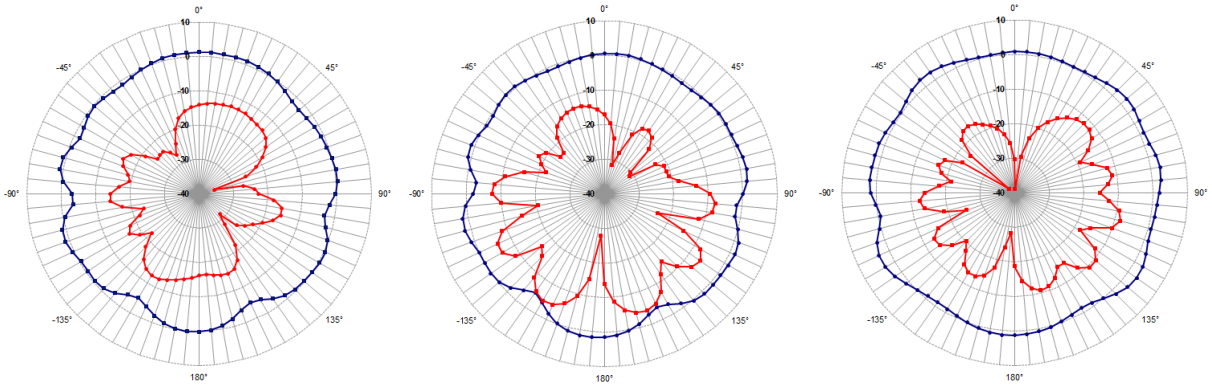

(d) ICS 1L at 1875MHz; Φ = 90°

(e) ICS 2L at 1895.5MHz; Φ = 90°

(f) Kapton at 2040MHz; Φ = 90°

Figure 43. Measured radiation patterns of inkjet printed dipoles at resonance frequency: (a) IF fabric 1 deposit at 1875MHz, Φ = 0°; (b) IF fabric 2 deposits at 1897.5MHz Φ = 0°; (c) Kapton at 2040MHz Φ = 0°; (d) IF fabric 1 deposit at 1875MHz, Φ = 90°; (e) IF fabric 2 deposits at 1897.5MHz Φ = 90°; (f) Kapton at 2040MHz Φ = 90°. Note EΦ is blue and Eθ is red and EΦ > Eθ for all plots.

These radiation patterns show that the printed antennas have dipole-like patterns [126]. The patterns were reasonably isotropic in the azimuth plane with a minor effect of the positioner. However, pattern asymmetry is noticeable in the elevation plane which is attributed to the dipole arms being not perfectly straight and asymmetrical. The positioner in the anechoic chamber as shown in figure 40 was included in the simulations as shown in figure 44.

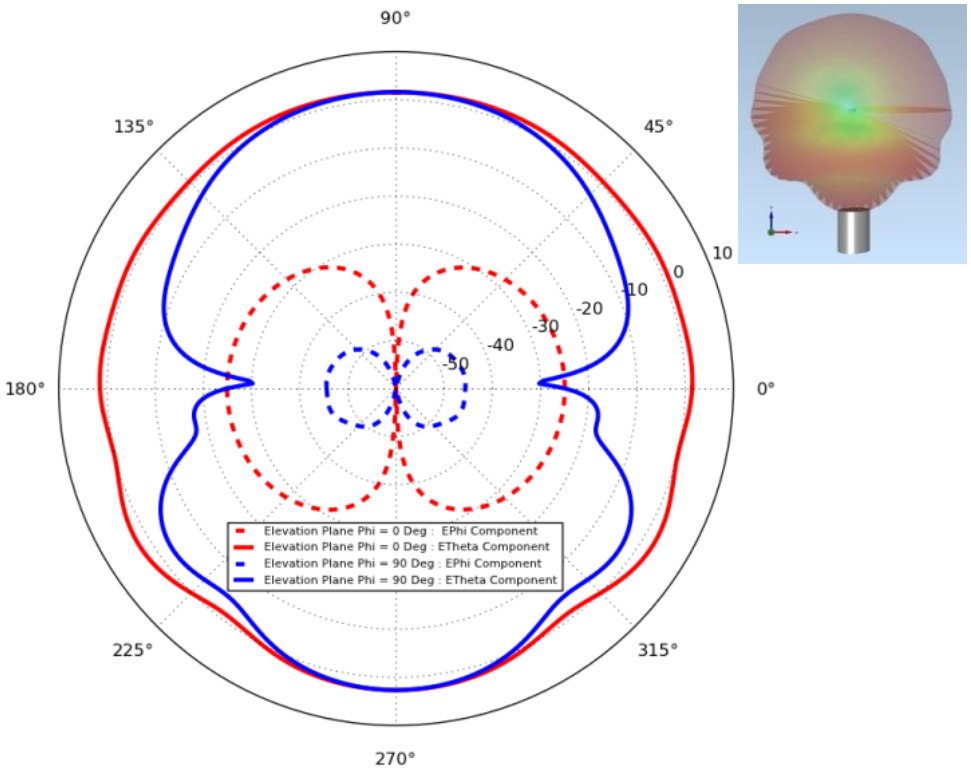

Figure 44. Simulated radiation patterns at 1.89GHz with the positioner and 3D view.

The vertical tower, which holds the testing antenna in the middle of the anechoic chamber, was covered with radar absorbing material and therefore was not included in the simulations. Figure 44 shows the 2-D simulated antenna pattern with the positioner included at 1890MHz. The positioner affects the radiation pattern which is particularly noticeable at about 225^{o} and 315^{o} in the 2-D polar plot, as it can be seen in figure 44 the non-circular pattern on the bottom half pattern. This shows that for antennas with no ground plane, it is important to consider the effect of the positioner. The radiation plot at 1.89 GHz shows that the positioner can enhance the directivity of the dipole. This explains the gain values above 2.2 dBi in table 10. Simulations verified that the effect of the positioner on the measurement results was minimised by increasing the separation of the dipole from the positioner.

Efficiencies of more than 70 % have been achieved. The efficiency was increased by using two inkjet printed deposits rather than one. The antenna efficiency with one deposit inkjet printed silver on the IF fabric was greater than that of an antenna using 5 inkjet deposits for one conductive layer without an interface layer.

5.4.2 Fabric patch antenna measurement

Three 2.4 GHz patch antennas were inkjet printed on to IF fabric as shown in figure 45. Three different designs, provided by Loughborough University were used. The fabrication process is the same as that used in fabricating the fabric half wavelength dipole antenna. Only the radiating element, the patch plane is inkjet printed in this research. All fabricated patch antenna samples were then sent to Loughborough for assembly and testing in their anechoic chamber.

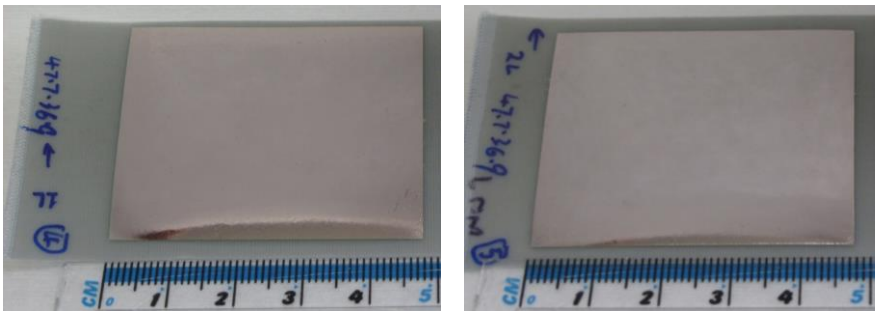

(a) (b)

Figure 45.(a) 1 silver deposit inkjet printed 47.7mm ×36.9mm patch, (b) 2 silver deposits inkjet printed 47.7mm ×36.9mm patch. All patch antennas are inkjet printed on IF fabric.

The fabric patch antenna was assembled as follows. Two layers of 0.8mm thick felt were attached to a 90 mm ×90 mm Nora Dell ground plane using commercially available upholstery glue that is activated by ironing. A probe feed was implemented by using an ultra-small flexible co-axial cable of diameter 1.32 mm. The inkjet printed side faced the ground plane, as shown in figure 46.

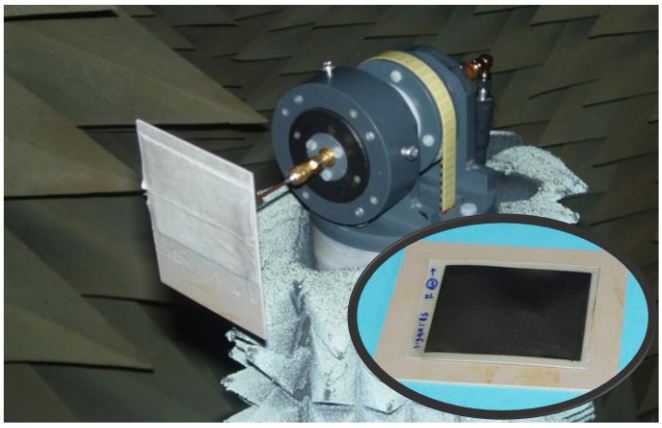

Figure 46. The inkjet printed patch antenna in the anechoic chamber and inset the patch antenna before the connection was made.

In order to assess the performance of the inkjet printed antennas, three antennas were compared with an etched patch antenna on a low loss substrate. The antennas were designed to resonate at approximately 2.4 GHz. Details of the geometry are given in figure 22 and the smaller patch

antenna was cut from the original design. The low loss substrate used was a Taconic RF45 (ε_r = 4.5 and $\tan\delta$ = 0.0037) substrate with a copper ground plane. To maintain the resonant frequency of 2.4 GHz with the felt substrate, the patch dimensions were reduced by cutting the inkjet printed patch plane.

The theoretical efficiency of the etched patch was calculated to be 85 % at 2.372 GHz on FR45 and 97 % at 2.6 GHz on felt using Personal Computer Aided Antenna Design (PCAAD) 6.0 software from Antenna Design Associates, Inc. The four antennas were measured in an anechoic chamber. The measured efficiency of the etched patch antenna was 79 %. The efficiency reduced to 57 % with the inkjet printed patch glued on the same substrate. A similar efficiency was measured with the felt substrate but this reduced to 37 % when only one layer of ink was used. Variations in the felt properties and thickness caused small variations in the frequency between the two inkjet printed fabric antennas. The simulated efficiency of the etched patch antenna on felt using a copper patch was 78 % using EMPIRE XCcel finite-difference time-domain (FDTD) software. Reducing the simulated conductivity of the ink layer to 1MS/m approximately replicated the measured efficiencies with both one and two deposits of ink. The results indicate that reasonable efficiency levels were achieved with just one layer of ink and were improved by the addition of a second inkjet printed layer. The above measured antenna results are summarised in table 11.

	Etched Copper Patch on FR45 substrate	Fabric Inkjet Patch on FR45 Substrate	Fabric Inkjet Patch on Felt	Fabric Inkjet Patch on Felt
Patch size (mm)	37.4 × 28.1	37.4 × 28.1	47.7 × 36.9	47.7 × 36.9
Substrate height (mm)	1.6	1.6	1.9	1.9
Silver ink deposits	35µm copper	2	1	2
Frequency (GHz)	2.378	2.480	2.405	2.505
S11(dB)	-13.39	-14.89	-10.05	-9.95
10dB Bandwidth (MHz)	22.5	24.5	17.5	N/A
Directivity (dBi)	7.39	7.55	8.38	8.72
Gain (dBi)	6.37	5.09	4.02	5.98
Efficiency (%)	79	57	37	53

Table 11. Measured results of inkjet printed patch antennas on different substrate, FR45 and felt.

Directivity in a given direction is defined as the ratio of radiation intensity and the intersity averaged over all directions. The radiation patterns of the four antennas were similar. Therefore, only the fabric antenna with two inkjet deposits for the conductive layer is shown in figure 47.

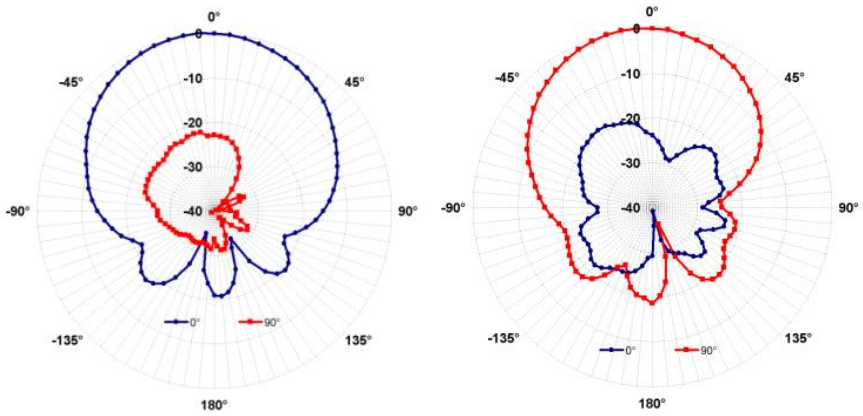

Figure 47. The measured patterns of the fabric inkjet patch with two deposits of ink on IF fabric at 2.505 GHz: (a) y-z plane (E-Theta Plot) and (b) z-x plane (E-Phi Plot).

Patch antenna is designed to radiate more power in a certain direction than another direction, as typically quoted as antenna directivity in the unit of dB. The radiation pattern of patch antenna is often described as a perfect from-to-back ratio, as all radiation toward the front and no radiation towards the back [127]. Figure 47 the inkjet printed fabric patch antenna radiation pattern shows it has very good front plane radiation pattern with a weak and random back plane radiation.

Inkjet printed antennas are sensitive to bending as the inkjet layer can be damaged by the physical act of compressing and tensioning the conducting surface. The fabric antennas were tested on a polystyrene cylinder of radius 70 mm and 125 mm. The patch antennas were bent in two dimensions with respect to the feed. The antennas on the larger cylinder 125 mm generally maintained their S11 performance compared to the flat antenna. The S11 results for the fabric antenna with one and two silver deposits for the conductive layer on the 70 mm radius cylinder are shown in figure 48 and figure 49 respectively.

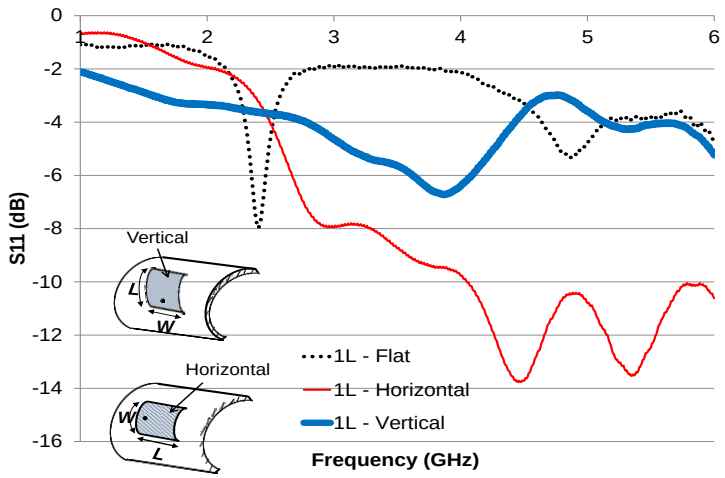

Figure 48. The measured S11 of the textile inkjet patch on felt with one deposit of ink bent around a 70 mm radius polystyrene cylinder.

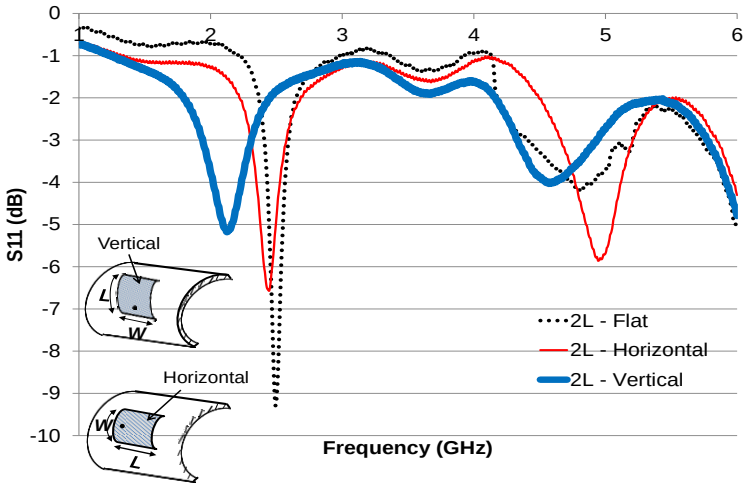

Figure 49. The measured S11 of the textile inkjet patch on felt with two deposits of ink bent around a 70mm radius polystyrene cylinder.

Figure 48 S11 result with one silver deposit inkjet printed layer show that the connectivity of the conductive layer is adversely affected by bending and the antenna becomes extremely lossy and does not function. However, the conventional resonance at 2.4 GHz resumed when the antenna was unbent even after approximately ten measurements. Figure 49 indicates that the antenna is reasonably robust to bending and this robustness is increased with a second deposit of ink. The S11 results indicate that bending in the horizontal direction is preferable as it has good correlation with the curve measured in free space.

5.5 Conclusions

All five selected substrates have been evaluated with regard their physical properties and potential for being direct write printing substrates in this research. An inkjet printed dipole antenna and patch antenna have been fabricated on standard fabric for the first time. The inkjet printed fabric dipole has been shown to achieve efficiencies up to 74.1 % at 1.897 GHz, compared to 77.5 % at 1.778 GHz from etched copper on low loss laminate. The inkjet printed fabric patch antennas has been shown to achieve efficiency up to 57 % at 2.48 GHz, compared to 79 % at 2.378 GHz from etched copper patch antenna on FR45 substrate. It was found experimentally that the optimum printing resolution of SunChemical silver ink on IF fabric was 15μm. This chapter has allowed the characterisation of the printing procedure for the fabrication of conductive layer on IF fabric. These results and experience also enable to inkjet print conductive tracks and plates for use as conductive electrodes on IF fabric in inkjet printed smart fabric parallel plate capacitors.

This page intentionally left blank

Chapter 6

6 Direct write printed smart fabric capacitor

6.1 Introduction

This chapter discusses two direct write fabrication methods: inkjet printing and pneumatic dispenser printing to realise direct write printed flexible capacitors. The performance of the direct write printed capacitors will be assessed and discussed. Three capacitors were direct write printed. Two flexible capacitors were fabricated by inkjet printing. The first was printed on a Kapton film using SU-8 as the dielectric material. The second used a new formulation of inkjet printable PVP dielectric on fabric. These two capacitors are compared to emphasize the new PVP inkjet printable dielectric ink's performance. The third capacitor is fabricated by pneumatic dispenser printing with the same active materials used in the first inkjet printed capacitor. It is compared with the inkjet printed capacitor and proves the capability of the pneumatic dispenser in direct write printed electronics.

This chapter starts with the background theory, design and architecture of printed capacitors. Then the active materials and substrates used in this research work are introduced, followed by two main sections on inkjet printed capacitors and pneumatic dispenser printed capacitors. Finally, a comparison between inkjet printing and pneumatic dispenser printing techniques is made and their techniques are discussed.

6.2 Theory, design and architecture of a printed parallel plate capacitor

A capacitor is typically a passive two terminal electronic component with a dielectric separator in between that can be used to store electrical energy when subjected to an electric field. In Chapter 4, two potential capacitor structures for direct write printing were evaluated. These are a parallel plate structure and an interdigital structure, as shown in figure 19. The parallel plate

structure was selected to be the second step for the reasons given in section 4.3, towards the all inkjet printed transistor after the achievement of inkjet printed fabric antenna.

The capacitor design involves direct write printing three layers, consisting of top and bottom electrodes with a dielectric layer in between. The dielectric material can be low temperature thermally curable or UV curable dielectric. The initial design is shown in figure 50. The black and grey layers represent the top and bottom electrodes respectively with the light blue the dielectric layer. The effective capacitive area is in the diameter of 5 mm.

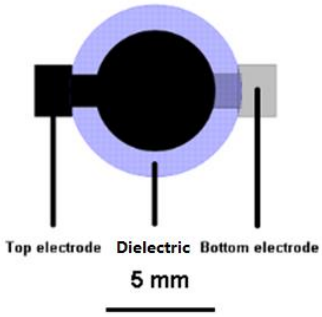

Figure 50. Plan view of the initial designed layout of inkjet printed flexible parallel plate capacitor.

The capacitance of a parallel plate capacitor can be determined using equation 8.

$$C = \frac{\varepsilon_o \varepsilon_r A}{d} \tag{8}$$

Where

C is the capacitance in F,
A is the effective area of the top and bottom two plates in m^2,
d is the distance between the two conductive electrodes in m,
ε_r is the relative permittivity of the dielectric layer,
ε_0 is the vacuum permittivity as a constant of 8.854×10^{-12} in F/m,

The static absolute permittivity is calculated by multiplying the relative permittivity by the vacuum permittivity. The relative permittivity is the key property of an electrical dielectric material and is equal to the ratio of the capacitance of a capacitor filled with the given dielectric material to the capacitance of an identical capacitor in a vacuum space without a dielectric material [128]. A high relative permittivity dielectric material is desirable in fabricating a

capacitor, because the overall capacitor structure can be much smaller as the reduced distance between the two electrodes, compared to a capacitor with a vacuum or air separator.

6.3 Selected inks and substrates for printed capacitors

Four potential inkjet printable dielectric inks were considered in addition to the inkjet printable conductive ink and the selected substrates used in fabricating direct write printed flexible capacitors. Inkjet printable inks have much stricter rheological requirements than pneumatic dispenser printer inks, which can potentially accept all inkjet printable inks and screen printable pastes. Therefore, in this section, only inkjet printable inks are discussed without mention of specific pneumatic dispenser printable materials.

6.3.1 Selected dielectric materials for printed capacitors

The dielectric layer is required to prevent electrons moving from one electrode of the capacitor to the other. It can be either organic or inorganic. An inkjet printed dielectric layer often produces poor layer smoothness, as the printed layer is typically non-uniform. Both thermally curable and UV curable dielectric layer thicknesses can be altered by varying the drop spacing. In the case of solvent based dielectric inks, varying the dielectric solid weight percentage in the solution can change the printed layer's thickness more significantly than altering the drop spacing. Typically UV curable inks are a 100 % solid system, which essentially means it does not contain solvent that must evaporate during the curing phase [129]. The printable dielectric inks frequently reported in publications are acrylate based UV curable inks and PVP based thermally curable inks, which have been fully reviewed in chapter 3.

In this material selection section, three dielectric material types (acrylate, SU-8 and PVP) will be introduced in terms of their potential to be used as inkjet printable UV curable dielectric inks. The use of UV curable dielectric inks for inkjet printed fabric devices are preferred since this approach will avoid the potential degradation caused by the heat required to cure a thermally curable dielectric ink. A thermally curable PVP ink will also be developed, as an intermediate ink to study the PVP based formulation towards a new UV curable PVP ink.

6.3.1.1 Inkjet printable UV curable acrylate dielectric ink

Inkjet printable UV curable dielectric inks are primarily based on acrylate materials. SunChemical U6415 UV curable dielectric ink for inkjet printing will be evaluated; it has the attraction of being commercially available and is based on acrylate which is very widely used in inkjet printable dielectric applications. The average viscosity is around 40 mPa s under an ambient room temperature. The datasheet suggested the viscosity of U6415 will lie in the viscosity range of 11 to 13 mPa s at a nozzle temperature of 50 ^{o}C. Its viscosity range at 50 ^{o}C overlaps the printer's ideal viscosity range of 10 to 12 mPa s. Later experimental work has shown it works well with the Dimatix inkjet printer in firing droplets with the desired performance. However since its cured layer surface energy is not sufficiently high enough to wet the subsequent inkjet printed silver ink, the viscosity of this acrylate ink at 50 ^{o}C is not measured. Details of this ink's printing trials will be shown in later section 6.4.1.4.

6.3.1.2 Inkjet printable UV curable SU-8 dielectric ink

MicroChem [130] PriElex V005 and V006 inkjet printable dielectric ink is based on SU-8, a photoresist widely used in subtractive microfabrication. PriElex V005 is a UV curable ink and PriElex V006 is a thermally curable ink. Both are designed for inkjet printing. These two products were still under development by MicroChem while this research work was carried out. They are designed to be the world's first inkjet printable SU-8 inks for use as dielectrics. A small sample quantity (4 ml) of PriElex V005 ink was provided by Printed Electronics Ltd (PEL) [131] as it was prohibitively expensive to obtain from the manufacturer. The quantity is less than the minimum amount 6 ml required to perform a viscosity measurement. Figure 51 shows the unpublished viscosity data provided by Printed Electronics Ltd (PEL) for V005 and V006 PriElex ink.

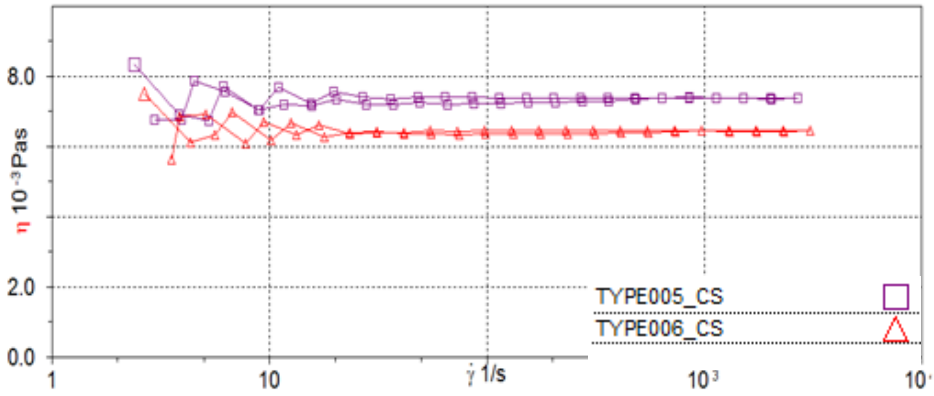

Figure 51. Viscosity measurements of MicroChem PriElex V005 and V006 SU-8 inkjet printable dielectric ink.

The x axis unit is called 'reciprocal seconds' which is recognised as the frequency of oscillation. The inkjet printer operates at 40 KHz which represents the 10^4 on the x axis in Figure 51. The average viscosity of V005 is about 7.3 mPa·s and V006 is about 8.5 mPa·s; both are outside the ideal viscosity range 10 to 12 mPa s but within the acceptable viscosity range of 2 to 30 mPa s.

6.3.1.3 Inkjet printable thermally and UV curable PVP dielectric inks

Inkjet printable PVP based dielectric ink is the most widely reported inkjet printable dielectric ink in inkjet printed electronics literature when both thermally and UV curable dielectric inks are considered. Therefore, PVP based dielectric ink is selected to be the one of the candidate for use in this research. Figure 52 shows that 7 wt% PVP in 1-hexanol with 3.5 wt% cross linking agent has an average viscosity value of 12.9 mPa s which is very close to the ink's ideal viscosity range of 10 to 12 mPa s.

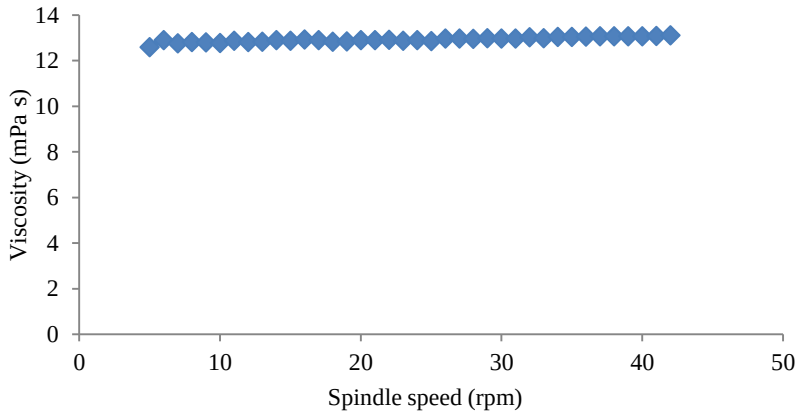

Figure 52. Viscosity of 7 wt% PVP dissolved in 1-hexanol solvent, measured using a Brookfield DV-II pro viscometer.

The PVP solvent based formulation will be explained in detail in later section 6.4.1. 1-Hexanol has a surface tension of 0.025 N/m at 25ºC [132]. 1-Hexanol's surface tension is very close to the lower limit of the suggested surface tension boundary of 0.028 N/m defined by Dimatix. If the surface tension is low then jetting will produce tails or satellite droplets after each droplet and a higher surface tension will prevent a droplet forming. In addition, the surface tension of the solvent typically increases after dissolving a high molecular polymer material, because the polymers typically have higher surface tension than the solvent [133]. The DMP 2831 inkjet printer can have 16 nozzles working with both the thermally and UV curable PVP dielectric ink. For the commercial SunChemical silver ink, only one or two nozzles work.

6.3.2 Selected conductive silver for printed capacitors

The printed antenna results from chapter 5 showed the conductive silver ink U5714 from SunChemical is compatible with the DMP 2831 inkjet printer and shows good conductivity and flexibility on the IF fabric substrate after a 150 ºC curing temperature for 10 minutes. Therefore, the conductive silver ink U5714 will be used as the only conductive ink for inkjet printing and pneumatic dispensing in this chapter. Its processing parameters will remain the same as in chapter 5; 15 µm drop spacing, 2 inkjet printed deposits of silver ink as one conductive layer, curing at 150 ºC for 10 minutes in a conventional thermal oven.

6.3.3 Selected flexible substrate for printed capacitors

For these printing trials carried out in section 5.3.1, Kapton film and IF fabric will be used for the direct write printed capacitors. Kapton will be used for initial printing trials using UV curable acrylate ink, SU-8 ink and thermally/UV curable PVP ink, then IF fabric will be used to realise the all inkjet printed fabric capacitor. The dispenser printed capacitor is made on Kapton film substrate as an incremental approach toward fabric substrate for the same reasons as chapter 5.

6.4 Inkjet printed capacitor

6.4.1 Fabrication

6.4.1.1 Multilayer device alignment in DMP 2831 inkjet printer

The previous inkjet printed fabric antenna only requires one electrically functional layer: the conductive layer. A capacitor will need three functional layers in a parallel plate structure including conductive and dielectric layers. Therefore, multilayer device alignment becomes a challenge in practical work. Well aligned layers between the two conductive electrodes will generate the maximum capacitance from the designed capacitor layout. Misaligned layers will reduce the capacitance by reducing the overlapping effective capacitive area between the two parallel conductive silver plates as shown in figure 53.

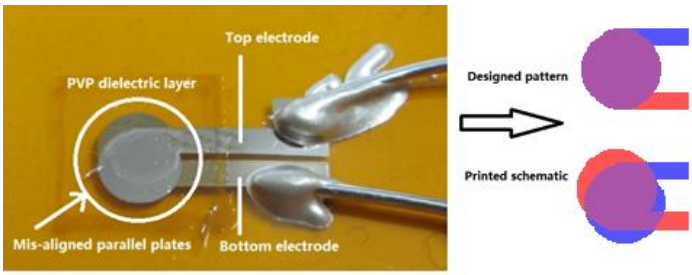

Figure 53. Top view of a misaligned inkjet printed capacitor with UV curable PVP dielectric on Kapton film.

This misalignment problem must be solved not only to improve capacitor performance but because it will be a significant problem for future devices. For example, the printed transistor will fail if the alignment of the different layers is incorrect.. There are two different alignment processes which are essential before each different material's deposition.

(1) X axis and Y axis alignments,
(2) Theta axis alignment.

These alignment processes are only required when printing different materials or patterns, additional printing of the same layer during the same process does not need re-alignment between prints. The two different alignment checks can be performed using the integrated alignment check function provided with the DMP 2831. X and Y axes alignment checks are achieved by locating the droplet actual location with the pre-set starting position as a reference

point to compensate the off-set distance in both X and Y directions. Theta axis alignment check is to pick up two points on the substrate which are designed to be level, then the system will rotate the platen to level the two points for printing. An example of the theta axis alignment process is given below in figure 54.

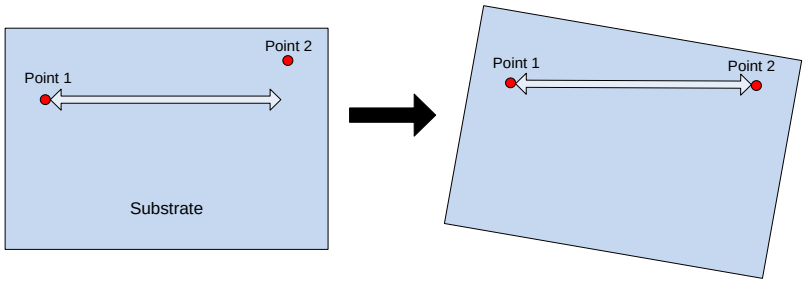

Figure 54. Example image of the integrated theta alignment function in the Dimatix inkjet printer; the printed pattern is rotated to match the chosen design alignment marks.

6.4.1.2 Inkjet printed parallel plate capacitor fabrication process

The chosen substrate surface is wiped with lint free cleanroom wipes dipped in DI water. This step is required to ensure the surface energy across the whole printing area is uniform. A 10 pL cartridge is used in this research work. 60 µm droplets diameter is the average value used in this thesis. The next step is to inkjet print two deposits of silver ink, with a drop spacing of 15 µm, as one conductive layer on to the substrate to form the lower electrode. After two deposits of silver ink, the conductive pattern is then cured for 10 minutes at 150 ^{o}C. The UV curable dielectric inks are then printed on top of the lower electrode from the designed dielectric pattern. Two inkjet printed deposits of the dielectric ink as one dielectric layer are deposited to avoid potential pin holes on the film causing device failure. The curing process for the inkjet printable SU-8 and UV PVP inks is 10 and 100 seconds respectively in a UV chamber with a power density of 31 mW/cm^2. A 365 nm wavelength mercury bulb is fitted in the UV chamber supplied by UV Light Technology Ltd [134].The top electrode is then inkjet printed and cured, using the same process as the lower electrode, to complete the capacitor structure. The upper and lower contact pads are then wired with silver epoxy for further electronic performance testing. Solder does not stick to the silver layer as stated in chapter 5. The fabrication flow diagram is shown in figure 55.

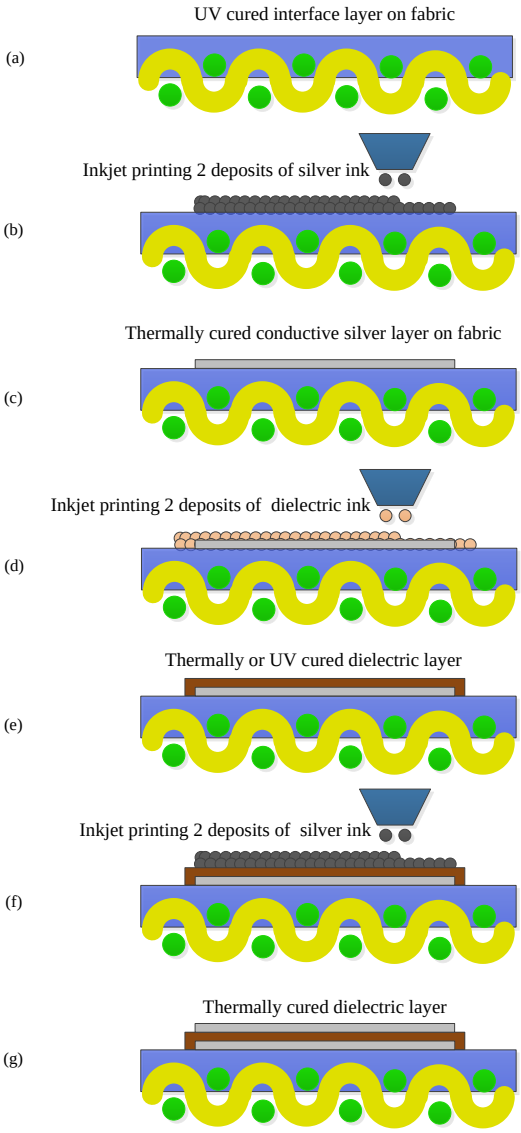

Figure 55. A flow diagram in the cross sectional view showing the fabrication of inkjet printed smart fabric parallel plate capacitor fabrication process.

6.4.1.3 Inkjet printing parameter optimisation

Several parameters can be set to reach the optimum jetting performance based on each different ink's rheological properties. All parameter setting in this research work are tested on the DMP 2831 inkjet printer with a 10 pL droplet volume cartridge head.

The first parameter is the nozzle temperature. It is typically used when the ink is too viscous beyond the printer's acceptable upper limit, 30 mPa s, then raising the temperature can achieve the desired jetting performance. SunChemical silver ink does not require a raised nozzle temperature to perform jetting based its datasheet values. Further investigation however revealed that raising the nozzle temperature up to 35 ^{o}C can reduce the chance of clogging the

nozzles while the inkjet printer is in operation. SunChemical dielectric requires 50 ^{o}C nozzle temperature to reach the viscosity range of 11 to 12 mPa s due to its datesheet value. MicroChem PriElex inks require 30 ^{o}C nozzle temperature based on their datasheets [135]. Both PVP based UV curable and thermally curable dielectric inks do not require raised nozzle temperature while jetting.

The second parameter is the firing voltage. The firing voltage is adjusted using the built in drop watcher to tune the droplets velocity range to between 7 and 9 m/s. The firing voltage for standard inkjet printable inks is around 20 V. However, with the Dimatix printer, each inkjet nozzle is not of identical quality. For examples, some nozzles do not fire droplets properly on first use and some nozzles require a higher firing voltage than others. There can be up to 2 V difference in firing voltage in the same inkjet printable ink within the same cartridge head. SunChemical silver ink requires a firing voltage in the range of 25 to 30 V. If a 35 ^{o}C nozzle temperature is applied, the nozzle voltage reduces down to between 20 and 25 V. SunChemical dielectric requires a 20 to 25 V nozzle voltage. MicroChem PriElex inks both require 15 to 20 V. Both PVP based UV curable and thermally curable dielectric inks typically require firing voltages in the range of 18 to 23 V.

The waveform is usually a standard setting for the majority of inkjet printable inks. Dimatix provides two standard waveforms:

(1) One is designed for low viscosity inks.
(2) The other is designed for ideal viscosity inks.

A high viscosity ink can be heated up to reduce its viscosity, but this can increase the ink's solvent evaporation rate resulting nozzles clogging. There are typically 4 segments in a standard waveform to achieve the 3 staged process of droplet formation as shown in figure 3. An example of SunChemical silver ink's waveform control panel is shown in figure 56 with the vertical lines indicating the transition rather than a time scale.

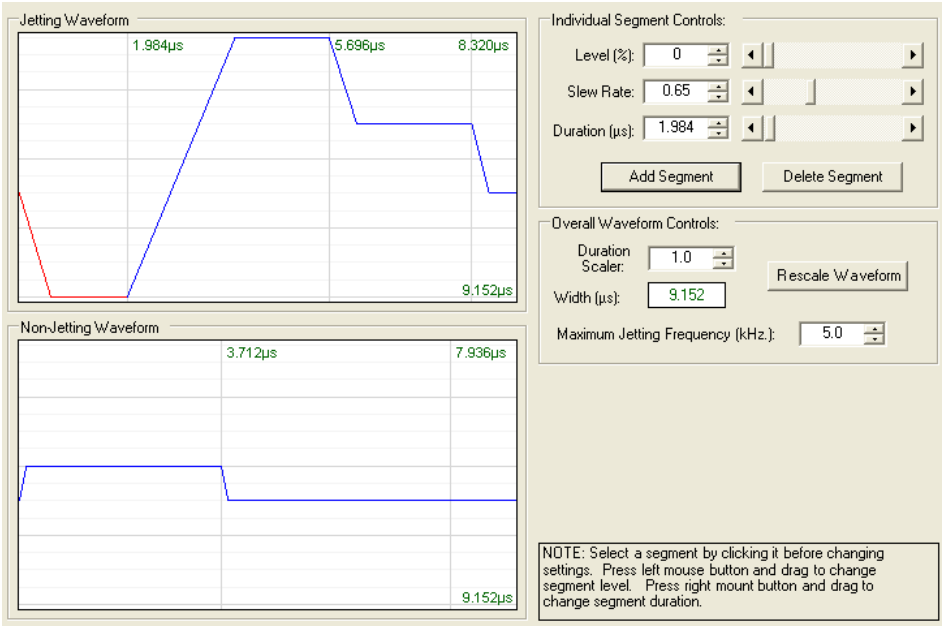

Figure 56. SunChemical silver ink's waveform in DMP 2831 inkjet printer showing the four segment levels of amplitude.

Adjusting the waveform helps to achieve a better droplet formation and avoid potential tails and satellite droplets with the main droplet each time the nozzle fires. As shown in the silver ink's waveform, there are three properties of each segment which can be changed:

(1) Level, this is the percentage of the amplitude relative to the other segment level.
(2) Slew rate, this is the slope of the line in the waveform during voltage ramps.
(3) Duration, this is the length of the segment in time.

Meniscus point is another parameter which can be set before printing which can slightly affect the jetting performance. Meniscus control is a low level vacuum applied to the ink reservoir to prevent ink from flowing out of the nozzle. Experimental work carried out in this research suggests the higher meniscus set-point is used for high viscosity and/or high surface tension inks while low meniscus control is used for low viscosity and/or low surface tension inks.

6.4.1.4 UV curable acrylate ink: printing trials, capacitor fabrication and interface printing trials

UV curable acrylate inks benefit from fast room temperature UV curing. The U6415 ink is compatible with the DMP 2831 inkjet piezo head and the pattern is sharp. There are around 5 continuous nozzles working at the same time compared with typically 1 or 2 continuous nozzles working for the SunChemical silver ink. A new design was used for these prints shown in figure

57, to shift the top electrode from the left to the right. This new design reduces the strain on the capacitive area due to the attached wires making the devices easier to print and handle. The new designed diameter has an effective capacitance area of 7.07 mm^2 in the diameter of 3 mm.

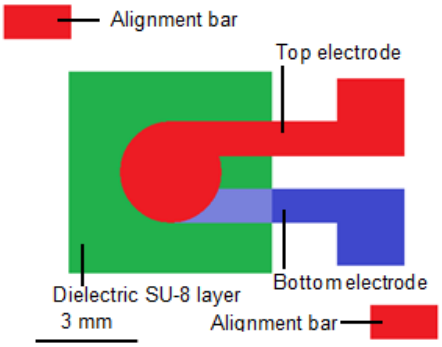

Figure 57. Plan view of the 2nd schematic design of the inkjet printed capacitor.

The alignment bars in the corners are added as a practical addition to help alignment between layers. Figure 58 shows the poor wetting of the inkjet printed silver on top of the acrylate dielectric layer in an all inkjet printed capacitor on Kapton substrate.

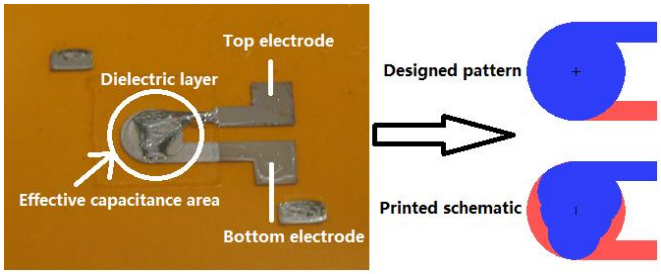

Figure 58. Plan view of inkjet printed capacitor on Kapton substrate.

The experimental work has proved it is not suitable for the all inkjet printed capacitor. This is because the surface energy of the UV cured acrylate dielectric layer is not sufficiently high to allow the subsequently printed silver layer to wet properly to form a conductive layer as in the designed pattern. Therefore this SunChemical U6415 acrylate dielectric ink was not further investigated regarding its use as an inkjet printable dielectric ink. However, due to its fast room temperature UV curing process SunChemical U6415 UV curable ink has been tested to be inkjet printed directly onto the standard polyester cotton fabric (standard fabric) to function as an interface layer. There are two reasons to do the printing trials of the UV 6415 as an interface layer after it has been proved that, it is not capable to be used as an dielectric layer:

(1) The fast UV curable ink can still fill in the weaves of the fabric to stop the fabric absorbing the subsequent printed functional inks.
(2) The low viscosity and high absorption of the ink result in poor surface smoothness, which can increase the average surface energy of the printed U6415 interface layer compared to a printed smooth U6415 layer.

Direct write printable interface layer on fabric has been mentioned only once in literature review as references [88] used PEDOT/PSS as the interface material on a fabric substrate for a subsequently printed silver ink. PEDOT/PSS is expensive and lost its conductive function being as an interface layer. A screen printed interface layer on fabric was introduced in chapter 5 on the inkjet printed fabric antenna. Figure 59 shows an SEM micrograph of an inkjet printed U6415 as an interface coating on the standard fabric in cross sectional view.

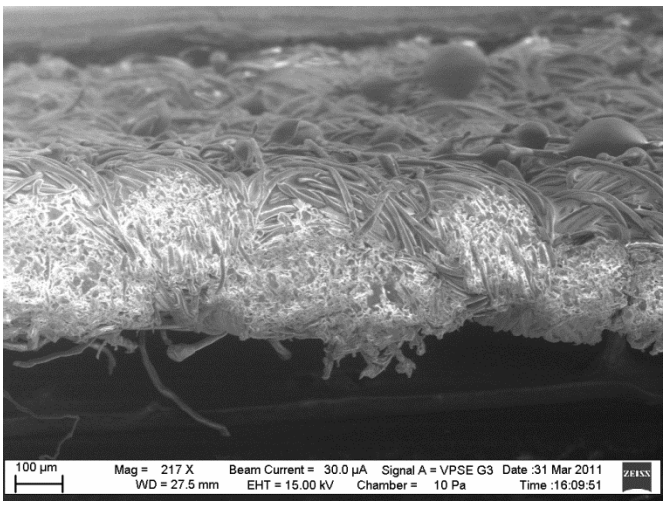

Figure 59. Isometric view SEM image of inkjet printed UV curable ink as interface coating on the standard fabric.

For these trials, there are six inkjet printed acrylate layers with a drop spacing of 15 µm. Each layer is fully UV cured before depositing the next layer. This method reduces the absorption rate of each subsequent printed layer on the polyester cotton fabric, even though the layers are completely absorbed into the yarns due to their low viscosity. The white bright area in figure 59 shows the highly charged dielectric material absorbed in the yarns on the SEM microgram. However, the roughness of the resulting surface suggests that this method is not suitable because test showed at least three deposits of silver inks were needed to create a conductive layer on this inkjet printed UV acrylate coated standard fabric. The surface roughness is still very poor even after six deposits U6415 as shown in figure 60.

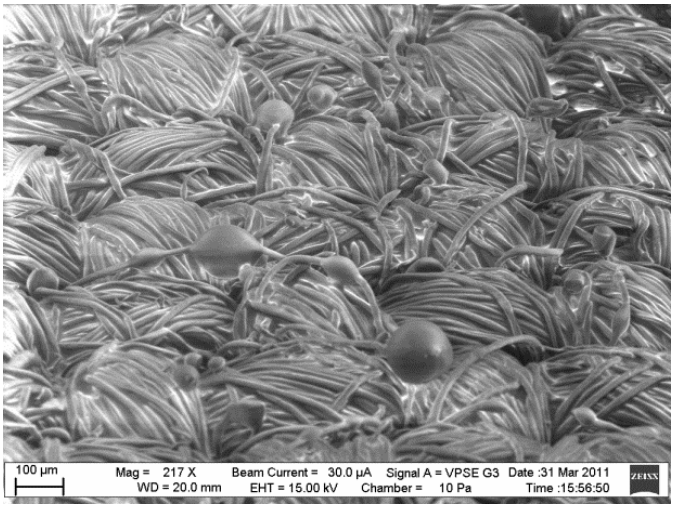

Figure 60. Plan view SEM image of inkjet printed UV ink as interface coating on the standard fabric.

Due to the low viscosity of typical inkjet printable inks (2 to 30 mPa s) and high solvent content (> 85 %), the inks are absorbed by the fabric substrate in a very short time whereas an interface ink is ideally expected to stay on top of the fabric to fill in the weave, especially after the first few prints. The top view image of inkjet printed interface layer on fabric shows the absorption of the inkjet printed ink has expanded into a much larger area than the designed area, as shown in figure 61.

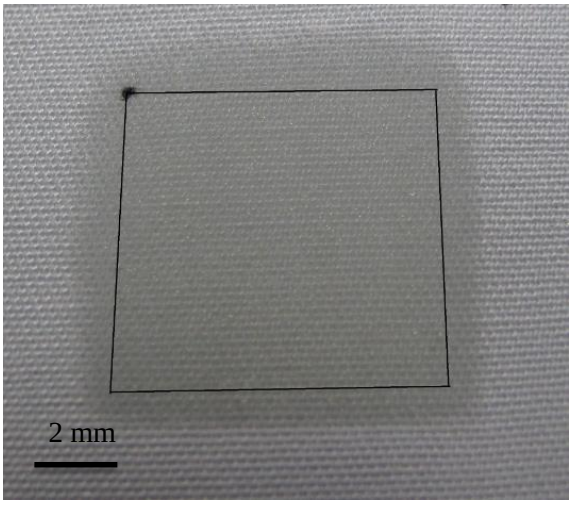

Figure 61. Plan view of inkjet printed interface layer on fabric substrate with U6415 ink.

In figure 61, the black lined square box represents the design area for inkjet printing interface layer. The ink covered area is beyond the boundary of the designed pattern which means the inkjet printed pattern is poor.

Partial UV curing of the UV dielectric ink can potentially be performed before the droplets land on the fabric surface to increase its viscosity by using the UV pinning curing method. UV

pinning curing method is to use a UV source to pin on the in-flight droplet before it lands on the substrate. Another possible method is instantly UV cure directly after each pixel line is printed. Printed Electronics Ltd (PEL) have developed a UV curing system that attaches to the left side of a DMP 2831 printer head to perform real time UV curing as each line of pixels is printed. In addition, these two suggested methods may potentially achieve an inkjet printed interface layer on top of the standard fabric.

6.4.1.5 UV curable SU-8 ink: printing trials and capacitor fabrication

An inkjet printed flexible capacitor was printed on a Kapton substrate without any surface modification, for example, pre-defining surface energy on desired printing pattern to achieve sharp pattern. MicroChem PriElex V005 ink is not easy to inkjet continuously as missing dots and lines occasionally occur when a new pixel line is started. Therefore the initial designed layout with two electrodes on two sides as shown in figure 50 and square sized dielectric layer in figure 57 were abandoned when using SU-8 ink. The new layout used in practical work for inkjet printing SU-8 capacitor is shown in figure 62. The new designed diameter has an effective capacitance area of 19.6 mm^2 in the diameter of 5 mm.

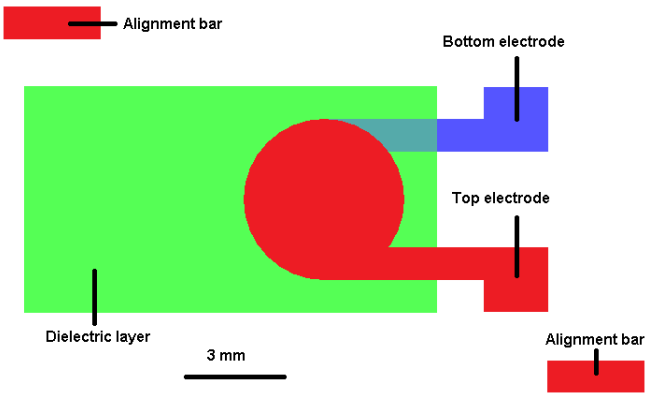

Figure 62. Plan view of the 3rd layout designed in L-Edit for an inkjet printed capacitor.

The new design has extended the dielectric area to avoid possible missing dots and lines when a new pixel line is started. The fabrication follows the described procedure in section 6.4.1.2. The final all inkjet printed capacitor based on SU-8 dielectric ink is shown in figure 63.

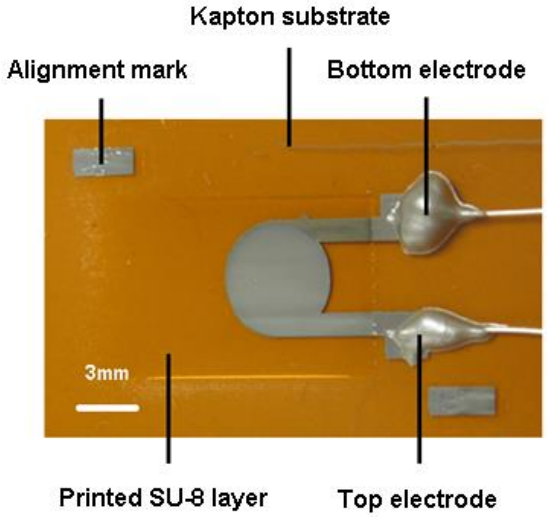

Figure 63. Plan view of all inkjet printed SU-8 capacitor on Kapton substrate.

The capacitor shown was connected to standard copper wires using silver epoxy to enable easier measurement of the device characteristics. The SU-8 layer is approximately 15 μm thick as shown in the cross sectional view micrograph of the all inkjet printed SU-8 capacitor in figure 64.

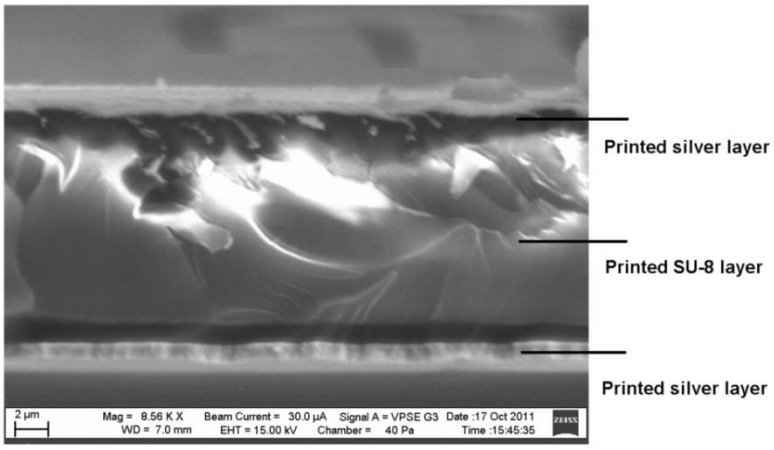

Figure 64. SEM cross sectional image of inkjet printed capacitor on Kapton substrate.

6.4.1.6 Thermally curable PVP ink: development, printing trials and capacitor fabrication

The majority of inkjet printable PVP inks use isopropanol (IPA) [38] or propylene glycol monomethyl ether acetate (PGMEA) as the solvent to dissolve the PVP [136]. However, experimental work during this research has revealed that IPA cannot dissolve 7 wt% PVP. Even by stirring it for over 5 hours resulted in more than 50 % PVP material remaining un-dissolved. PGMEA can dissolve PVP material easily as most publications suggest. However, the Dimatix inkjet printer is unable to jet the PVP/PGMEA ink properly. The main factor is the viscosity

of PGMEA at only 0.8 mPa s at 25 ºC [137]. Ko et al [138] reported hexanol being used as the solvent to form a stable PVP ink for inkjet printing. There are three types of hexanols: 1-hexanol, 2-hexanol and 3-hexanol. 1-hexanol has the highest polarity because it has a hydrogen bond on the end of the chemical chain. 1-hexanol has the highest boiling point 157 ºC [139] among the other two types, 2-hexanol and 3-hexaol. Therefore, 1-hexanol is selected to be the solvent for dissolving the PVP material. Experimental results showed 1-hexanol to be the best candidate from a printing perspective compared to the other two potential solvents, IPA and PGMEA. All 16 nozzles can inkjet print the UV curable dielectric PVP ink continuously without clogging, which will significantly reduce the fabrication time. This significant advantage will reduce the requirement for the extended dielectric pattern required for the printed SU8 capacitor design.

Poly(melamine-co-formaldehyde) methylated solution (PMF) is the most widely used cross linking agent in PVP solvent based thermally curable inks as reported in the majority of publications. The formulation of PVP in 1-hexanol with cross linking agent (PMF) in the ratio of 2:1 was tested by inkjet printing. The thermally curable formulation used here is 7 wt% PVP in 1-hexanol solvent with the 3.5 wt% PMF.

The previous substrate evaluation section in chapter 5 has stated the standard fabric can only survive under 150 ºC for a maximum of 45 minutes without visible degradation. In capacitor fabrication, top and bottom electrodes will take 10 minutes each at 150 ºC for curing. The total thermal curing condition is 20 minutes under 150 ºC for both electrodes. The thermal curing condition for testing the thermally curable PVP ink can therefore be a maximum of 25 minutes at 150 ºC. However, it normally requires 200 ºC for one hour [140]. The result shows the PVP wasn't cross linked after the thermal curing at 150 ºC for 25 minutes. The subsequent inkjet printed silver layer completely dissolved the un-cross linked PVP layer as shown in figure 65.

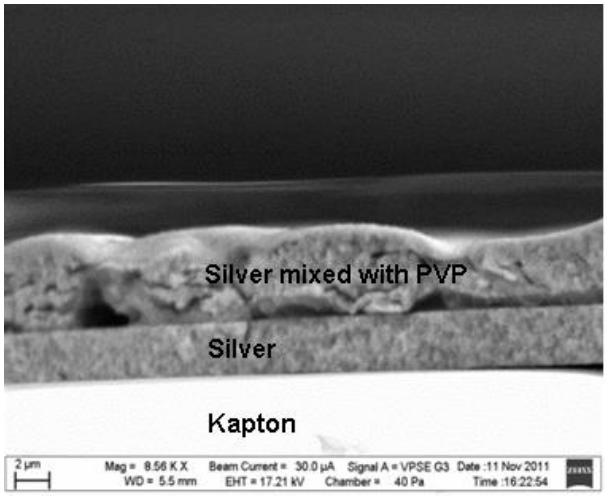

Figure 65. Cross sectional view SEM image of a mixture of PVP and silver layer on top of a thermally cured silver layer.

Figure 65 is taken from the all inkjet printed flexible capacitor on Kapton substrate with PVP thermal curing condition of 150 ^{o}C for 25 minutes. The whole printed capacitor is shown in figure 66, showing the high roughness top surface caused by the mixing of the silver and un-cross linked PVP layer.

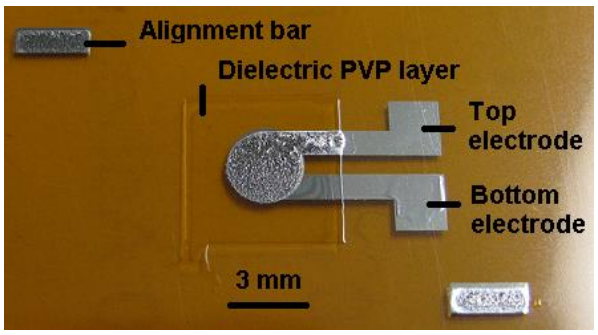

Figure 66. Plan view of a failed all inkjet printed capacitor on Kapton substrate with thermally curable PVP dielectric.

For comparison purpose, one hours thermal curing at 200 ^{o}C for the inkjet printed thermally curable PVP ink was tested during fabrication of a parallel plate capacitor. The PVP layer is fully cross linked as shown in figure 67, with three inkjet printed active layers clearly shown in a capacitor on Kapton film substrate.

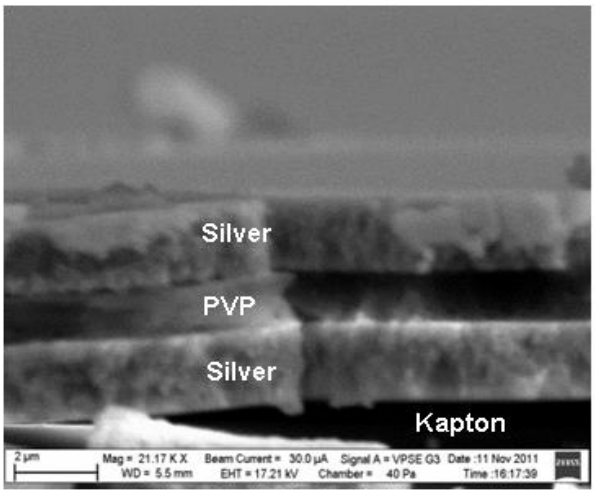

Figure 67. Cross sectional SEM image of an all inkjet printed thermally curable PVP capacitor.

The fabric is not capable of sustaining this high temperature curing process required to fully cross link the thermally curable PVP, this is not therefore a viable process for a smart fabric capacitor.

Choi et al [57] reported a spin coating formulation of poly(4 vinylphenol) (PVP) insulator solution that can be cross linked at 70 ^{o}C. Later in this research work it was proved that this insulator formulation cannot cross link at under 70 ^{o}C with the recipe provided in the inkjet printed parallel plate capacitor. This could be because, the repeated experiment used inkjet printed silver on top of the cured PVP, rather than the evaporating electrode as described in the paper. The strong solvent could dissolve the un-cross linked PVP layer as the evaporated electrode could not.

6.4.1.7 UV curable PVP ink: development, printing trials and capacitor fabrication

The thermally curable PVP ink has been shown to be unsuitable for low temperature curing conditions and therefore an alternative process is desired. Therefore in this research, a new novel UV curable solvent based PVP ink has been developed to achieve the inkjet printed thin dielectric film using UV curing at room temperature.

The new formulation is inspired by a papers related to a UV curable dielectric ink [140], which is not directly on the topic of inkjet printable UV curable PVP ink. Yang et al [140] reported that a photo-acid generator can be used to trigger the polymerisation reaction of spin coatable PVP ink under UV exposure. A photo-acid generator can create localised acidic environments

upon UV exposure [141]. The photo-acid generator (PAG) used in reference [140] is {4 - [(2 - hydroxyltetradecyl) oxy] phenyl} phenyliodonium hexa-fluoroantimonate, supplied from Sartomer [142]. The new formulation does not use the same solvent or the photo-acid generator as reported in reference [140]. The PAG used in reference [140] is not commercially available. A polymerisation initiator (PI), bis(4-tert-butylphenyl)iodonium triflate (DtBPIT), is used to replace the photo-acid generator. PI can produce reactive atoms used to polymerise vinyl chloride, methyl methacrylate and other monomers [143]. Thermally curable PVP ink has the exact substances for the PI to polymerise, as PMF is based on methacrylate solution and PVP is a vinyl based polymer material. The selected PI has a similar catalyst functional monomer group to the photo-acid generator. The selected PI can be dissolved in 1-hexanol easily. 1-hexanol has been shown to dissolve the PVP materials well and work well with the Dimatix inkjet printer previously (section 6.4.1.6). Therefore, 1-hexnaol is used to replace the PGMEA reported in reference [140].

The new UV curable PVP inkjet printable dielectric ink is prepared from a mixture of PVP and PMF solution in 1-hexanol with an additional polymerization initiator. PMF is used as the cross linking agent to polymerise the PVP monomers into a giant cross linked polymeric chain. The PI is used to catalyse the polymerization between PVP and PMF under UV exposure. The catalysing reaction is triggered by the UV source. PVP has 7 wt% of the mixture. The mixture ratio is 4:2:1 for PVP:PMF:PI. The UV curable PVP ink is cured for 100 seconds in a UV chamber at power density 31 mW/cm^2.

Following on from the previous work, this all inkjet printed flexible PVP smart fabric capacitor will be printed using SunChemical silver ink for the electrodes and the new UV curable PVP ink for the dielectric layer. The fabrication procedure will follow the same process as the previous section 6.4.1.

After the all inkjet printed smart fabric capacitor was made, both the printed silver and PVP layers exhibited good chemical resistance to commonly used solvents in printed electronics, for example, IPA (cleaning solvent) and ethanol (U5714 ink's solvent). In addition, depositing the UV curable PVP ink in a layer thickness of 2 to 4 μm did not change or damage the fabric interface layer observably. All three layers showed good smoothness across the effective area of the capacitor. The plan view image of the all inkjet printed fabric capacitor is shown in figure 68.

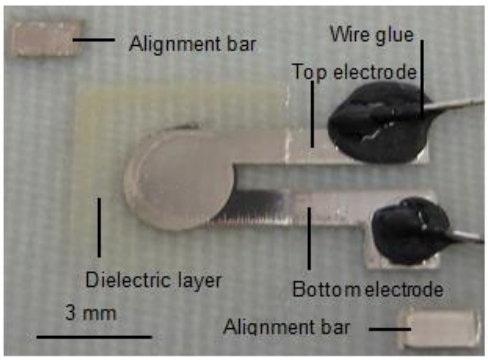

Figure 68. Plan view of the all inkjet printed capacitor; wires have been added using wire glue for further measurement.

The wire glue is used instead of the silver epoxy to connect the device for testing, because silver epoxy is expensive to purchase. However, this trial proved the wire glue did not give strong adhesion as silver epoxy to between wires and printed silver electrodes. The thicknesses of the three functional layers were measured using the SEM, as its cross sectional view micrograph is shown in figure 69.

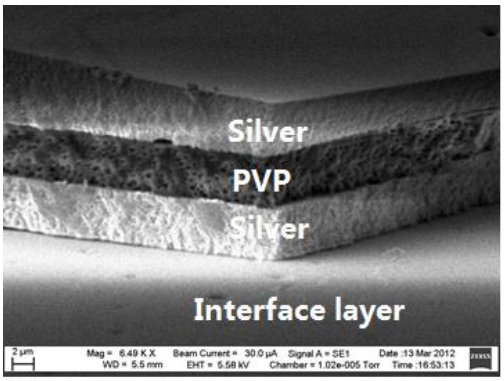

Figure 69. SEM cross sectional micrograph of an all-inkjet printed capacitor on fabric with U5714 silver ink and the developed UV curing PVP ink.

The UV cured PVP layer thickness is around 4.5 µm and the silver thickness is around 4.5 µm. Figure 70 shows that there is a random series of 100-300 nm diameter air bubbles in the PVP layer.

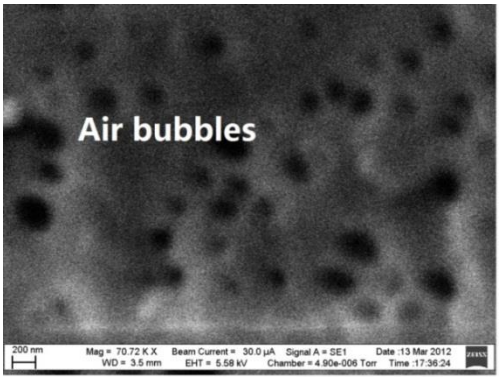

Figure 70. SEM cross sectional images of the printed PVP layer showing air bubbles with diameters in the order of hundreds of nanometres.

These bubbles are hypothesised to be a result of the curing process. The UV source triggers the chemical polymerisation reaction to cross link the PVP material in the ink. The PVP material is dissolved in the solvent. Sudden heat can be generated by cross linking reactions which will make the solvent evaporate in the printed PVP layer. Then the solvent evaporation rate is lower than the polymerisation reaction, which causes the air bubbles to become trapped in the solid PVP cured dielectric layer. This series of chemical and physical reactions occurring during the UV curing process can generate and trap the air bubbles in the cured dielectric PVP layer which will adversely affect the dielectric properties of the PVP layer.

6.4.1.8 Summary

One inkjet printed UV curable SU-8 dielectric layer thickness is typically around 15 µm thick for 2 deposits of silver ink per electrode. The UV curable dielectric inks can produce a thicker film compared to solvent based dielectric inks, which are typically around 2 µm thick. This is because solvent based solution evaporates the solvent at thermal curing stage resulting in a thin solid content. However, UV curable dielectric inks are cured at low temperatures whereas solvent based dielectric inks tend to require high curing temperatures, typically at or above 200 ^{o}C. A solvent based inkjet printable dielectric ink is therefore usually used for inkjet printed electronic devices where a thin dielectric layer is required. The UV curing ink is used in those applications which have less restriction on the thickness of the dielectric layer, for example, an insulation layer between two crossed conductive tracks to avoid potential electric field interference. Therefore, in this research a new inkjet printable solvent based PVP dielectric ink was developed which is UV curable. The new formulated dielectric ink was used to realise an all inkjet printed capacitor. Because of its low temperature processing properties, the all inkjet

printed smart fabric flexible capacitor with thin dielectric layer is realised for the first time on a fabric substrate.

6.4.2 Device testing

6.4.2.1 Inkjet printed SU-8 capacitor on Kapton

The capacitance of the device was measured using a Wayne Kerr 6500B precision impedance analyser. The measured value of the capacitance is 48.5 pF at 100 Hz, 48.3 pF at 1 kHz, 46.5 pF at 100 kHz and 43.6 pF at 1 MHz. The variation across the frequency range from 100 Hz to 5 MHz is shown in figure 71.

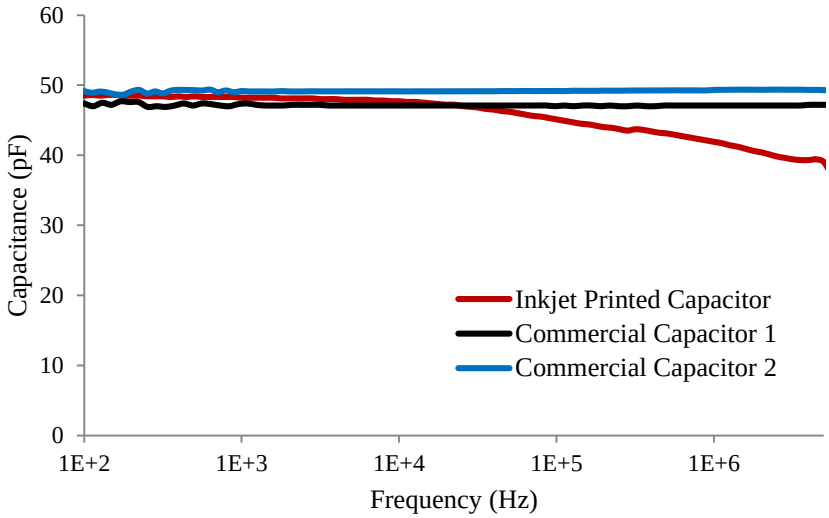

Figure 71. Capacitance as a function of frequency for the inkjet printed capacitor and two commercial 47 pF capacitors.

Assuming that the inkjet printed SU-8 layer has a relative permittivity of 4.2 [144] and the measured thickness of 15 µm, the theoretical capacitance based on equation 4 can be calculated as 48.59 pF. The measured capacitance value is very stable up to 10 kHz at around 48 pF with an capacitance per unit area of 2.4 pF/mm^2. The discrepancy is around 0.2 % compared to the actual measured capacitance value at 100 Hz, 0.6 % at 1 kHz, 4.3 % at 100 kHz and 10 % at 1 MHz shown in figure 71. Figure 71 also shows a comparison with two commercial single layer 47pF ceramic capacitors. Commercial capacitor 1 was supplied by NOVA Comp-Card System (Type CCC-31). Commercial capacitor 2 was supplied from Rapid Electronics (08-0054). The results show that up to 5 MHz there is no reduction in capacitance for the two commercial one layer ceramic capacitors. However, for the inkjet printed capacitor, the capacitance begins to

drop slightly after 10 kHz. The capacitance value of the inkjet printed capacitor reaches 40 pF at a frequency of 5 MHz, a reduction of around 15 %.

The capacitance value of the inkjet printed capacitor starts to decrease after 10 kHz. A high dielectric loss tangent of SU-8 means there is a large dielectric absorption causing a more pronounced deterioration of capacitance with frequency. The dielectric loss tangent is the ratio at any particular frequency between the real and imaginary parts of the impedance of a capacitor. Typically high dielectric loss tangent means more effect on the capacitance loss with increasing operating frequency; this is called the dielectric absorption. Equation 9 [145] shows the measured capacitance as a function of frequency.

$$C_f = C_0 \cdot (\frac{j \cdot f}{f_0})^k \tag{9}$$

Where

C_f is the capacitance as a function of frequency f in F,

C_0 is the capacitance at one particular frequency of f_0 in low frequency range in F,

j is the square root of minus one,

k is a negative constant that sets the rate of deterioration in capacitance per decade of frequency.

Referring to equation 5, the term of C_0 is the capacitance measured without any deterioration at low frequency. There are two terms extracted from the term $(\frac{j \cdot f}{f_0})^k$: the pure phase part j^k and the magnitude part $(\frac{f}{f_0})^k$. While the frequency increases, the term $(\frac{f}{f_0})^k$ decreases. The magnitude is determined by the dielectric loss tangent which decreases proportionally as the frequency increases. Figure 72 compares the impedance change between the three devices. The graph shows that there is good correlation between the three measured results.

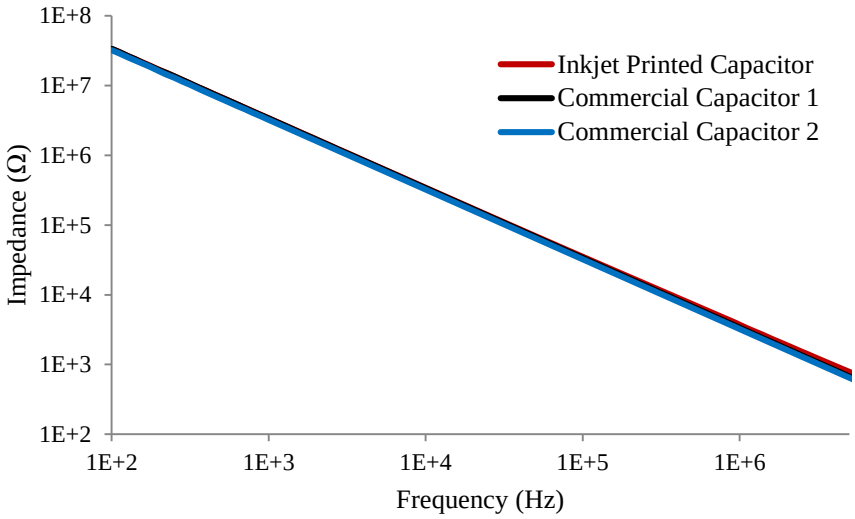

Figure 72. Impedance as a function of frequency for the inkjet printed capacitor and two commercial 47 pF capacitors.

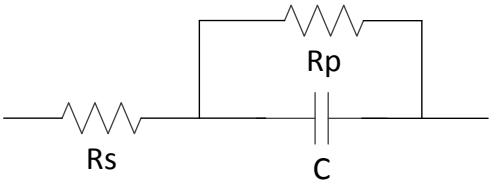

Figure 73 shows the equivalent circuit of a capacitor with an internal parallel resistor and an internal series resistor.

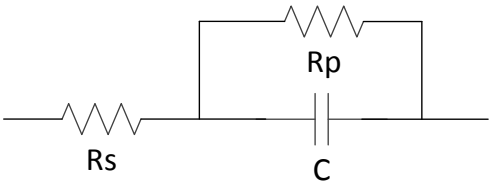

Figure 73. The equivalent circuit of a capacitor with a parallel resistor and a series resistor.

The total impedance equation is derived from equation 10 and equation 11 to equation 12.

$$Z = R_s + Z_{R_p+C} \tag{10}$$

$$Z_{R_p+C} = \frac{R_p}{R_p \omega c + 1} \tag{11}$$

$$Z = R_s + \frac{R_p}{R_p \omega c + 1} \tag{12}$$

Where

Z is the total impedance of the whole equivalent capacitor circuit in Ω,

R_s is the internal series resistance in the equivalent capacitor circuit in Ω,

$Z_{equivalent\ parallel}$ is the internal parallel circuit impedance including capacitance and internal parallel resistance in Ω.

R_p is the internal parallel resistance in Ω,

ω is the natural frequency, 2πf in Hz,

c is the capacitance in F.

Equation (12) can be re-arranged into the relationship in the equation 13.

$$\log Z \propto -\log f \tag{13}$$

Therefore, the $\log Z$ is linearly proportional to the $-\log f$ as shown in the previous Figure 72.

An ideal capacitor has infinite parallel and zero series resistance. In practice, capacitors have imperfections which create equivalent parallel and series resistances. A finite parallel resistance occurs as a result of the conductivity of the dielectric. Therefore, a small leakage current flows between the two electrodes. Ultimately, the capacitor will be discharged by the parallel resistance with a discharge time controlled by its value. The internal parallel resistance only becomes significant when the frequency approaches 0 and then the capacitive part of the impedance approaches infinity which results an equivalent circuit of the internal resistor and the internal parallel resistance in series. The measurement can be done by applying a small load in series to the printed capacitor. The measurement of the total resistance including the internal and parallel resistance needs to be taken at very low frequency. The equivalent circuit is shown in Figure 74.

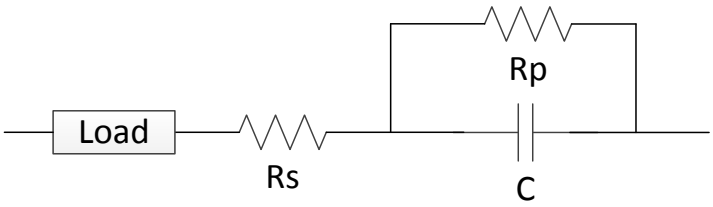

Figure 74. A small load in series to the printed capacitor to measure the R_s + R_p values in series at low frequency to disable the capacitor as an open circuit.

As the load in series to the printed capacitor results from the analyser, it is very small compared to the internal parallel capacitance. Therefore, the series load value is ignored in this measurement. However, such equipment covering low frequency is not available in this

research group. Figure 75 shows a Rs+Rp resistance measurement as a function of frequency for the inkjet printed and two commercial capacitors.

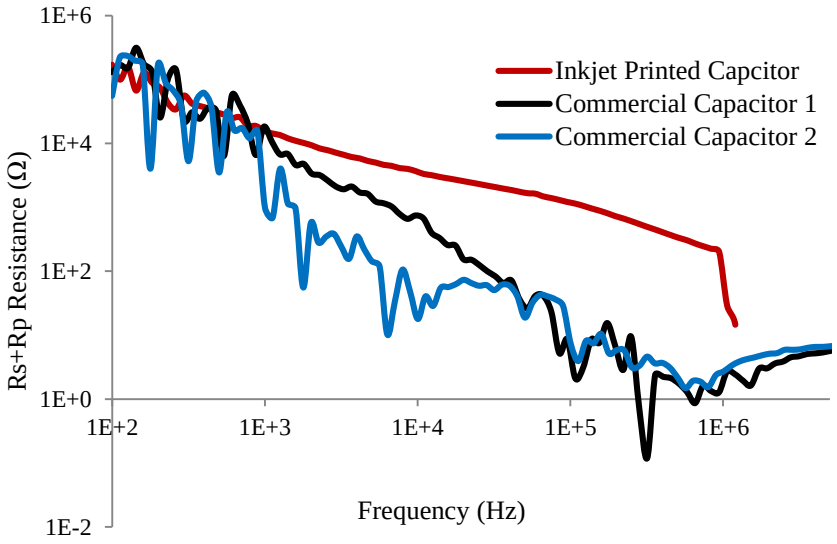

Figure 75. Rs + Rp resistance measurement as a function of frequency for the Inkjet printed capacitor and two commercial 47 pF capacitors.

It can be seen that total resistance is at 10^5 Ω at 100 Hz. Estimation of Rs+Rp, when the frequency approaches 0, can be made by extrapolating the experimental results to cut the y axis at a frequency of 0 Hz. This estimates the total resistance Rs+Rp in the order of 10^7 Ω. The equivalent internal series resistance is determined by the resistance of the electrodes and the loss tangent of the dielectric. The series resistance only becomes significant when the frequency approaches infinity and the capacitive part of the impedance approaches zero which results an equivalent circuit of a single internal series resistor. The internal series resistance is low resistance compared to the internal parallel resistance. Therefore the small load in the circuit will become significant in Figure 74 under these conditions. Therefore the measurement method has been adapted to connect a large load in parallel to the printed capacitor as shown in Figure 76.

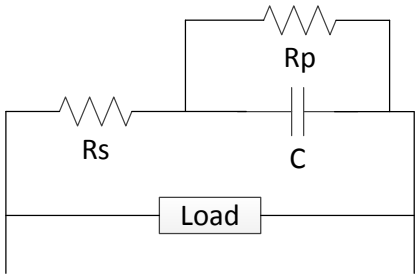

Figure 76. A large load in parallel to the printed capacitor to measure the R_s values at very high frequency to pass out the capacitor as a closed circuit to avoid R_p.

The measurement can be done at very high frequency to effectively short circuit the capacitor. This results in the resistance of the Rs in parallel to the large load. As the load connected to the printed capacitor is very large, it is effectively an open circuit. In addition, equation 14 shows that, when the load approaches infinity, the total resistance approaches Rs.

$$R_{total} = \frac{R_s R_L}{R_s + R_L} \tag{14}$$

However, such equipment covering sufficiently high frequencies is not available in this research group. Figure 77 shows the Rs resistance measurement as a function of frequency for the inkjet printed capacitor and two commercial capacitors in the frequency range of 100 Hz to 10 MHz.

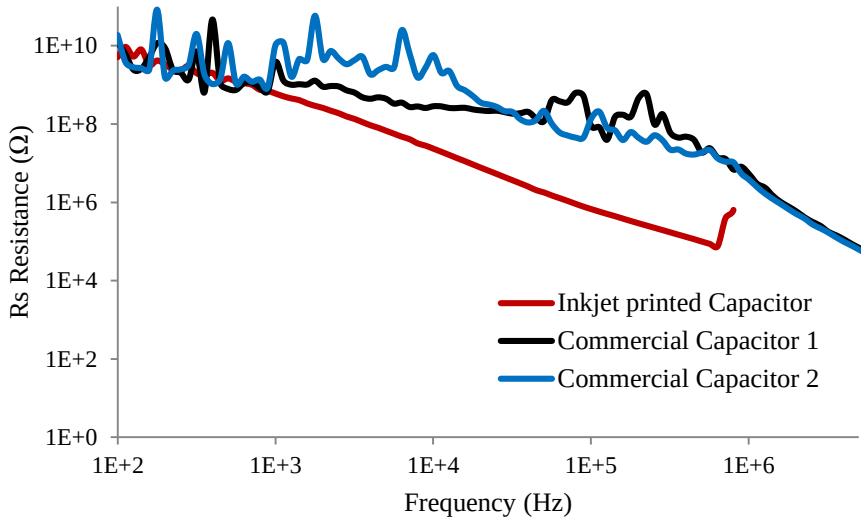

Figure 77. Rs resistance measurement as a function of frequency for the inkjet printed capacitor and two commercial 47 pF capacitors.

It can be seen that the internal series capacitance cannot be obtained as the frequency can only reach 10 MHz. In addition, at 700 KHz, a polymer dielectric breakdown may have happened, indicated by the sharp transition at the high frequency end of the plot.

6.4.2.2 Inkjet printed PVP capacitor on fabric

Two inkjet printed fabric PVP capacitors and a commercial 150 pF capacitor were evaluated using a Wayne Kerr 6500B precision impedance analyser. The black line in figure 78 is the

commercial 150 pF capacitor. The capacitance of the printed samples varies from 163 pF at 100 Hz to 113 pF at 9 MHz with a reduction of around 29 % as shown in figure 78.

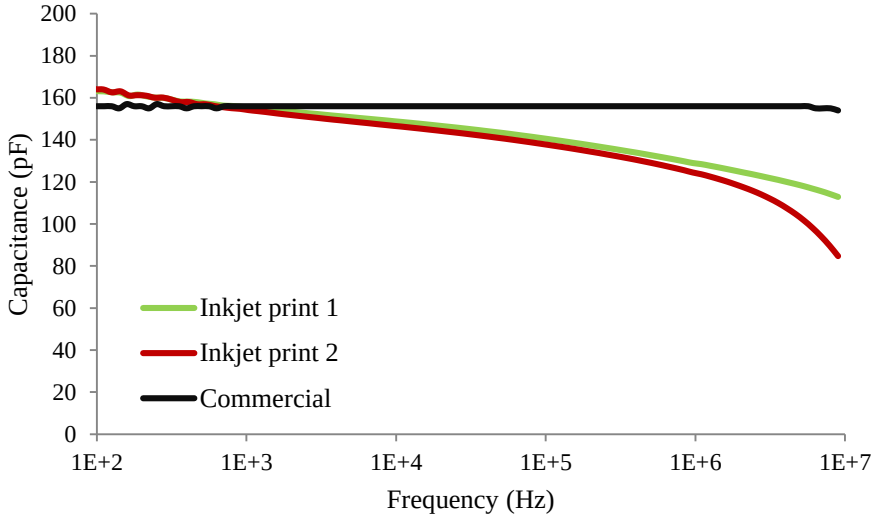

Figure 78. Capacitance as a function of frequency for the two inkjet printed capacitors and one commercial 150 pF capacitors.

The capacitance per unit area can be calculated as 23.1 pF/mm^2 at a 100 Hz. The capacitance per unit area is ten times higher than the all inkjet printed SU-8 capacitor reported 2.4 pF/mm^2 in the section 6.4.2.1. The printed PVP fabric capacitor's capacitance values start to decrease steadily at the beginning of the frequency sweep. This may be caused by the high dielectric loss tangent, which means there is a large dielectric absorption causing a more pronounced deterioration of capacitance with increasing frequency, as defined by equation 5. The capacitor area is 7.07 mm^2 based on the designed diameter of 3 mm. The measured thickness of the cross linked PVP dielectric layer is 4.5 μm, as shown in figure 69. Therefore the relative permittivity of inkjet printed PVP layer is 11.7 based on equation 4. This almost doubles the highest previously reported solution processed PVP relative permittivity of 6.4 [10]. This high relative permittivity value may be caused by the additives added into the PVP formulation, for example, cross linking agent and polymerisation initiator. For the commercial 150 pF ceramic capacitor (TruCap 150P50V10%), there is no reduction in capacitance up to a frequency of 9 MHz. Figure 79 compares the impedance change with increasing frequency of the three devices. The results show that there is good correlation between the three measured results.

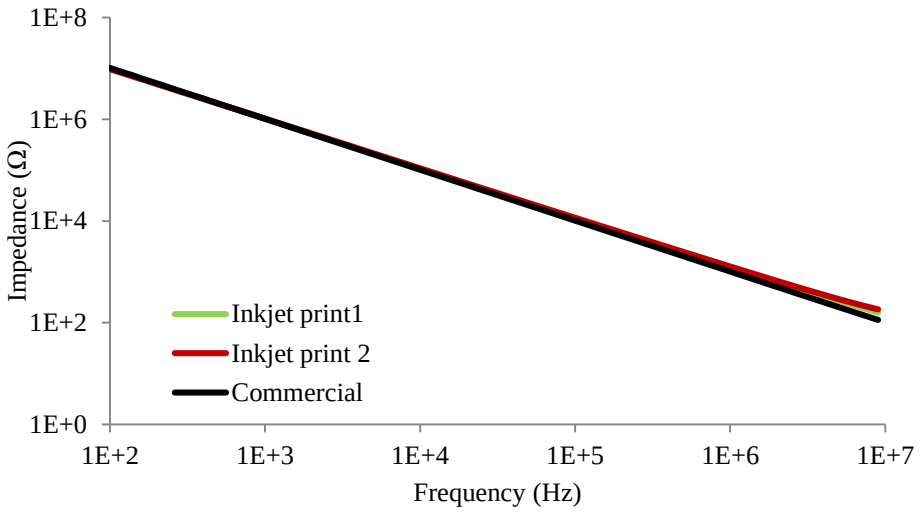

Figure 79. Impedance as a function of frequency for the two inkjet printed capacitors and one commercial 150 pF capacitors.Figure 80 shows the Rs + Rp resistance measurement over the same frequency range, which ideally should be performed at low frequency

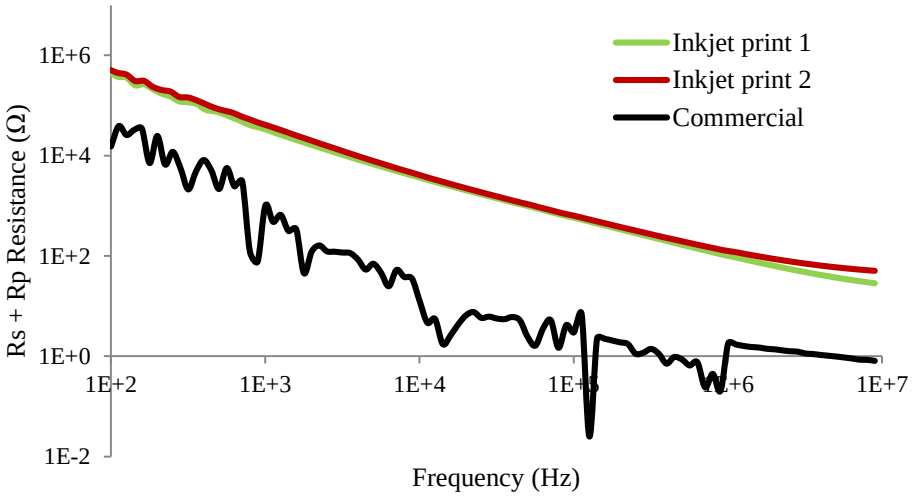

Figure 80. Rs + Rp resistance measurement as a function of frequency for the two inkjet printed capacitors and one commercial 150 pF capacitors.

The two inkjet printed capacitors' Rs + Rp resistances are very similar whilst the commercial capacitor's series resistance is around 1 to 2 orders of magnitude lower. However, the three measured results follow the same trend, with the resistance of the commercial capacitor decreasing at a slightly higher rate as the frequency increases. It can be seen the two printed capacitor plots tend to have 10^7 Ω resistance due to the plots gradient. The printed capacitor has a higher internal parallel capacitance than the commercial one.

Error! Reference source not found. shows the change in Rs resistance measurement as a function of frequency for the same three capacitors towards high frequency to pass out the capacitor as the close circuit.

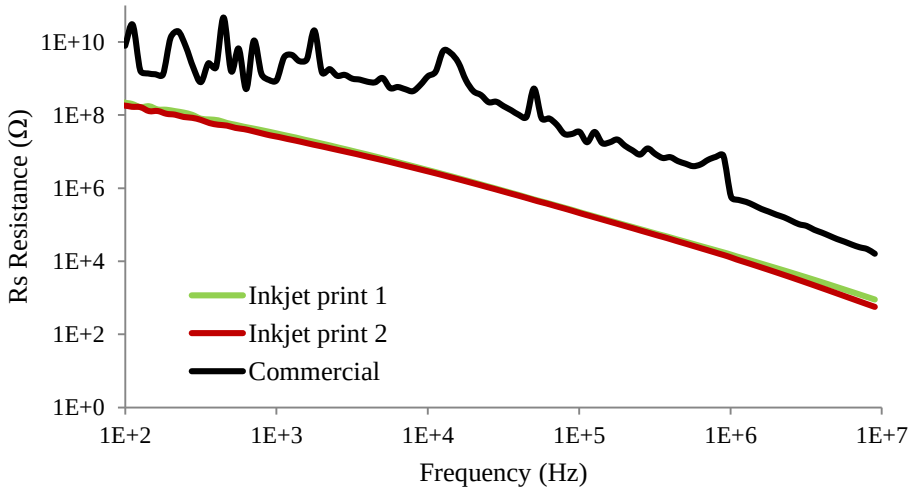

Figure 81. Rs resistance measurement as a function of frequency for the two inkjet printed capacitors and one commercial 150 pF capacitors.

The two inkjet printed capacitors' series resistance values are very similar, while that of the commercial capacitor is around 1 to 2 orders of magnitude higher. However, the three results show the same general trend. It shows the printed capacitor has a lower internal series resistance than the commercial one.

6.5 Pneumatic dispenser printed capacitor

6.5.1 Theory of volumetric flow rate of pneumatic dispenser

The viscosity of the ink has the most significant effect on the printability of an ink. The flow rate (m^3/s) of an ink through a needle is approximated by measuring the volume of ink (m^3) extruded from the syringe for a given dispensing time (s).The equation 15 [146]:

$$\int_0^R V_z r 2\pi dr = \left[\frac{\left(P_{top} - P_{bottom}\right)}{L} + \rho g\right]\left(\frac{\pi R^4}{8\mu}\right) = Flow\ rate \tag{15}$$

Where

V_z is the velocity in m/s;

$P_{top} - P_{bottom}$ is the pressure applied to the ink P_{Δ} in Pa;

L is the needle length in m;

ρ is the density of the ink in kg/m^3;

g is the gravitational force in m/s^2;

π is the mathematical constant, 3.1415927;

R is the inner diameter of the dispensing needle in m;

μ is the viscosity of the dispensing liquid in Pa s;

Flow rate is measured in m^3/s.

The Matlab simulated results are based on equation 6 in the function of two variables of liquid density and viscosity. Figure 82 shows the relationship between the volumetric flow rate, the liquid viscosity and density changes under the same 20 kPa pressure and a 2.54 cm needle length with a 100 μm inner diameter. 20 kPa is the minimum pressure input the pneumatic dispenser used in this work can be set. 2.54 cm needle length is the standard one inch needle with 100 μm inner diameter size.

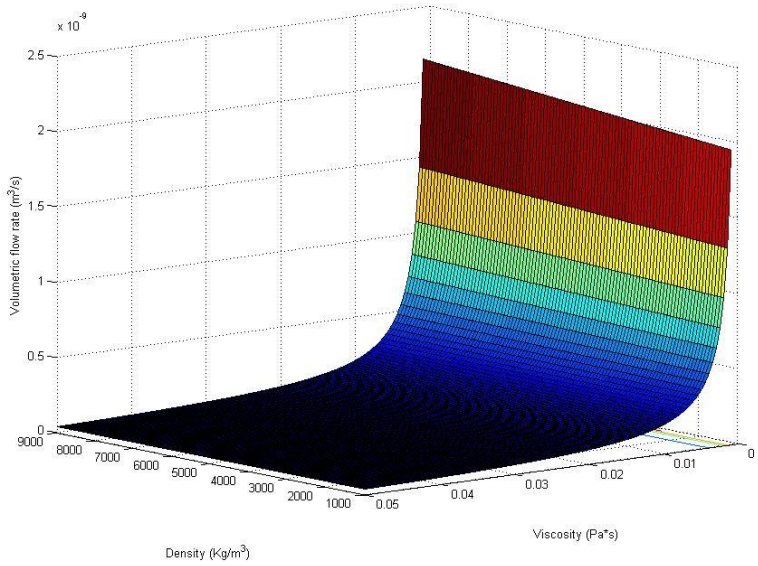

Figure 82. Volumetric flow rate against liquid viscosity and density changes using 20 kPa pressure with a 100 inner diameter 2.54 cm needle length.

Figure 82 shows there is a minimal change in the flow rate as the liquid density changes. The liquid density variable can consequently be neglected, as a variation will affect the flow rate minimally compared to the other variables. Figure 83 shows the volumetric flow rate against the liquid viscosity under the same pressure of 20 kPa and a 2.54 cm needle with inner diameter of 100 μm with liquid density changes ignored.

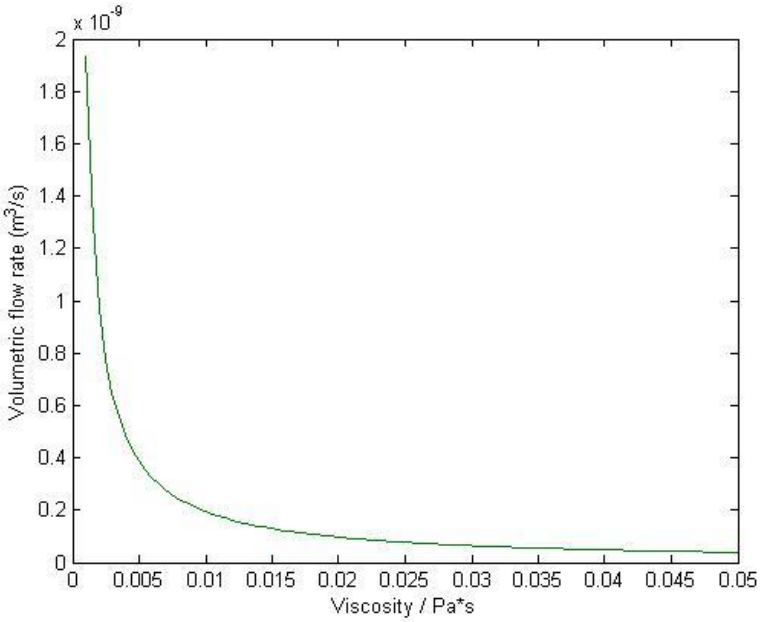

Figure 83. Volumetric flow rate against the liquid viscosity under the same 20 kPa pressure with a 100 inner diameter 2.54 cm needle length condition.

For example, at a 20 kPa dispensing pressure with a 2.54 cm needle with a 100 μm inner diameter and an ink with viscosity 11 mPa s, the flow rate is 175.68 pL/s. 11 mPa s is selected because this value is in the ideal viscosity range of an ideal inkjet printable ink. The dispenser controller dispenses highly precise drops of liquid, about 1 pL in 5.7 ms, under the same dispensing conditions stated above. However, the minimum dispensing time is limited to 10 ms by the dispenser controller, so the minimum dispensable volume of an ideal inkjet printable ink is about 1.76 pL under the above stated conditions and printing parameter.

The volumetric flow rate has been studied in this section. Assuming the dispensing nozzle inner diameter is fixed for the selected application, a long dispensing needle can be used to reduce the volumetric flow rate for a low viscosity liquid, for example with inkjet printable inks. A short dispensing needle or tapered nozzle can be used to increase the volumetric flow for a highly viscous liquid, for example a screen printable paste.

6.5.2 Fabrication

6.5.2.1 Dispenser printing operating procedure

Pneumatic dispenser has a simple operating principle and a very wide range of acceptable liquid rheological properties, there are fewer precautions to take while dispensing compared to inkjet printing, for example, adjusting the dispensing gap from the substrate and dispensing

resolution. Pneumatic dispenser printing has much wider tolerance in printing the inks in volume, for example, various commercially available syringes sizes. The dispensing nozzles are more robust and much lower cost compared to the inkjet printing nozzles. In this section, the operational procedure of using pneumatic dispensing is briefly introduced as this is a customised system. The designed pattern, loaded into the bespoke Labview control software, is digitised into a pixel array. The array is evenly divided by the printing resolution which is equivalent to the drop spacing used by the inkjet printer. The operational procedure is quite similar to that of an inkjet printer:

1) Load the liquid barrel with electronic functional ink.
2) Degas it under vacuum before loading the barrel into the dispenser.
3) Load the barrel into the dispenser.
4) Set the vacuum level on the dispenser to hold the liquid meniscus point at the dispenser needle (or nozzle) tip.
5) Set the dispensing time and pressure.
6) Load the bitmap image of the design into the system.

Creating a suitable bitmap image is the key stage for this custom pneumatic dispenser, because the program can only analyse an 8-bit depth image and resolution changes will cause the pattern to change in the final printed sample.

The pneumatic dispenser operates based on an air pulse generated by the controller to push the liquid out of the barrel through the tip (or nozzle). Therefore the whole system can be very robust. The printing process can be interrupted if the vacuum is set too high for a very low viscosity liquid, causing reflux from the barrel. This can be avoided by installing a liquid filter to prevent reflux.

6.5.2.2 Dispenser printed capacitor fabrication process

The fabrication procedure is similar to the inkjet printed capacitor and is shown in figure 55. The main difference is to replace the deposition of inkjet printed layers by pneumatic dispenser printed layers. The first step is to choose the substrate to inkjet print on. The surface is then wiped with lint free cleanroom tissues dipped in DI water. The next step is to pneumatic dispenser print one conductive silver layer on to the substrate to form the lower electrode. The conductive pattern is then cured for 10 minutes at 150 ^{o}C. The UV curing dielectric inks are

then printed on top of the lower electrode in the designed dielectric pattern. One dielectric layer is deposited per device. Because it is contact dispensing mode in droplet format, there is not any pin holes in the film. Gaps between each two pixels are dragged through which results no pin holes. The top electrode is then dispenser printed and cured to complete the capacitor structure. The fabrication flow diagram is shown in figure 84 based on the pneumatic dispenser printed capacitor on Kapton film.

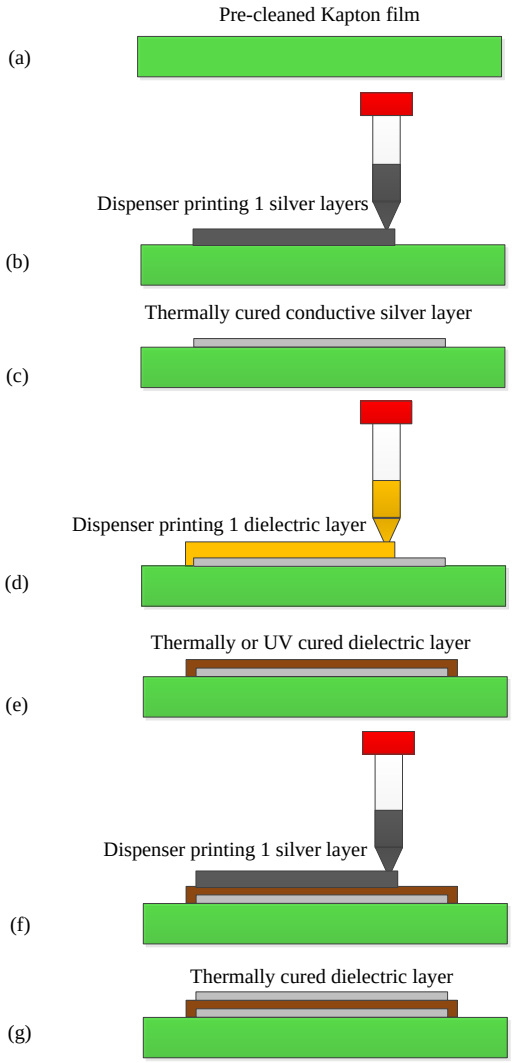

Figure 84. A cross sectional view flow diagram showing the fabrication of dispenser printed parallel plate capacitor fabrication process.

6.5.2.3 Dispenser printable materials, printing trials and capacitor fabrication

This section summarises the initial dispenser printing trials with four materials. First two screen printable pastes, as shown below, were selected not for their electrical functions, as these printing trials were to test the dispenser capability to print the standard screen printable pastes.

(1) Screen printable sacrificial paste, Fabink-SF-11 supplied from Fabinks.
(2) Screen printable structural paste, Fabink-IF-UV1 supplied from Fabinks.

The two inkjet printable inks were selected to further dispenser print the flexible SU-8 capacitor on Kapton to compare the results with the inkjet printed SU-8 capacitor in section 6.4.2.1.

(1) Inkjet printable SunChemical silver ink, U5714 supplied from SunChemical.
(2) Inkjet printable SU-8 ink, PriElex V005 supplied from MicroChem.

There are two parameters, time and pressure, which can be balanced to dispense the same amount of liquid in different combinations. There are two typical combinations summarised based on practical work and equation 6:

(1) Higher pressure and a shorter dispensing time are used for low viscosity liquids.
(2) Lower pressure and a longer dispensing time are used to perform contact mode dot and line extruded direct write printing.

Inkjet printable inks can be potentially jetted as droplets in a similar fashion to inkjet printing. The droplet's kinetic energy plus the force of gravity needs to be sufficient to break the surface tension of the liquid at the needle tip. The resultant droplet volume will spread after landing causing the area covered by a droplet to be significantly larger than the in-flight droplet diameter. The printing resolution can be limited so as to achieve small pixels (droplet landing area) and hence limit the printed line width. More importantly, only low viscosity liquids equivalent to inkjet printable inks can be jetted with pneumatic dispensing as the shear rate is a limiting factor for highly viscous liquids.

With pneumatic dispensing, material is dispensed through the needle tip which is placed very close to the substrate, typically 200 μm. As the needle is moving, the dispensed liquid adheres to the substrate due to surface energy, stiction and gravity. The optimum line width written by needle dispensing is 2.5 times the inner diameter of the needle [147]. Preliminary dispenser printing trials are tested in only in droplet based dispensing mode. The dispenser parameter

settings are: 20 KPa dispenser pressure, 0.01 s dispenser time, 50 μm inner diameter size nozzle is selected to test the dispenser printing capability of printing fine features. Figure 85 shows a Fabink-IF-UV1 dot dispensed with 50 μm inner diameter nozzle.

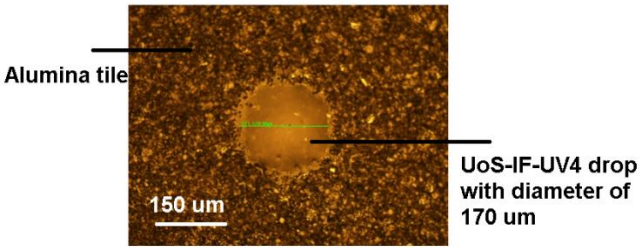

Figure 85. Plan view of a dispenser printed 170 um diameter dot by a 50 μm inner diameter nozzle.

The diameter of the dispensed dot is about 170 μm. The theoretical optimum minimum value is 125 μm as this is 2.5 times of the inner diameter. Figure 86 shows a Fabink-IF-UV1 line dispensed with a 50 μm inner diameter nozzle with a line width of about 210 μm.

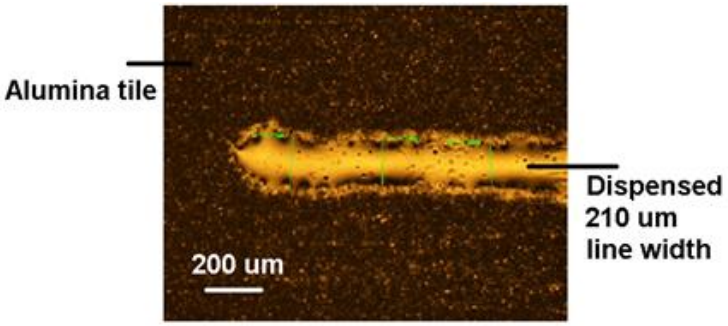

Figure 86. Plan view of a line dispensed with 50 um inner diameter nozzle with a 210 um line width feature.

In this initial test of the dispenser printing process, line widths three and four times the size of the nozzle's inner diameter have been achieved. Further work could decrease the line width with the same needle feature by adjusting the dispenser nozzle moving speed and dispensing gap to avoid the ink spreading. In addition, an increased the substrate temperature can also expect a finer line width, because heated substrate can stop the paste spreading.

A free standing cantilever structured pattern was selected to be dispensed with the two screen printing pastes: Fabink-IF-UV1 and Fabink-SF-11 as the structural and the sacrificial paste respectively. The dispenser parameter settings are: 200 KPa dispenser pressure, 0.02 s dispenser time and a 25 gauge tapered dispensing nozzle with 250 μm inner diameter size. Figure 87 shows a pneumatic dispensed free standing cantilever structure before sacrificial

layer removal. This printing trial has proved that screen printable pastes can be used with a dispenser printing technique.

Figure 87. Pneumatic dispensed free standing cantilever structured pattern.

All inkjet printable inks used in this work use the same dispenser printing parameter settings. The dispenser pressure is set to the minimum value of Musashi ML-808FXcom-CE dispenser, 20 kPa. The dispensing time for each shot is set to the minimum time length of 0.01 s. The 100 µm needle inner diameter is selected; the longer the needle the lower the dispensed droplet volume as per equation 6. The dispensing gap between the nozzle and substrate is around 200 µm to avoid droplet spreading caused by excessive impact force on the Kapton substrate. Figure 88 shows capacitors' bottom electrodes being dispenser printed.

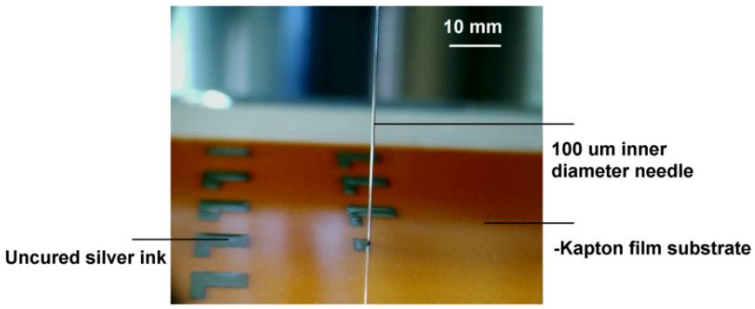

Figure 88. An image of capacitors' bottom electrodes being dispenser printed.

After dispenser printing trials, a parallel plate capacitor was built by dispenser with the same inkjet printable inks used for the inkjet printable SU-8 capacitor in section 6.4.2.1. Figure 89 shows the dispenser patterned the lower electrode with SunChemical inkjet printable U5714 silver ink. Figure 89 shows pneumatic dispensed capacitors being fabricated, before the upper electrode is added and after the SU-8 layer has been UV cured.

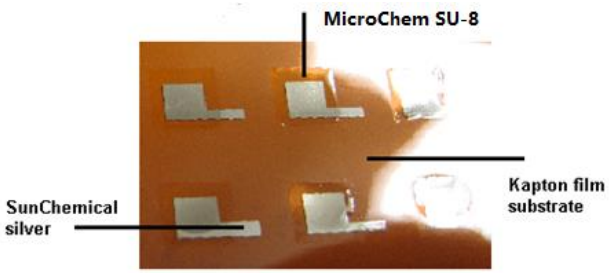

Figure 89. Isometric view of pneumatic dispenser printed capacitor two layers including bottom electrode and dielectric layers.

An entirely dispenser printed flexible capacitor was constructed by two functional inkjet printable inks: SunChemical U5714 and MicroChem PriElex V005 SU-8. Consequently, the curing conditions are the same as the inkjet printed flexible SU-8 capacitor on Kapton. Figure 90 shows a plan view of capacitors printed with the pneumatic dispenser on a Kapton substrate, two of which have been connected with wires using silver epoxy for further electronic performance testing.

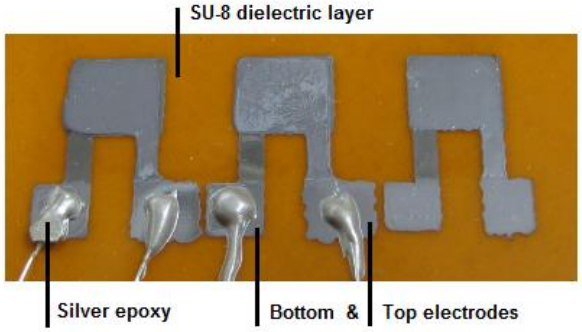

Figure 90. Plan view of pneumatic dispenser printed capacitors on Kapton substrate with silver epoxied wires for testing.

6.5.3 Device testing

6.5.3.1 Pneumatic dispenser printed SU-8 capacitor

The dispenser printed capacitor is designed to have an effective capacitance area of 36 mm^2. The average thickness of the dispenser printed SU-8 is 9 μm. Using equation 4, the theoretical capacitance is calculated to be 35.4 pF. The measured capacitance is around 45 pF with capacitance per unit area 1.25 pF/mm^2. The capacitance difference between the theoretical calculated value and the measured value can be caused by the uneven dispenser printed dielectric layer, because a thin area in the capacitance could increase the capacitance significantly. The three measured capacitance values are close to the capacitance of the inkjet printed SU-8 capacitor. Therefore, the values are compared here with the inkjet printed SU-8

capacitor. Three capacitors were fabricated by dispenser printing and their capacitance measurement results are shown in figure 91.

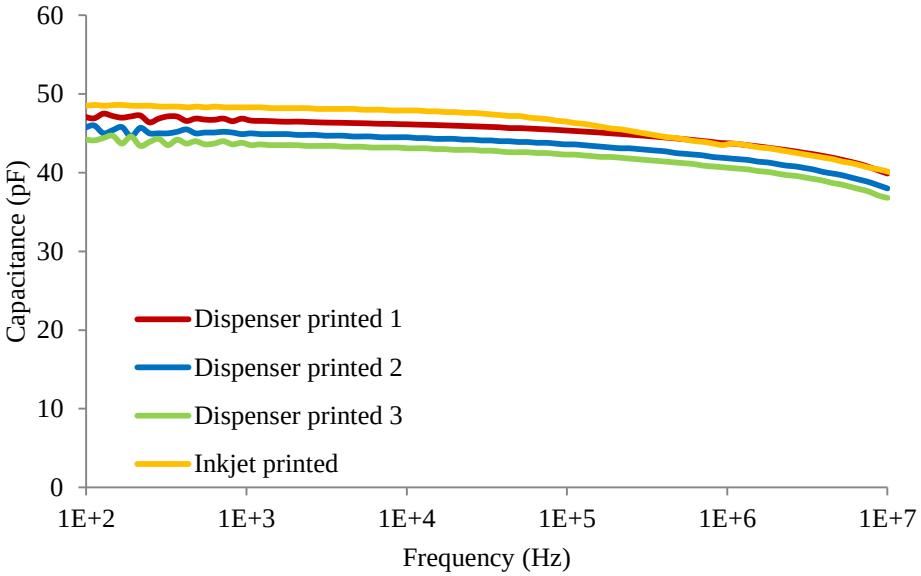

Figure 91. Capacitance as a function of frequency for the three dispenser printed and one inkjet printed SU-8 capacitors.

The dispenser printed capacitor shows a decreasing capacitance slightly as frequency increases up to 10 MHz compared to the inkjet printed SU-8 capacitor. The deterioration of capacitance can be explained by the dielectric loss tangent as discussed in section 6.4.2.1. Figure 92 compares the impedance change between the three devices and the inkjet printed SU-8 capacitor.

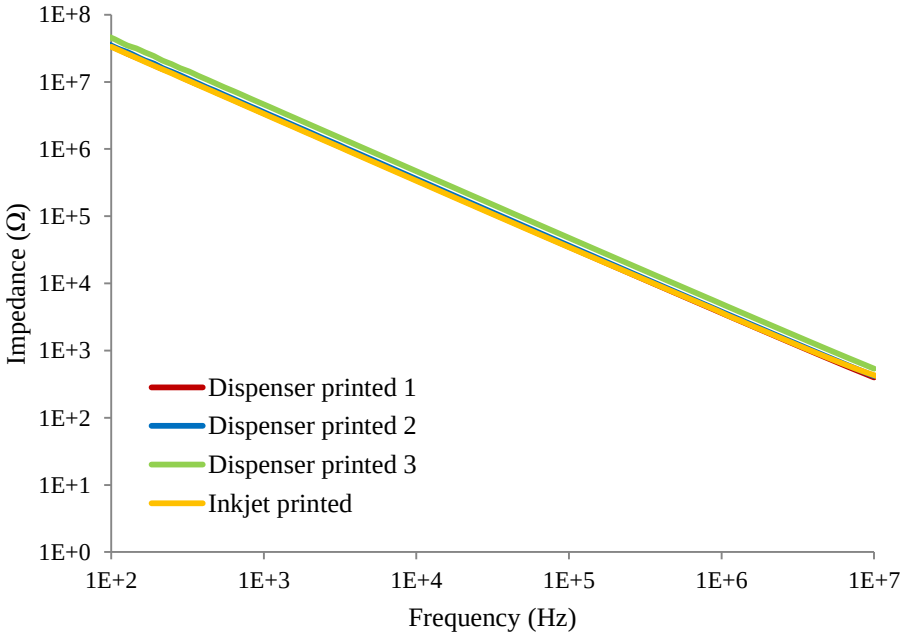

Figure 92. Impedance as a function of frequency for the three dispenser printed and one inkjet printed SU-8 capacitors.

The results show that there is good correlation between the three dispenser printed and one inkjet printed capacitors.

Error! Reference source not found. compares the Rs + Rp resistance measurement towards low frequency between the three devices and the inkjet printed SU-8 capacitor. The results also show that there is good correlation between the four capacitors measured results down to 100 Hz.

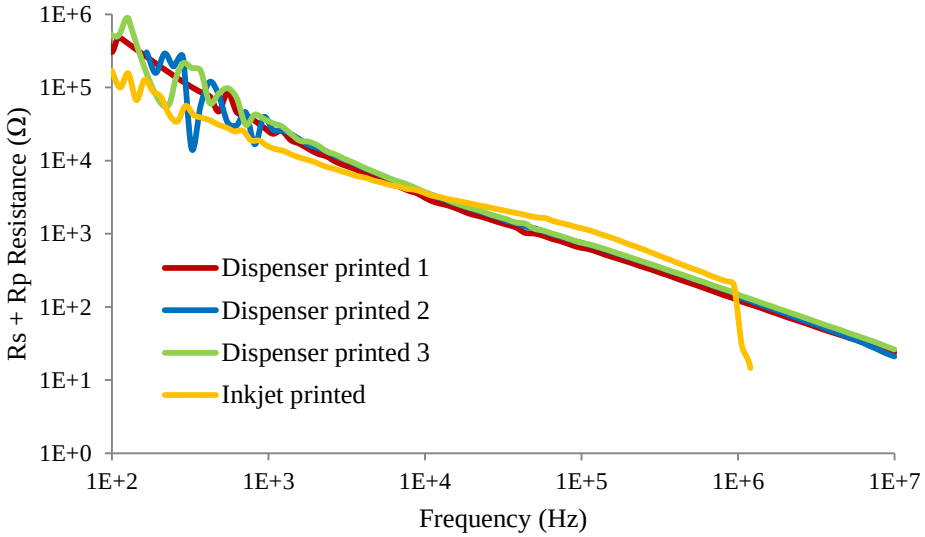

Figure 93. Rs + Rp resistance measurement as a function of frequency the three dispenser printed and one inkjet printed SU-8 capacitors.

Figure 94 compares the Rs resistance measurement between the three dispenser printed and one inkjet printed SU-8 capacitors towards high frequency.

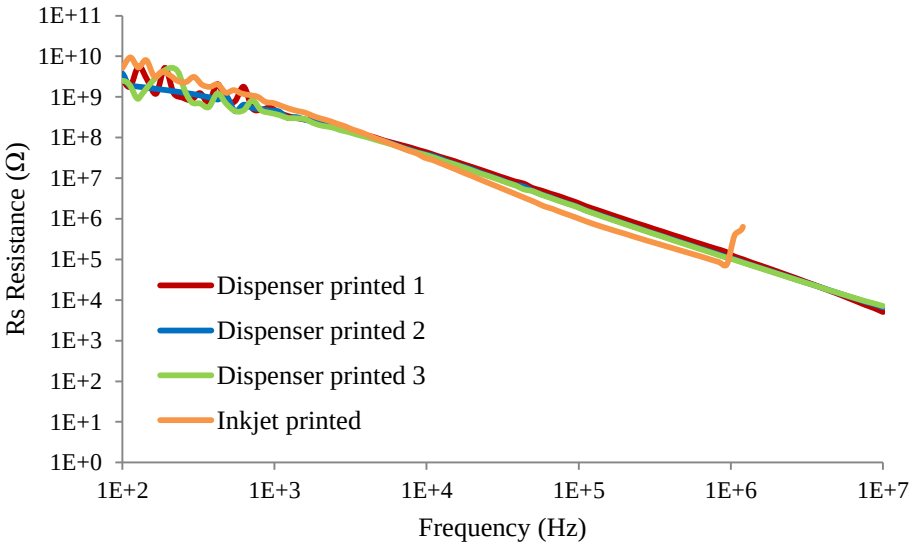

Figure 94. Rs resistance measurement as a function of frequency for the three dispenser printed and one inkjet printed SU-8 capacitors.

The results show that there is good correlation in the internal series resistance measurement between the three dispenser printed and one inkjet printed capacitors measured results until 1MHz.

A parallel plate flexible capacitor was entirely fabricated using pneumatic dispenser printing. The functional materials used here are the same as those used in the all inkjet printed SU-8 capacitor as described in section 6.4. The fabrication process of the dispenser printed capacitor is also the same as the inkjet printed capacitor fabrication process. There is good correlation in electronic performance between the three dispenser printed capacitors and the inkjet printed SU-8 capacitor. This experiment has proved the feasibility of inkjet printable inks deposited with dispenser printing. The results show that the capacitance, impedance, serial and parallel resistance values are highly comparable to the inkjet printed SU-8 capacitor.

6.6 Comparison between pneumatic dispenser and inkjet printing

For inkjet printing, the acceptable materials range is very strictly limited, especially as regards viscosity, surface tension, particle size and solid content. Most of the organic electronically functional materials can be dissolved into organic solvents to form inkjet printable inks, whereas some other inkjet printable inks are based on nanoparticle dispersions or dissolved precursors to the functional materials. Viscosity, surface tension, evaporation rate and stable suspension can be key barriers that prevent the ink from jetting properly. In addition, the

solvent content of inkjet printable ink is typically over 85 % resulting in thin film disposition, which is good for most of the thin film based applications, for example, inkjet printed transistor. However, inkjet printing a thick functional layer over 5 μm poses a significant challenge except for UV curable dielectric ink, for example, inkjet printable acrylate can easily build up thicker layer up to 15 μm thick based on two inkjet printed deposits of UV curable ink. Inkjet printable UV inks are good for applications which need thick layer.

However, pneumatic dispensing benefits from all the advantages of the inkjet printing technique, as it is additive, maskless and a rapid prototyping technique. These advantages have been defined in chapter 2. While at the same time, due to its operating principles, it imposes no strict limitations on the physical or chemical properties of the printed material compared to the inkjet printable ink selections. Pneumatic dispenser printing also benefits from various printing nozzle sizes and shapes to form various thicknesses, shapes and fine feature sizes. In addition, inkjet printing is difficult to achieve on non-flat surfaces. In inkjet printing, the droplets have to be fired vertically down to the substrate due to the gravitational force. With pneumatic dispenser printing, the nozzle is moved to where the desired pattern is. The deposition angels can vary depend on applications, for example, rotary dispensing.. Therefore, pneumatic dispenser can pattern on any uneven 3D arbitrary surface with a pre-programmed route; for example, rotary dispensing, dispensing pattern inside a box and dispensing active materials vertically.

6.7 Conclusions

Three direct write printed flexible capacitors have been achieved for the first time using different printing materials and processes. The first flexible capacitor has been achieved using only inkjet printing on Kapton as an initial test sample with the conventional subtractive microfabrication material of SU-8. The measured capacitance was 48.5 pF at 100 Hz which compares favourably to the theoretical calculated capacitance of 48.59 pF. In addition, a new inkjet printable UV curable PVP ink has been developed for low temperature processing. Then the first all inkjet printed capacitor on fabric has been made by replacing the SU-8 dielectric with this new UV curable dielectric PVP ink. The calculated relative permittivity of the printed PVP layer reaches 11.7 which doubles the highest value previously reported. The first all inkjet printed fabric capacitor has a capacitance per unit area of 23.1 pF/mm^2, which is 10 times that

of the all inkjet printed SU-8 capacitor at 2.4 pF/mm^2. In addition, the flexibility of the printed capacitor increases significantly as the thickness decreases and the PVP layer (4.5 μm) has greater flexibility than SU-8 (15 μm).

A bespoke pneumatic dispenser printer was used to fabricate a parallel plate capacitor to prove the capability of pneumatic dispensing in patterning inkjet printable and screen printable materials. The practical work performed in this chapter has increased the knowledge and experience of how to customise inkjet printable solvent based inks for use with the interface coated fabric (IF fabric). The new inkjet printable PVP dielectric ink will be used as the insulator layer material for the proposed inkjet printed transistor in the final development stage. The results show that it is possible to inkjet and pneumatic dispenser print thin (2 μm) and thick (>15 μm) dielectric layers on IF fabric for direct write printed smart fabric applications.

Chapter 7

7 Inkjet printed transistor suitable for fabric applications

7.1 Introduction

This chapter discusses the use of an inkjet printable active semiconductor ink suitable for fabricating an inkjet printed transistor on fabric. Organic semiconductor materials are being developed to facilitate the inkjet printing of transistors. In this chapter the active materials and substrates used in this research are introduced, followed by the fabrication and device testing. The performance of the inkjet printed transistors will be evaluated and discussed.

The semiconductor ink used in this research is based on amorphous polymer polytriarylamines (PTAA). The transistors are inkjet printed on to silicon wafer with a silicon dioxide layer. Infrared spectroscopic analysis is used to study the failure mechanism of the printed semiconductor layer. This inkjet printed transistor work is a collaboration between the University of Southampton and Sichuan University. All the fabrication work including active ink formulation and transistor characteristic measurements were done by the author at the University of Southampton. Sichuan University performed the infrared spectroscopic analysis of the inkjet printed PTAA layer.

7.2 Theory, design and architecture selection of printed transistors

This section introduces the two most widely used transistor types: bipolar junction transistor (BJT) and the field effect transistor (FET). The BJT subsection starts with an introduction of BJT structure, followed by the relationship between the carrier diffusion length and the carrier mobility to assess the potential of realising an inkjet printed BJT. The FET subsection introduces theory and then the selection of the inkjet printed FET architectures is made and the initial design layout is shown.

7.2.1 Bipolar junction transistor

The two dimensional structure of a p-n-p bipolar junction transistor is shown in figure 95.

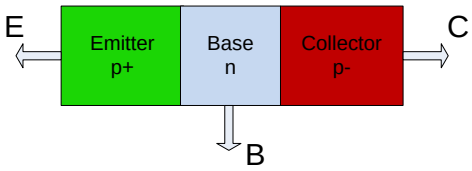

Figure 95. Two dimensional schematic of a p-n-p bipolar transistor.

A bipolar junction transistor typically has three separately doped regions, forming two pn junctions. The heavily doped p+ region is called the emitter, denoted as E in the figure 95. The central n- region with moderate doping is called the base, B. The width of the base has to be narrower than the minority carrier diffusion length to operate the BJT. The lightly doped p- region is called the collector, C.

The carrier diffusion length is proportional to the root of the semiconductor carrier mobility of the n type semiconductor as shown in equation 16 [148], with an n type equation selected as an example.

$$L_n = \sqrt{D_n \cdot \tau_n} = \sqrt{(\frac{kT}{q})\mu_n \tau_n} \tag{16}$$

Where

L_n is the diffusion length of the electrons in m,
D_n is the diffusivity of the carriers in cm^2/s,
τ_n is the lifetime in s,
kT is the thermal energy is eV,
q is the electrical charge on a electron, 1.602×10^{-19} C,
μ_n is the n type carrier mobility in $cm^2/V\ s$,

Therefore,

$$L_n \propto \sqrt{\mu_n} \tag{17}$$

Since all the other terms are constants in equation 16.

Where

L_n is the n type semiconductor diffusion length in m,
μ_n is the n type carrier mobility in $cm^2/V\ s$,

In a crystalline silicon wafer, the minority carrier diffusion length is about 100 nm [149]. The silicon wafer average mobility is about 1430 $cm^2/V\ s$ [150], however the mobility of organic semiconductors is in the range from 10^{-3} to 1 $cm^2/V\ s$ [8]. The diffusion length of an organic semiconductor obtained from equation 7 is therefore 2.6 nm based on mobility of 1 $cm^2/V\ s$, 37.8 times shorter than that of silicon. However, current inkjet printing technology cannot deposit a layer down to a few nanometre featured thickness even with solvent based inks. In theory a few nanometre thick layer can be achieved by formulating low weight percentage solvent based ink, but it can easily generate pin holes on the layer resulting in device failure. Therefore fabricating an organic bipolar junction transistor with current inkjet printing technology is not realistic, especially on IF fabric as the surface roughness is up to 5 μm.

7.2.2 Field effect transistor

The inkjet printed FET has been widely reported and is described in section 4.4 on inkjet printed transistors. Equation 18 [151] describes the semiconductor carrier mobility when the transistor operates in its saturation region:

$$\mu = \frac{2I_D L}{WC_i(V_G - V_T)^2} \tag{18}$$

Where

μ is the field effect mobility in $cm^2/V\ s$,
L and W are the channel length and width respectively in m,

C_i is the insulator capacitance per unit area in F/cm^2,

V_T is the transistor threshold voltage in V,

I_D is the drain/source current flowing through the channel in A,

V_G is the gate voltage applied in V,

Equation 8 will be used to evaluate the inkjet printed semiconductor layer's carrier mobility in the saturation region as a comparison with other researcher's reported values.

There are two main groups of field effect transistor architectures: bottom gate or top gate. Top/bottom gate represents the position of the gate electrode with reference to the position of the semiconductor layer. Each top or bottom gate group can be divided into bottom contact and top contact transistors as shown in figure 96.

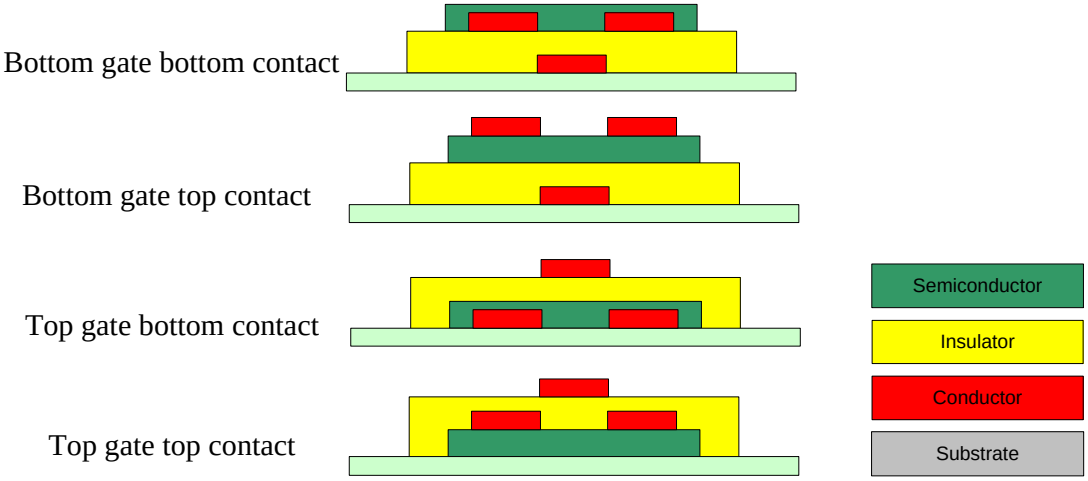

Figure 96. Four different architectures of potential inkjet printed transistors.

For the inkjet printing fabrication, these four transistor architectures each has a different deposition sequence of the four layers. In selecting the appropriate transistor architecture for this work, inkjet printing fabrication issues and the electronic performance of materials need to be carefully considered.

A screen printed interface layer on polyester cotton fabric has a surface roughness up to 5 µm, which is much higher than the thickness of the effective active semiconductor layer in a transistor which is in the 10 nm scale. Consequently, this means that the transistor channel cannot be flat due to the effect of the rough interface. In addition, the bottom gate transistor architecture has the source/drain electrodes and the semiconductor layers on the top of the printed insulator layer. Therefore, the semiconductor layer will be inkjet printed after the gate

electrode and insulator layer depositions to avoid damage caused by the subsequent deposition curing stage. Therefore, the top gate structure is not further considered.

The bottom electrode contact structure is selected from the two possible variations in the bottom gate architecture group. There are two reasons for selecting the bottom contact structure:

(1) The active semiconductor layer deposition will be the last deposition stage which can avoid any potential degradation caused by the thermal or UV curing of previous layers' deposition.
(2) While the gate voltage is applied, a layer is formed at the boundary between the semiconductor layer and the insulator layer by the mobile charge carriers (holes or electrons). Therefore the bottom contact structure does not have any resistance generated by the thickness of the semiconductor layer. The charged carriers in figure 97 (a) do not have to travel through the semiconductor layer to reach the source/drain electrodes as it is in figure 97 (b).

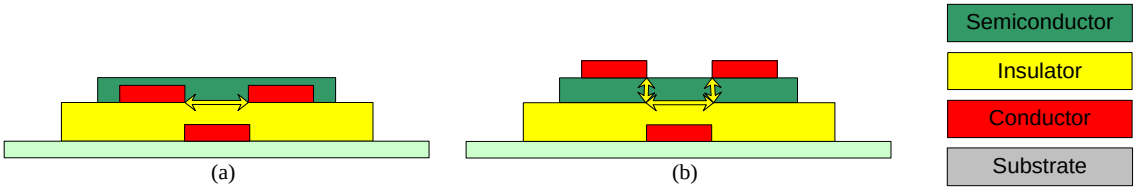

Figure 97. Schematic cross sectional views of the charged carriers path in (a) bottom gate and bottom contact, (b) bottom gate and top contact transistor structures.

In the bottom gate top contact structure, additional resistance is generated and can be altered by changing the thickness of the semiconductor layer. In the bottom gate bottom contact structure, the printed semiconductor layer thickness does not add the additional resistance and so this structure is selected.

Table 12 has summarised the four FET structures for inkjet printing with each advantages and disadvantages. Potential solutions are given.

FET architecture	Advantages	Disadvantages	Potential solutions
Bottom gate bottom contact	Inkjet printed semiconductor layer is the last deposition in fabrication to avoid degradation caused by subsequent deposition stage, including curing process.	Semiconductor layer is exposed to atmosphere so it can be easily oxidised and lost its electronic function.	An inkjet printed additional insulator layer on top to seal up to avoid semiconductor layer failure mechanism.
Bottom gate top contact	No benefit compared to bottom gate bottom contact.		
Top gate bottom contact	No benefit compared to top gate top contact.		
Top gate top contact	Subsequent inkjet printed insulator layer can protect previous inkjet printed semiconductor layer on the bottom to avoid exposing to atmosphere, resulting in oxidation.	Screen printed interface layer has up to 5 µm surface roughness, which can cause printed FET failure or resulting low grade performance.	An additional inkjet printed insulator layer on top of interface layer to further smooth the screen printed interface layer on standard fabric substrate.

Table 12. Summary table of four field effect transistor structures for inkjet printing.

The transistor layout of the bottom gate bottom contact transistor architecture is based on a straight transistor channel and consists of four deposition layers. The four layers are inkjet printed in the following sequence: gate electrode layer, insulator layer, source/drain electrodes layer and semiconductor layer. The design is shown in figure 98.

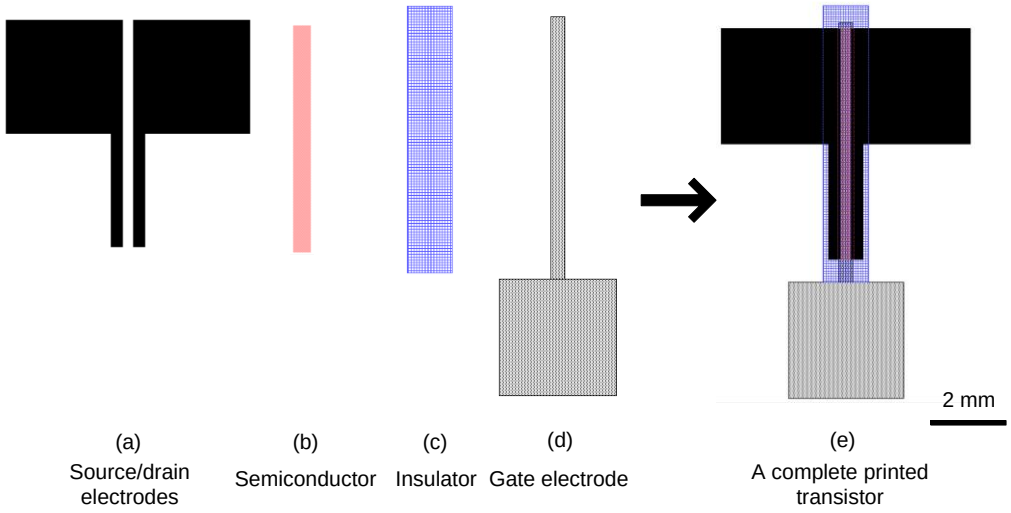

Figure 98. Plan views of schematic designed layout of each functional layer and a complete inkjet printed organic FET.

7.3 Methodology to achieve all inkjet printed smart fabric transistor

To achieve an all inkjet printed smart fabric transistor several technical challenges must be solved. These are the development of a new inkjet printing process, the investigation of active materials and control of the interactions between the different layers required for an inkjet printed smart fabric transistor. This section will discuss the methodology planned and used in this research to work towards an all inkjet printed smart fabric transistor.

The use of a screen printable interface layer (IF) is the first stage to realise inkjet printed electronic devices on fabric. Then the advances of chapters 5 and 6 are the second part of the research path to realise a fabric transistor by investigating and achieving inkjet printed conductor and insulator inks. Chapter 5 proved the inkjet printable conductive silver ink works well on IF fabric with suitable low temperature processing. Chapter 6 described the development of the new UV curable PVP insulator ink which can be used to inkjet print thin insulator films on fabric to construct a parallel plate capacitor which can now be used as the insulator for a printed transistor on fabric.

An inkjet printable semiconductor ink is a further advance which is investigated. The semiconductor performance can be lost under various circumstances, for example, oxidation and during the curing process. The requirements of an inkjet printable semiconductor ink are:

(1) Low temperature processable ($\leq 150\ ^{o}C$),
(2) Fabric compatible (Standard polyester cotton fabric),
(3) Inkjet printable (Dimatix DMP 2831),
(4) Flexible,
(5) Good semiconductor properties.

After the inkjet printable PTAA semiconductor ink is formulated, the inkjet printing process has to evaluate and confirm that the inkjet printed PTAA layer has semiconductor characteristics. The research in printed fabric transistor has been broken down to several progressive stages:

1. A silicon dioxide coated silicon wafer is used as the initial substrate for the inkjet printed transistor, which means the gate electrode and insulator layers do not need to be inkjet printed. The silicon wafer acts as the gate electrode and the silicon dioxide

layer acts as the insulator. This allows performance the testing of the inkjet printed semiconductor layer without combining the other challenges and uncertainties.

2. Once the inkjet printable PTAA layer has been proved to have semiconductor characteristics, the next stage is to inkjet print the transistor on a silicon wafer, which means the gate electrode does not need to be inkjet printed. This stage is to test the inkjet printable insulator and its capability to work with the subsequent inkjet printed semiconductor layer.
3. The next stage is to all inkjet print the full transistor on to a glass slide. This stage is to examine the performance and interaction between all four layers of an all inkjet printed transistor on an ideal surface.
4. Kapton film is then used to replace the glass slide to achieve an all inkjet printed flexible transistor whilst maintaining an ideal smooth surface. This stage is to examine the transistor performance during and after mixing.
5. The last stage is to migrate the whole processes obtained to achieve the final objective of an all inkjet printed smart fabric FET on the IF fabric.

7.4 Selected inks and substrates for printed transistors

Three different electronically functional inks are needed to fabricate an all inkjet printed transistor. These are insulator, conductor and semiconductor inks, which must all be inkjet printable and low temperature processable. In this section, the inkjet printable semiconductor ink is selected and discussed.

7.4.1 Selected organic semiconductor material for inkjet printed transistors

There are two groups of semiconductors analogous to the conductor groups discussed earlier: organic and inorganic. Organic semiconductors themselves are also categorised into two groups based on their chemical structure; these groups are polycrystalline and amorphous materials as described in section 3.2.3.

Inorganic semiconductor requires a high curing temperature (over 300 ^{o}C), therefore, only the organic semiconductors are examined. Section 3.2.3 discussed, F8T2 as a typical advanced model of polythiophene polycrystalline semiconductors. To reach its optimum value it must be cured to a crystalline structure which requires a 265 ^{o}C curing temperature [38]. This

temperature will destroy the fabric substrate and therefore this ink is unsuitable in its current form. PTAA is the most advanced amorphous organic semiconductor and does not require a high curing temperature (100 ^{o}C). This means PTAA has the most potential for use in an inkjet printed transistor on fabric. However, as discussed in section 3.2.3, amorphous semiconductors generally have low carrier mobility compared to the polythiophene semiconductors.

To achieve an inkjet printable organic semiconductor ink, a solvent must be used to dissolve the semiconductor material. 1, 2-dieleclorobenzene is the organic solvent used in Fauzia et al [152] on printed organic semiconductor ink using the Dimatix 2831 inkjet printer. It is one of the most widely used aromatic solvents for dissolving polymer semiconductors. Experimental work performed by the author shows the 1, 2-dichlorobenzene aromatic solvent dissolved organic semiconductor ink does not last long (< 5 minutes) in good jetting performance after the ink is inserted in to the ink cartridge. The PETEC company [153] found that the 1, 2-dichlorobenzene solvent could damage the DMP 2831 PZT/silicon bimorph nozzles. PETEC suggests to use tetralin as the organic solvent to dissolve organic polymer semiconductors. This was supported by Ossila, another printed electronics company, who also suggested tetralin is an alternative organic solvent to dissolve polymer semiconductor materials [154]. Inkjet printable PTAA formulation and performance will be discussed further in section 7.4.4.

7.4.2 Selected conductive silver for printed transistor

Chapters 5 and 6 showed that the SunChemical silver ink, U5714, is suitable for this application. Its printing parameters settings remain the same, with a 15 μm drop spacing and 2 inkjet printed deposits per conductive layer. However, its curing process is changed to be compatible with the silicon dioxide coated silicon wafer. The new curing process uses a hotplate for 10 minutes at 150 ^{o}C rather than using the box oven. This new process takes advantage of the fact that the silicon dioxide coated silicon wafer offers good thermal transfer and the printed silver tracks do not require flexibility. In addition, the printed samples does not have to be removed from the printing platform for each curing stage, as this curing stage could be integrated in the production line. Previous chapter 5 and 6 cannot use the hotplate to cure the fabric substrate because the fabric does not conduct heat as good as silicon wafer.

7.4.3 Selected insulator PVP for printed transistor

In chapter 6 the development of an all inkjet printed smart fabric capacitor proved that the new UV curable PVP insulator can be printed with the DMP 2831 inkjet printer with good insulating properties. The printed PVP layer shows good adhesion to the silver layer, the Kapton film and the IF fabric substrates. The printed layer also has good flexibility and transparency which can be desirable in some applications. Therefore, in this chapter, the printable insulator ink is not discussed further; the UV curable PVP insulator ink is selected as the insulator layer for the transistor. Its processing parameters remain the same as in chapter 6, with a 15 µm drop spacing and 2 inkjet printed deposits in one insulator layer, UV cured for 100 s in a UV chamber with power density 31 mW/cm^2.

7.4.4 Selected substrates for printed transistor

A silicon dioxide coated silicon wafer is used to perform the initial printing trials of the inkjet printable semiconductor ink. The silicon dioxide coated silicon wafer functions as an integration of the gate electrode and insulator layers. Therefore, only the source/drain electrode and the semiconductor layers are required to be inkjet printed on top of the silicon dioxide layer. After the semiconductor ink has been shown to work on the silicon dioxide layer, it was planned to migrate the process to an intrinsic silicon wafer, glass slide, Kapton film and IF fabric in that order as described in section 7.3.

7.5 Fabrication

7.5.1 Inkjet printed transistor fabrication process

A fabric substrate is the ultimate target substrate for an inkjet printed smart fabric transistor and therefore each intermediate step is aimed, and restricted in terms of available processing, by this goal. The structure of the inkjet printed transistor on a silicon dioxide coated silicon wafer is illustrated in figure 99.

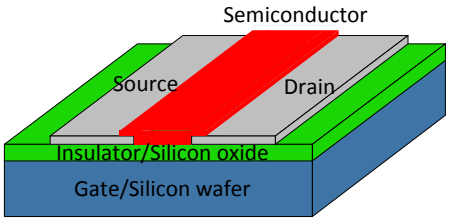

Figure 99. Isometric view of the schematic diagram of an inkjet printed transistor on silicon dioxide coated silicon wafer.

The silicon wafer acts as the gate electrode. The 90 nm thick layer of silicon dioxide acts as the gate insulator layer. Therefore, this reduces the required inkjet printed layers to the source and drain electrodes layer on the wafer followed by an inkjet printed semiconductor layer between the source and drain electrodes.

Inkjet printed transistor fabrication process on Silicon dioxide coated silicon wafer

The wafer is cleaned in an ultrasonic bath with DI water to ensure uniform surface energy across the whole printing area. The next step is to inkjet print two conductive silver tracks to form a conductive layer as the source and drain electrodes. The printed tracks are cured for 10 minutes at 150 ^{o}C on a hot plate. The final inkjet printed layer is the active semiconductor layer. Two deposits of PTAA ink are inkjet printed sequentially as the semiconductor layer. Two deposits are used to avoid pin holes as the layer's thickness is not important in a bottom gate and bottom contact transistor architecture. The semiconductor layer is then dried at 100 ^{o}C for 1 minute on a hotplate. No curing process is needed for amorphous semiconductor materials. The fabrication flow diagram of an inkjet printed transistor on a silicon dioxide coated silicon wafer is shown in figure 100.

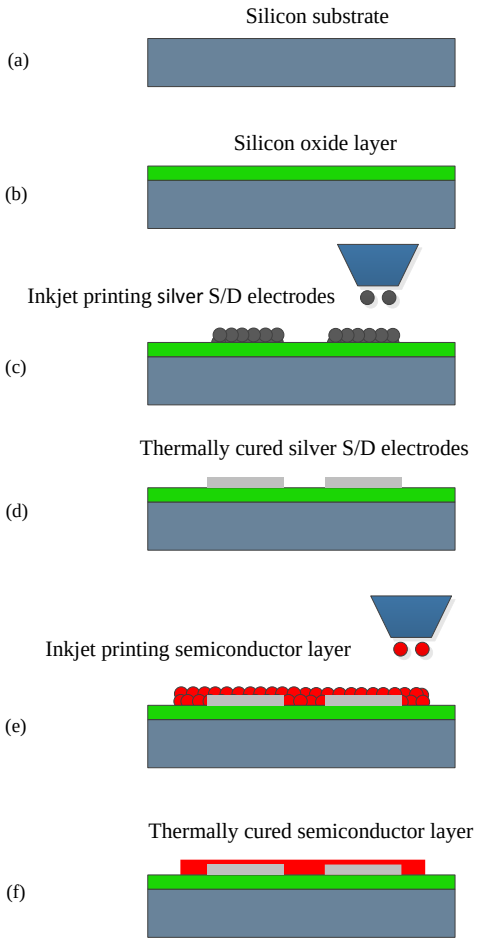

Figure 100. A flow diagram in the cross sectional view showing the fabrication of inkjet printed transistor on a silicon dioxide coated silicon wafer substrate.

Processing steps to achieve an inkjet printed transistor on fabric

A full fabrication process of inkjet printed smart fabric transistor is described here. The interface layer on the fabric is wiped with lint free cleanroom tissues dipped in DI water. The next step is to inkjet print two conductive silver deposits sequentially on the interface layer to form a single gate electrode. After printing, the gate electrode is cured for 10 minutes at 150 ^{o}C in a box oven. The UV curable PVP insulator ink is then printed on top of the gate electrode. Two insulator deposits are printed to avoid pin holes in the film, which can cause insulator breakdown and hence device failure. The curing process for the inkjet printable PVP ink is 100 s in a UV chamber at power density of 31 mW/cm^2. The source and drain electrodes are then inkjet printed and cured in the same way as the gate electrode. The final inkjet printed layer is the active semiconductor layer. Two deposits of the PTAA ink are inkjet printed to create the semiconductor layer which is then dried at 100 ^{o}C for 1 minute in a box oven. The fabrication flow diagram is shown in figure 101.

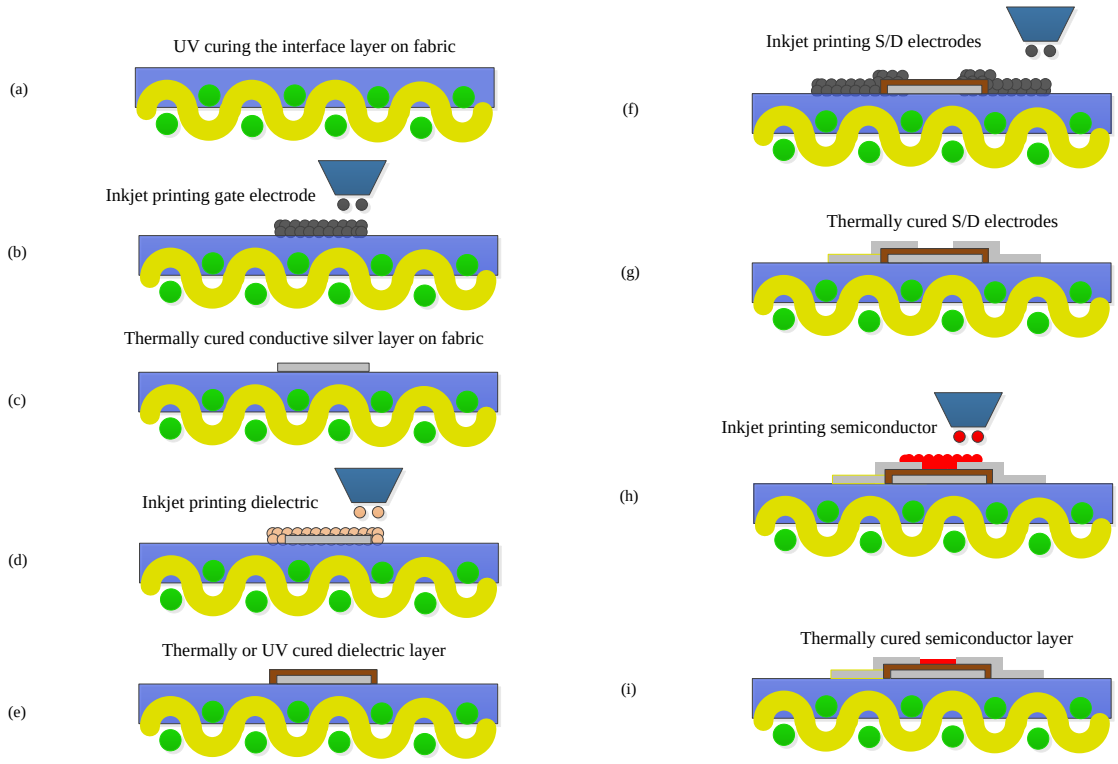

Figure 101. A flow diagram in the cross sectional view showing the fabrication process of an inkjet printed smart fabric transistor on fabric substrate.

7.5.2 Silicon dioxide layer deposition

Two silicon dioxide coated silicon wafers were prepared by the Nanofabrication Group at the University of Southampton [155]. The silicon dioxide layer was made using wet oxidation which uses water vapour at 1000 ^{o}C in a Tempress annealing furnace. The silicon dioxide layer has a target thickness of 100 nm. Two average layer thickness has been measured for each silicon dioxide layer across the whole wafer as shown in figure 102.

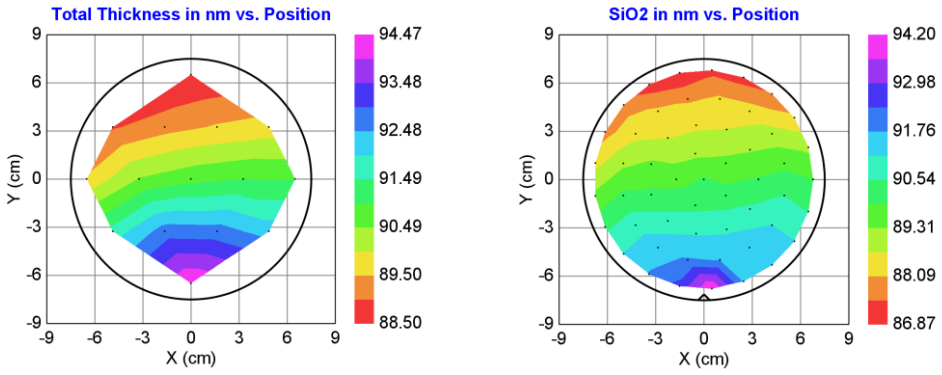

(a) (b)

Figure 102. Silicon dioxide layer thickness measurements at selected locations on silicon wafer.

The average thickness of the silicon dioxide layer is 90 nm and therefore this is the value used in further calculations in this chapter.

7.5.3 Thermally curable PTAA ink: development, printing trials, optimisation and transistor fabrication

PTAA has exceptional electronic performance among the available amorphous organic semiconductors [37]. It can be easily dissolved in an aromatic solvent to form a stable inkjet printable semiconductor ink. The printed PTAA layer does not require a curing stage, as it is an organic amorphous semiconductor. A drying stage is sufficient to evaporate the solvent used and realise its semiconductor performance.

The PTAA solid powder is supplied by PETEC [153]. The formulation suggested by PETEC, uses 1, 2, 3, 4-tetrahydronaphthalene (tetralin) as a solvent to dissolve the PTAA powder without any further additives. The inkjet printable PTAA ink is made from 1 wt% PTAA in tetralin. Tetralin has a viscosity of 2 mPa s [156] at room temperature which is at the lower end of the acceptable DMP 2831 printer range. 1 wt% of PTAA is dissolved in tetralin. This formulation has an average viscosity of 2.8 mPa s at 21.1 ^{o}C. Figure 103 shows the stable viscosity result of the PTAA in tetralin ink under different shear rates.

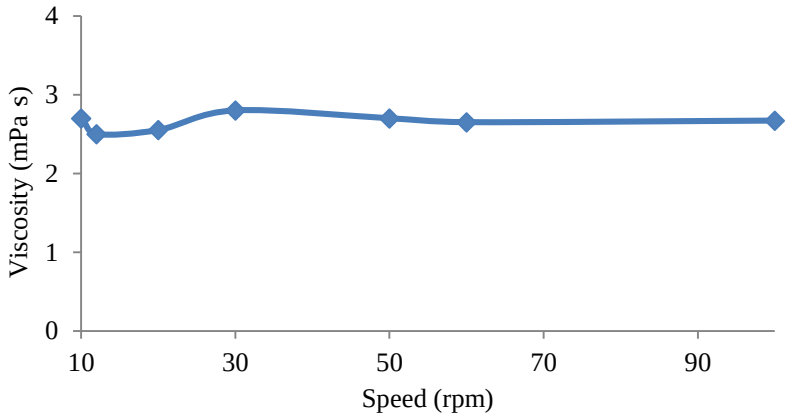

Figure 103. Viscosity of 1 wt% PTAA in tetralin, measured using a Brookfield DV-II pro viscometer.

The measured viscosity value of 2.8 mPa s is relatively low compared to the ideal viscosity range 10 to 12 mPa s, but within the acceptable range of 2 to 30 mPa s. Having established the viscosity was suitable, the PTAA ink was successfully printed using the DMP 2831. The PTAA ink produced consistent droplet firing resulting in a good pattern definition in the

millimetre scale. Figure 104 shows the inkjet printed transistor design and the actual prints on the silicon wafer with a silicon dioxide layer.

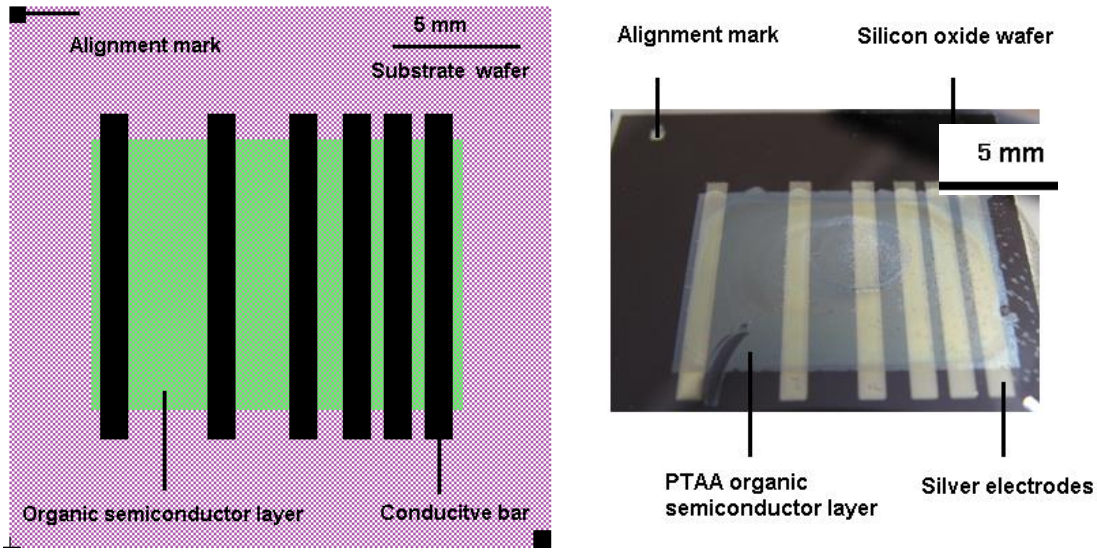

(a) (b)

Figure 104. (a) Schematic designed inkjet printed transistor on a silicon dioxide coated silicon wafer, (b) Inkjet printed transistor on a silicon dioxide coated silicon wafer.

The six parallel thin rectangular bars are the source and drain electrodes for the printed transistors with different spacing to provide a range of channel lengths to test, as shown in figure 104. The channel lengths chosen are: 3 mm, 2 mm, 1 mm, 0.5 mm and 0.5 mm from left to right. During testing, the two silver bars on either side of a given channel can be used as the source and drain. There are some satellite droplets on the right hand side of the desired PTAA pattern as shown in figure 104 (b). This is caused by the ink's low viscosity, which typically generates a tail after each fired droplet. The organic PTAA layer is very soft. It can be easily scratched off by a plastic tweezers as shown in the bottom left corner of the printed PTAA layer. Therefore, an encapsulation layer may be required to protect the active layer from physical damage. Figure 105 is focused in on a single inkjet printed transistor with a channel length of 1 mm.

Figure 105. One inkjet printed transistor on a silicon dioxide coated silicon wafer with channel length of 1 mm.

The uneven PTAA surface can be seen on the left hand side in figure 105. This is caused by the thermal drying of the solvent based ink. Because of the ink's low viscosity and accumulated ink deposit, the ink tends to shrink when thermally dried as shown in the left part of figure 105. This will result in an uneven surface. This effect cannot be avoided in a thermally curable solvent based ink for inkjet printing. However, UV curable inks do not have this issue, as the volume of the UV cured layer does not change compared to its liquid phase as discussed in section 6.3.1.

The 1 wt% PTAA in tetralin wets the silicon dioxide layer well, as shown in figure 106 (a). However, three weeks after the PTAA was formulated, the wetting is much poorer, as shown in figure 106 (b).

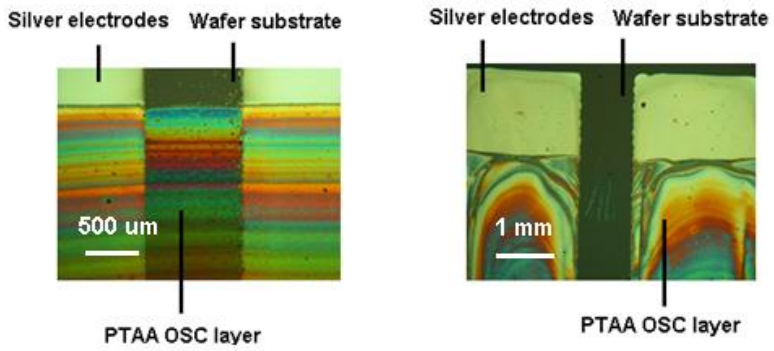

(a) (b)

Figure 106. Comparison of the PTAA ink wetting to the silicon dioxide layer, (a) Plan view of an inkjet printed transistor channel with the PTAA ink formulated on the same day, (b) Plan view of an inkjet printed transistor channel with three weeks old PTAA ink.

The substrate was re-cleaning again in the ultrasonic bath to ensure the surface energy is uniform. However, this did not improve the wetting and therefore it is believed the surface tension of PTAA ink has therefore increased significantly over three weeks due to settling.

7.6 Device testing

7.6.1 Performance testing of the inkjet printed transistor on a 90 nm silicon dioxide layer coated silicon wafer

Only one batch of 30 inkjet printed organic transistors were tested once in Nano Research Group at University of Southampton. During the work only a single access was possible to the required semiconductor analyser with probe station. The materials selected are discussed in

section 7.4, the transistor fabrication process was discussed in section 7.5.1 and the transistor layout was discussed in section 7.5.3. All 30 printed transistor devices are tested. The test involves the source/drain voltage being swept from -15 V to 15 V with a constant gate voltage of -15 V. 29 of the inkjet printed transistors show no significant transistor characteristic output due to a failure of the printed organic semiconductor layer or the silicon dioxide layer breakdown. The transistor failure mechanism is studied in the next section. Only a single device showed the performance characteristics of a transistor. However, it only worked for 2 measurements before failure. Figure 107 shows the gate current leakage measurement graph at a constant gate voltage of -15 V.

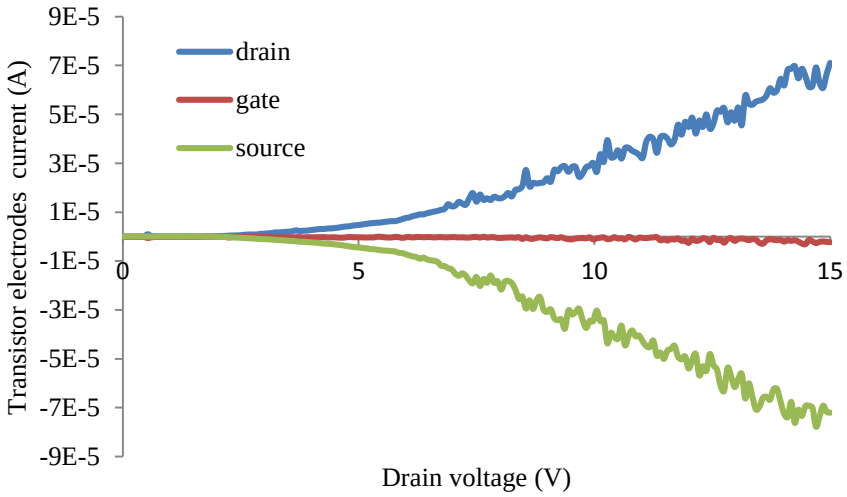

Figure 107. Transistor gate leakage current measurement plot while gate voltage -15 V.

The gate current is very small compared to the drain and source current. The gate current is of the order of magnitude 10^{-7} A and the source/drain currents are of the order of magnitude 10^{-5} A. The drain current is roughly equal to the source current from the plot. A negative voltage was applied to a p type semiconductor in order to achieve an accumulation layer of the FETs rather than an inversion layer, as the organic semiconductor suffers from poor electron carrier mobility but good hole carrier mobility. Figure 108 shows a gate voltage sweep output graph when the drain voltage is set to either 500 mV or 1 V.

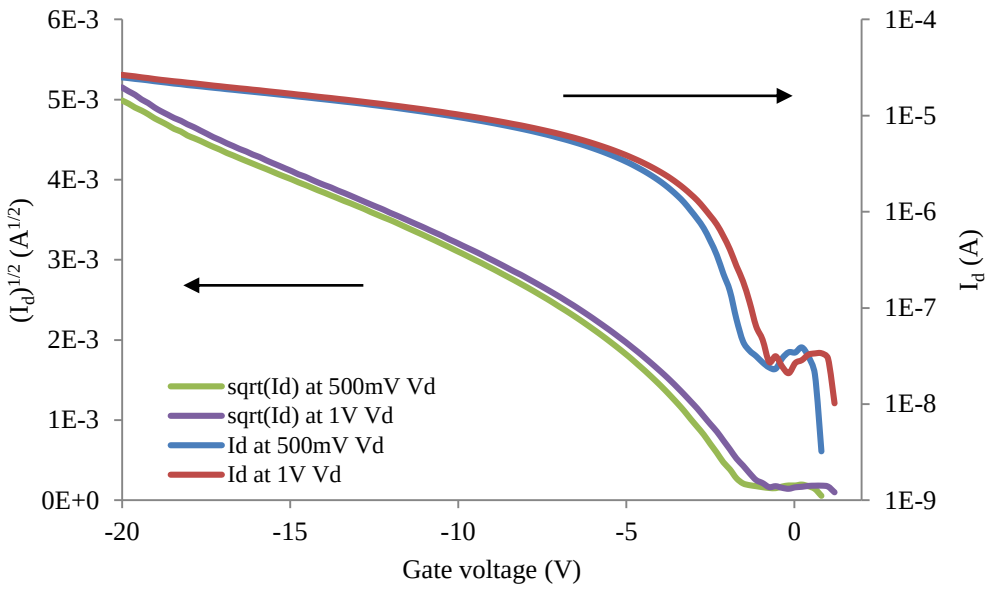

Figure 108. Transistor drain current output in the function of the gate voltage sweep while drain voltage is constant at 500 mV and 1 V respectively.

It can be seen that the on/off ratio is about 10^3, which is lower than the 10^4 Sigma Aldrich reported for PTAA [157]. The measured on current of the printed transistor is the same as the Sigma Aldrich reported in range of 10^{-5} A, but the off voltage of the Sigma Aldrich reported is in the range of 10^{-9} A [157] at the same time the measured off current is in the range of 10^{-8} A. Therefore, 10 times higher measured off current compared to Sigma Aldrich's may be caused by the gate leakage current or possibly the intrinsic conductivity of the printed PTAA layer.

The inkjet printed PTAA semiconductor carrier mobility is calculated based on its saturation region as shown in figure 108, when a -10 V gate voltage is applied. The relative permittivity of silicon dioxide of 3.7 is used in the calculation of the capacitance per unit area of the silicon dioxide layer [158]. Table 13 shows the sampling point information taken to calculate the inkjet printed organic transistor carrier mobility in the ON state in its saturation region.

V_g (V)	I_g (A)	I_d (A)	I_s (A)	Vt (V)	L (m)	W (m)	C_i (F/cm)
-10.083	5.171×10^{-10}	9.7337×10^{-6}	9.7299×10^{-6}	-1.1389	1×10^{-3}	10×10^{-3}	3.638×10^{-8}

Table 13. Sampling point taken to calculate the inkjet printed organic transistor's carrier mobility at ON state.

In Figure 108, the slope of the square root of the drain current is not constant as typically occurs. Therefore, the transistor threthold voltage was extracted from the point of the gate voltage when the drain current starting to increase. The holes mobility is calculated to be 0.669 cm^2/V s based on equation 8. Yadav et al [159] reported that simulated results on the electron mobility in a PTAA transistor reached 5×10-5 cm^2/V s and that the hole mobility reached 0.7

$cm^2/V\ s$. This is very close to the mobility value extracted from the author's PhD work. Sigma Aldrich reported the spin coated PTAA ink dissolved in chlorobenzene solvent and obtained carrier mobility of 0.004 $cm^2/V\ s$ [160]. The solution processed organic transistor performance varies between different publications due to the deposition process and measuring conditions since there is no standard process in these new organic semiconductor devices. Sigma Aldrich used spin coating method to deposit the PTAA layer, which achieves a smoother layer and therefore increases its transistor carrier mobility. However, Sigma Aldrich used the top gate bottom contact transistor structure, which added additional resistance from the carriers passing twice through the PTAA layer, as explained in section 7.2.1. In this example, the semiconductor layer is protected by the insulator layer. However, the semiconductor can be damaged or degraded by subsequent active layer deposition. Another possible explanation of the high carrier mobility compared to the Sigma Aldrich's is the performance of the PTAA powder is supplied by the PETEC company. PETEC may use different chemical approach to syntheses the PTAA than Sigma Aldrich. There are other parameters used in this research which are different from Sigma Aldrich's process, for example, a 250 nm thick silicon dioxide layer and higher gate and drain voltages are used in the transistor testing by Sigma Aldrich.

7.6.2 The failure mechanism of the inkjet printed PTAA transistor

Section 7.4.1 showed that only a single transistor out of 30 samples worked. In addition, the only working transistor lost its semi-conducting properties after one cycle of the two performance tests.

The breakdown of the transistor devices can be caused by instability of PTAA layer caused by oxidation in the atmosphere. This phenomenon is suggested to be the failure mechanism of the printed PTAA layer. In this collaboration work with Sichuan University, the formulated PTAA ink and inkjet printed transistor on a silicon dioxide coated silicon wafer were sent to Sichuan University. A new 10 samples of inkjet printed transistors were inkjet printed and sent to Sichuan University before testing to avoid damages on the printed transistors caused by the characteristic testing. To further prove the printed PTAA layer's failure mechanism, PTAA layers were inspected using an infrared spectroscope by Sichuan University with the following drain voltages: 0V, 20 V and 40 V. The following results were obtained from Sichuan University. Figure 109 shows the infrared spectroscopic diagram of PTAA layer with no voltage applied.

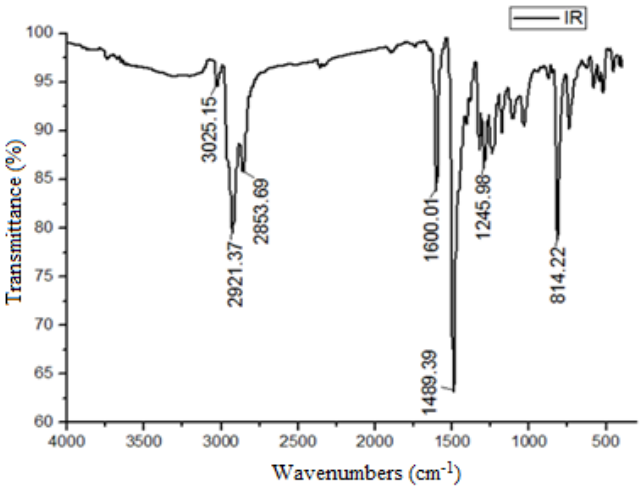

Figure 109. Infrared spectrum diagram of PTAA layer after a drain voltage of 0 V applied.

Reference [161] states the first absorption peak at 3025.15 cm^{-1} represents the C=C-H asymmetric stretch bond vibration from the aromatic rings. Two strong absorption peaks at 2921.37 and 2853.69 cm^{-1} represent H-C-H asymmetric and symmetric stretch alkanes group. The absorption peak at 1600.01 represents the C-C=C symmetric stretch bond vibration from the aromatic rings. The absorption peak at 1489.39 cm^{-1} represents the C-C=C asymmetric stretch bond vibration from the aromatic rings. The region to the right hand side of the infrared spectrum diagram from 1450 to 500 cm^{-1} usually contains a very complicated unique series of absorption peaks [162]. These are mainly due to various bending vibrations within the molecule [163]. This region is called the fingerprint region, where most absorption peaks cannot relate to specific bonds from chemically functional groups. Figure 109 shows the absorption peaks related only to the aromatic rings in the PTAA material. Figure 110 shows the infrared spectroscopic diagram of the PTAA layer after 20 V is applied across the layer.

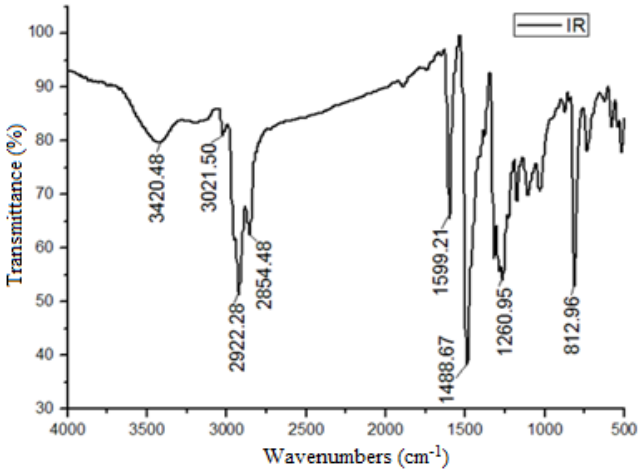

Figure 110. Infrared spectrum diagram of PTAA layer after a drain voltage of 20 V applied.

The main absorption peaks shown in figure 109 related to aromatic rings remain in the diagram. However, there are two new absorption peaks visible in the diagram. The absorption peak at 3420.48 cm^{-1} represents the high concentration of hydrogen bonded O-H stretch bond vibration from the phenol group's rings. In addition, reference [161] suggests that this peak usually appears as a much broader peak than the other infrared absorptions, which is observable in figure 110. Another new absorption peak at 1260.95 cm^{-1} represents C-O stretch bonds, which can be generated by ester or ether groups. These two new absorption peaks are both consistent with an oxidisation reaction on PTAA layer when 20 V is applied. Figure 111 shows the infrared spectroscopic diagram of a PTAA layer after 40 V is applied across the layer.

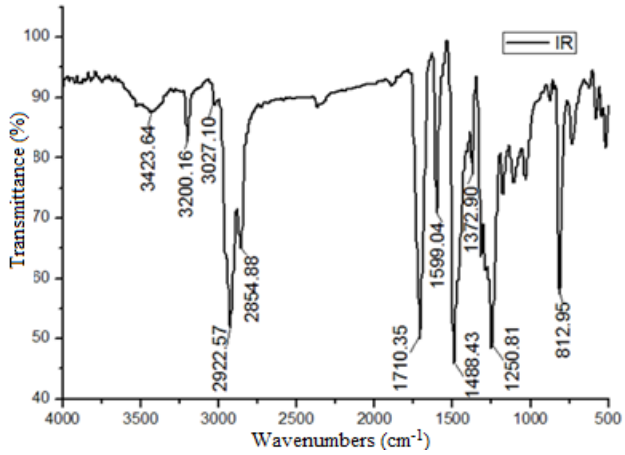

Figure 111. Infrared spectrum diagram of PTAA layer after a drain voltage 40 V applied.

The main absorption peaks seen in figure 109 related to the aromatic rings and oxidised chemical bonds, explained in figure 110, all remain in figure 111. However, there are three new absorption peaks in the diagram. Reference [161] states that an absorption peak at 3200.16 cm^{-1} represents N-H stretch bond vibration from an amine group. The absorption peak at 1710.35 cm^{-1} represents C=O stretch bond vibration from ester or aldehyde groups. The absorption peak at 1372.90 cm^{-1} represents N=O bend bond vibration from a nitro group. These three new absorption peaks show the aromatic structure based PTAA polymer chains have been broken up in to smaller chains or monomers. The breakdown phenomenon is caused by the oxidation reaction catalysed by voltage applied to the transistor while in operation. While the transistor is in operation, the semiconductor layer is in an active state with increased energy level. Therefore, the inkjet printed PTAA layer in an operating transistor has less chemically stability than no voltage applied on to the PTAA layer in ambient atmosphere without further encapsulation.

7.7 Conclusions

An inkjet printed transistor with processing suitable for fabric has been printed on a silicon wafer with silicon dioxide layer. This inkjet printed transistor was fabricated to study and test the inkjet printable PTAA semiconductor ink. The inkjet printed PTAA semiconductor layer within a transistor shows basic semiconductor characteristics. The inkjet printed transistor on a silicon dioxide coated silicon wafer has an on/off ratio of 10^3. The PTAA layer has a carrier mobility of 0.669 $cm^2/V\ s$ when a -10.083 V gate voltage is applied on a 90 nm thick insulator. The inkjet printed PTAA semiconductor on a silicon dioxide coated silicon wafer has been proved to function as a semiconductor layer, but had very short operating life time when in ambient atmosphere. The inkjet printed PTAA layer was tested under infrared spectroscopy which shows its chemical instability due to oxidising reactions. It has been demonstrated that an encapsulation layer on top of the active semiconductor layer is essential.

The inkjet printed smart fabric transistor research did not proceed beyond this stage. This was due to a number of factors; the high cost of the semiconductor materials and the timescales required for further development would go beyond the limits of the PhD. However, the study has identified the key objectives for inkjet printing a transistor on fabric and a clear pathway for future work has been laid out in section 7.3 and 7.5.1.

Chapter 8

8 Conclusions and future work

In this thesis, the objective was to provide solutions that merge direct write technology into smart fabric fabrication. It is noted that most research projects concerning smart fabrics with electronic functionality are more focused on achieving the end application rather than the fabrication methods. This thesis has introduced the two most promising direct write techniques, inkjet printing and pneumatic dispenser printing methods, to the fabrication of fundamental flexible electronic components on a fabric substrate. Both direct write techniques' operating principles and limitations have been examined in detail. These developed solutions will assist and contribute to realise printed integrated circuits with functional electronic applications on fabric including sensing and reaction to external stimuli, without the attachment of rigid electronic modules.

In this research, a novel inkjet printed smart fabric half wavelength dipole antenna has been achieved with efficiencies up to 74.1 % at 1.897 GHz and a novel inkjet printed smart fabric microstrip patch antenna has been achieved with efficiency up to 57 % at 2.48 GHz. The inkjet printed fabric antenna has proved the capability of inkjet printing conductive tracks on fabric substrate. The inkjet printed smart fabric dipole antenna is considered to be the world first inkjet printed fabric antenna. A novel inkjet printed fabric dipole antenna conference paper has been published and a journal paper on a novel inkjet printed fabric patch antenna result has been submitted.

A novel inkjet printed SU-8 capacitor on Kapton film has been achieved with a capacitance per unit area of 2.47 pF/mm^2. A novel inkjet printed smart fabric capacitor has been made with the same process on fabric substrate, but with tenfold increase in the capacitance per unit area, achieving 23.1 pF/mm^2. A new inkjet printable UV curable PVP dielectric ink is the key to this result which was formulated to increase the capacitance per unit area value by forming an inkjet printed thin dielectric film. The calculated relative permittivity of the inkjet printed PVP layer reached 11.7 compared to previous the highest value of 6.4 reported in the literature. Both

novel inkjet printed flexible capacitors and the new inkjet printable dielectric ink formulation have been published in two conference papers.

A precision pneumatic dispenser printer has been developed in this research work and used to prove the capability of dispenser printing in direct write printed electronics applications. Both inkjet and screen printable materials have been shown to work with the dispenser on various designs including a cantilever structure and multilayer capacitor. A dispenser printed flexible capacitor has been made from the identical inks as for the printed SU-8 capacitor to show the results are highly comparable. This work has lead to the writing of a successfully funded EU Framework 7 project called CREATIF [164].

An inkjet printed organic transistor has been made on a silicon dioxide coated silicon wafer to prove the functionality of an inkjet printable organic semiconductor PTAA ink. The inkjet printed transistor had an on/off ratio of 10^3 and carrier mobility reached 0.669 cm^2/V s. However, this inkjet printed transistor had a very short life time. Infrared spectroscopic analysis was used to examine the transistor failure mechanism caused by oxidisation reaction, which is catalysed by applying the operational voltage to the printed transistor. The infrared spectrum diagrams show the oxidation reaction and polymer chains breakdown according to the individual strong absorption peaks. This transistor failure mechanism has been examined and novel results have been published.

Future work can achieve smart fabric RF applications using a simple geometric design; the key novelty is the fabrication. Further optimisation of previous inkjet printed fundamental smart fabric electronic components can be achieved.

1. The frequency selective surface on fabric can be inkjet printed with screen printed interface layer, which is a further part of collaboration work with Loughborough University.
2. The flexibility and adhesion of the inkjet printable silver ink can be further developed to avoid the printed layer's cracks and it peeled off the substrate when bending.
3. An inkjet printable, low processing temperature thermally curable PVP based insulator ink to form thin insulator films is of great interest to research of this nature. This ink could potentially increase the capacitance per unit area in a printed capacitor and avoid the PVP layer's surface energy being altered by the UV exposure.

4. An all inkjet printed smart fabric transistor can be investigated and achieved based on the inkjet printable PTAA semiconductor ink. A clear pathway and methodology for achieving a printed transistor on fabric have been defined in section 7.3 and 7.5.1. As more organic semiconductors become commercially available and reasonably priced, the aim of a printed transistor on fabric could realistically be achieved.

This page intentionally left blank

References

1. X. Tao, *Smart fibres, fabrics and clothing*, Woodhead Publishing Limited, 2001, Cambridge, England, ISBN: 1-85573-546-6.
2. C. Dalsgaard and A. Jensen, *White paper on smart garments: a market overview of intelligent textile technologies in apparel*, Ohmatex of Smart Textiel Technology, January 2011, 11 pages.
3. H. Reiter, *The development of E-health in the field of cardiovascular medicine – The role of smart textiles*, Philips Research Europe, EHRA Summit 2010.
4. *Luminescent fabric*, LumiGram SARL, France, http://www.lumigram.com, access date: 08/08/2013.
5. *Pharad antenna*, Antenna, Photonic & RF Communications, http://www.pharad.com, access date: 01/10/2013.
6. A. C. Arias, S. E. Ready, R. Lujan, W. S. Wong, K. E. Paul, A. Saleo, M. L. Chabinyc, Y. Wu, P. Liu, B. Ong, *All jet-printed polymer thin film transistor active-matrix backplanes*, Applied Physics Letters, volume 85, number 15, 2004, pp. 3304-3306.
7. D. Kim, S. H. Lee, S. Jeong, J. Moon, *All-Ink-Jet Printed Flexible Organic Thin-Film Transistors on Plastic Substrates*, Electrochemical and Solid-State Letters, volume 12, 2009, pp. H195-H197.
8. T. Kawase, T. Shimoda, C. Newsome, H. Sirringhaus, R. H. Friend, *Inkjet printing of polymer thin film transistors*, Thin Solid Films, volume 438-439, 2003, pp. 279-289.
9. J. N. H. Shepherd, S. T. Parker, R. F. Shepherd, M. U. Gillette, J. A. Lewis and R. G. Nuzzo, *3D microperiodic hydrogel scaffolds for robust neuronal cultures*, Advanced Functional Materials, 2011, Vol. 21, pp. 47-54.
10. Dimatix Materials Inkjet Printer DMP-2831, FUJIFILM Dimatix Materials Printer, USA, http://www.fujifilmusa.com/products/industrial_inkjet_printheads/deposition-products/dmp-2800/index.html, access date: 01/10/2013.
11. Micropen pneumatical syringe dispensing operation principle, Micropen Technology, http://www.micropenmedical.com/micropenning/, access date: 01/10/2013.
12. Micro to pico-liter dispensing systems with patented micro dispense pump, nScrypt, http://www.nscrypt.com/direct-print-smartpump/ access date: 01/10/2013.
13. *Jettable fluid formulation guidelines*, Dimatix Materials Printer, FUJIFILM.
14. X. Zhao, J. R. G. Evans, M. J. Edirisinghe and J. H. Song, *Formulation of a ceramic ink for a wide-array drop-on-demand ink-jet printer*, Ceramics International, Vol. 29, 2003, pp. 887-892.
15. *Dimatix Material Printer DMP 2831 data and specification sheet*, Dimatix FUJIFILM.
16. *Different valves for precision dispensing*, Fisnar – The art of Dispensing (Europe), http://www.fisnareurope.co.uk/valves_index, access date: 31/08/2013.
17. *Fisnar - Dispensing dynamics - Part 1 - Fluidic*, Fisnar to The art of Dispensing http://www.fisnar.com/media/technical/Dynamics_Part_1.pdf, access date: 01/10/2013.
18. Y. Zhang, C. Liu and D. Whalley, *Direct-write techniques for maskless production of microelectronics: a review of current state of the art technologies*, 2009 International Conference on Electronic Packaging Technology & High Density Packaging (ICEPT-HDP).
19. B. King and M. Renn, *Aerosol Jet Direct Write Printing for Mil-Aero Electronic Applications*, http://www.optomec.com/, access date, 01/10/2013.
20. P. E Sheehan, W. P. King, A. R. Laracuente, M. Yang and L. J. Whitman, *Thermal Dip Pen Nanolithography*, NRL Review Chemical/Biochemical Research, 2006, pp.1-2.

21. U. Geiser. *Toward crystal design in organic conductors and superconductors*, In Proceedings of the 28th International School of Crystallography, Erice, Italy, May 1999.
22. Richard C. Dorf and James A. Svoboda, *Introduction to Electric Circuits*, 7th Edition, Section 2.4 Resistors. Published by Wiley, ISBN: 0-471-73042-4.
23. H. Akamatu, H. Inokuchi, Y. Matsunaga, *Electrical conductivity of the perylene-bromine complex*, Nature, Vol. 173, 1954, pp. 168-169.
24. P. W. Anderson, P. A. Lee and M. Saitoh, *Remarks on giant conductivity in TTF-TCNQ*, Solid State Communications, Vol. 13, Iss. 5, 1973, pp. 595-598.
25. A. A. Bright, A. F. Garito and A. J. Heeger, *Optical conductivity studies in one-dimentional organic metal: tetrathiofulvalene tetracyanoquinodimethan (TTF) (TCNQ),* Physical Review B, Vol. 10, No. 4, 1974, pp. 1328-1342.
26. K.M. Coakley and M.D.McGehee, *Conjugated polymer photovoltaic cells*, Chemistry of Materials, 2004, Iss. 16, pp. 4533-4542.
27. D.Zou, D. Wang, Z. Chu, Z. Lv and X. Fan, *Fiber-shaped flexible solar cells,* Coordination Chemistry Reviews, 2010. 254(9to10), pp. 1169-1178.
28. X. Yang, S. Shang, L. Li, X. M. Tao and F. Yan, *Vapor phase polymerization of 3, 4-ethylenedioxythiophene on flexible substrate and its application on heat generation,* Polymers for Advanced Technologies, 2011. 22(6), pp. 1049-1053.
29. D. N. Batchelder, *Colour and chromism of conjugated polymers*, Contemporary Physics, 1988. 29(1), pp. 3-31.
30. T. Bashir, *Conjugated polymer-based conductive fibres for smart textile applications*, thesis for the degree of Doctor of Philosophy, University of Boras. http:// publications.lib.chalmers.se/records/fulltext/173652/173652.pdf, access date: 10/10/2013.
31. Y. Liu, T. Cui and K. Varahramyan, *All-polymer capacitor fabricated with inkjet printing technique*, Solide-State Electronics, Vol. 47, 2003, pp.1543-1548.
32. V.G. Shah, D. J. Hayes, *Trimming and printing of embedded resistor using demand mode inkjet technology and conductive polymer*, IPC Printed Circuit Expo, 2002.
33. H. Koezuka, A. Tsumura and T. Ando, *Field effect transistor with polythiophene thin film*, Synthetic Metals, Vol. 18, Iss. 1-3, 1987, pp. 699-704.
34. S. Chung, S. O. Kim, S. K. Kwon, C. Lee and Y. Hong, *All-inkjet-print organic thin film transistor inverter on flexible plastic substrate*, IEEE Electron Device Letters, Vol. 32, No. 8, 2011, pp. 1134-1136.
35. J. Kim, J. Jeong, H. D. Cho, C. Lee, S. O. Kim, S. K. Kwon and Y. Hong, *All-solution-processed bottom-gate organic thin-film transistor with improved subthreshold behaviour using functionalised pentacene active layer*, Journal of PhysicsD: Applied Physics, Vol. 42, 2009, pp. 115107-6.
36. S. C. Lim, Y. S. Yang, S. H. Kim, Z. S. Kim, D. H. Youn, T. Zyung, J. Y. Kwon, D. H. Hwang and D. J. Kim, *Fabrication and characterisation of an OFET-based biosensor using a biotinylated F8T2 polymer*, ETRI Journal, Vol. 31, No. 6, 2009, pp. 647-652.
37. Z. Bao and J. Lockin, *Organic Field Effect Transistors*, Chapter 2.3 Charge Transport Physics of Solution-Processed Organic Field-Effect Transistor, Published by CRC Press, ISBN 0-8493-8080-4.
38. H. Sirringhaus, T.Kawase, R. H. Friend, T. Shimoda, M. Inbasekaran, W. Wu, E. P. Woo, *High Resolution Inkjet Printing of All-Polymer Transistor Circuit*, Science, volume 290, 2000, pp. 2123-2126.
39. P. Buffat and J. P, Burrel, *Size effect on melting temperature of gold particles*, Physics Review A, Vol. 13, Iss. 6, 1976, pp. 2287-2298.
40. J. Perelaer, C. E. Hendriks, A. W. M. De Laat and U. S. Schubert, *One-step inkjet printing of conductive silver tracks on polymer substrates*, Nanotechnology, Vol. 20, Iss. 16, 2009, pp. 165303/1-165303/5.

41. J. Perelaer, A. W. M. De Laat, C. E. Hendriks and U. S. Schubert, *inkjet printed silver tracks: low temperature curing and thermal stability investigation*, Journal of Materials Chemistry, Volume 18, Iss. 27, 2008, pp. 3209-3215.
42. B. S. Cook, T. Fang, S. Kim, T. Le, W. B. Goodwin, K. H. Sandhage and M. M. Tentzeris, *Inkjet catalyst printing and electroless copper deposition for low cost patterned microwave passive devices on paper*, Electronic Materials Letters, Vol. 9, No. 5, 2013, pp. 669-676.
43. *Znic oxides dispersion*, 50 wt% in water, Supplied by Buhler AG via Sigma Aldrich, http://www.sigmaaldrich.com/catalog/product/aldrich/721077?lang=en&region=GB, access date: 13/10/2013.
44. E. M. C. Fortunato, P. M. C. Barquinha, A. C. M. B. G. Pimentel, A. M. F. Gonçalves, A. J. S. Marques, R. F. P. Martins and L. M. N. Pereira, *Wide-bandgap high-mobility ZnO thin-film transistors produced at room temperature*, Applied Physics Letters, Vol. 85, Iss. 13, 2004, pp. 2541-2543.
45. A. S. G. Khalil, S. Hartner, M. Ali, A. Gupta, H. Wigger and M. Winterer, Stable aqueous dispersion of ZnO nanoparticles for inkjet printed gas sensors, Nanoelectronics Conference (INEC), 2010 3rd International, pp. 440-441.
46. C. Liu, W. Lee and T. Shih, *Synthesis of ZnO nanoparticles to fabricate a mask free thin film transistor by inkjet printing*, Journal of Nanotechnology by Hindawi Publishing Corporation, Vol. 2012, ID 710908, pp. 8.
47. M. N. Kamalasanan and S. Chandra, *Sol-gel synthesis of ZnO thin films*, Thin Solid Films, Vol. 288, Iss. 1-2, 1996, pp. 112-115.
48. S. P. Singh, Z. Ooi, S. N. L. Geok, G. K. L. Goh and A. Dodabalapur, *Electrical characteristics of zinc oxides organic semiconductor lateral heterostructure based hybrid field effect bipolar transistors*, Applied Physics Letters, Vol. 98, 073302, 2011, pp. 3.
49. *Inkjet printable silicon ink*, Kovio, http://www.kovio.com/, access date: 01/10/2013.
50. *Inkjet printable silicon ink*, Intrinsiq Materials, http://www.intrinsiqmaterials.com/, access date: 01/10/2013.
51. *Printed transistor announced*, New Electronics website, 14 November 2007, http:// www.newelectronics.co.uk/electronics-news/printed-transistor-announced/12084/, access date: 01/10/2013.
52. A. N. Goldstein, *The melting of silicon nanocrystals: submicron thin film structures derived from nanocrystal precursors*, Applied Physics A, Vol. 62, 1996, pp. 33-37.
53. T. Shimoda, Y. Matsuki, M. Furusawa, T. Aoki, I. Yudasaka, H. Tanaka, H. Iwasawa, D. Wang, M. Miyasaka and Y. Takeuchi, *Solution-processed silicon films and transistors*, Nature, Vol. 440, Iss. 6, 2006, pp. 783-786.
54. *Coating Guide Clevios P Formulations*, CLEVIOS, http://www.clevios.com, access date: 01/10/2013.
55. S. Jeong, D. Kim and J. Moon, *Inkjet printed organic inorganic hybrid dielectric for organic thin film transistors*, The Journal of Physical Chemistry Letters, Vol. 112, 2008, pp. 5245-5249.
56. C. L. Munsee, Master thesis '*Characterization of Solution-Based Inorganic Semi-conductor and Dielectric Materials for Inkjet Printed Electronics'*, Oregon State University, 2006.
57. Y. Choi, H. Kim, K. Sim, K. Park, C. Im and S. Pyo, *Flexible complementary inverter with low temperature processable polymeric gate dielectric on plastic substrate*, Organic Electronics, Vol. 10, 2009, pp. 1209-1216.
58. E. Braun and B. C. Levin, *Polyesters: a review of the literature on products of combustion and toxity*, Fire and Materials, Vol. 10, 1986, pp. 107-123.

59. C. S. Beroes, *Chapter 1 Elements of combustion and modes of heat transfer, The dangerous flammable fabrics: burning ourselves, our children and our senior citizens*, Publised by Authorhouse, 2004, ISB: 10-1418446742.
60. J. Bharathan and Y. Yang, *Polymer electroluminescent devices processed by inkjet printing: I. polymer light-emitting logo*, Applied Physics Letters, Vol. 72, No. 21, 1998, pp. 2660-2662.
61. T. Sekitani, Y. Noguchi, K. Hata, T. Fukushima, T. Aida, T. Someya, *A rubberlike stretchable active matrix using elastic conductor*, Science, 2008, volume 321, pp, 1468-1472.
62. K. Chun, Y. Oh, J. Rho, J. Ahn, Y. Kim, H. R. Choi, S. Baik, *Highly conductive, printable and stretchable composite films of carbon nanotube and silver*, Nature Nanotechnology, 2010, volume 5, pp. 853-857.
63. R. Purohit, D. Gosain, G. Gupta, R. Sagar, *Metal rubber: the new age nanomaterial*, International Journal of Nanomanufacturing, 2008, volume 6, number 2, pp. 659-666.
64. J. A. Rogers, T. Someya, Y. Huang, *Materials and Mechanics for Stretchable Electronics*, Science, 2010, volume 327, pp. 1603-1607.
65. S. P. Lacour, J. Jones, Z. Suo and S. Wagner, *Design and Performance of Thin Metal Film Interconnects for Skin-Like Electronic Circuits*, IEEE Electron Device Letters, Vol. 25, No. 4, 2004, pp. 179-181.
66. D. J. Lipomi, J. A. Lee, M. Vosgueritchian, B. C. K. Tee, J. A. Bolander and Z. Bao, *Electric properties of transparent conductive films of PEDOT:PSS on stretchable substrate*, Chemistry of Materials, Vol. 24, 2012, pp. 373-382.
67. *SWEET: Stretchable and Washbale Electronics for Embedding in Textiles*, http:// tfcg.elis.ugent.be/projects/sweet/index.html, access time: 15/07/2011.
68. *STELLA Project*, http://www.stella-project.de/, access time: 15/07/2011.
69. A. Arriola, J. I. Sancho, S. Brebels, M. Gonzalez and W. D. Raedt, *Stretchable dipole antenna doe body area networks at 2.45 GHz*, IET Microwaves, Antennas & Propagation, Vol. 5, Iss. 7, 2011, pp. 852-859.
70. M. Kubo, X. Li, C. Kim, M. Hashimoto, B. J. Wiley, D. Ham and G. M. Whitesides, *Stretchable microfluidic radiofrequency antennas*, Advanced Materials, Vol. 22. 2010, pp. 2749-2752.
71. Q. Liu, K. L. Ford, R. Langley, A. Robinson and S. Lacour, *Stretchable antennas*, 6th European Conference on Antennas and Propagation (EUCAP), 2011, pp. 168-171.
72. Z. Konstas, A. Rida, R. Vyas, K. Katsibas, N. Uzunoglu and <. Tentzeris, *A novel gree inkjet printed Z shaped monopole antenna for RFID applications*, Antennas and Propagation, EuCAP 2009.
73. N. J. Kirsch, N. A. Vacirca, E. E. Plowman, T. P. Kurzweg, A. K. Fontecchio and K. R. Dandekar, *Optically transparent conductive polymer RFID meandering dipole antenna*, IEEE International Conference on RFID, 2009, pp. 278-282.
74. I. Ortego, N. Sanchez, J. Garcia, F. Casado, D. Valderas and J. I. Sancho, *Inkjet printed planar coil antenna analysis for NFC technology applications*, International Journal of Antennas and Propagation, Vol. 102, ID. 486565.
75. T. Yasin and R. Baktur, *Inkjet printed patch antennas on transparent substrates*, IEEE Antennas and Propagation Society International Symposium (APSURSI), July 2010.
76. V. K. Palukuru, A. Pekonen, V. Pynttari, R. Makinen, J. Hagberg and H Jantunen, *An inkjet printed inverted F antenna for 2.4 GHz wrist applications*, Microwave and Optical Technology Letters, Vol. 51, Iss. 12, 2009, pp. 2936-2938.
77. P. S. Hall and Y. Hao, *Antennas and Propagation for body-centric wireless communications*, Second revised edition, Artech House Publishers, 2012, ISBN-10: 1608073769.

78 . Fabric Antenna, Patria, http://www.patria.fi/EN/Products+and+services/Situational+ Awareness/Textile+Antennas/index.html, access date: 01/10/2013.
79. *Wearable Antenna Technology*, Inc, http://wearableantenna.com/, access date: 01/10/2013.
80. P. Salonen and H. Hurme, *A novel fabric wlan antenna for wearable applications*, IEEE Antenna and propagation society international symposium, 2003, pp. 700-703.
81. M. Tanaka and J. H. Jang, *Wearable microstrip antenna*, Antenna and Propagation Society International Symposium IEEE, Vol. 2, 2003, pp. 704-707.
82 . P. J. Massey, *Mobile phone fabric antennas integrated within clothing*, IEE 11th International Conference on Antenna and Propagation, 2001, pp. 344-347.
83. M. Klem, I. Locher and G. Troster, *A novel circularly polarised textile antenna for wearable applications*, European Conference on Wireless Technology, 2004, pp. 285-288.
84. P. Salonen, Y. R. Samii, H. Hurme, M. Kivikoski, *Dual-band wearable textile antenna*, IEEE Antennas and propagation society international symposium, 2004, pp. 463-466.
85. T. Kellomaki, J. Virkki, S. Merilampi, L. Ukkonen, *Towards washable wearable antennas: a comparison of coating materials for screen-printed textile-based UHF RFID tags*, Hindawi Publishing Corporation, International Journal of Antennas and Propagation, Vol. 2012, Article ID 476570.
86. P. Vincenzini, C. Carfagna, *Washable screen printed textile antennas*, Advances in Science and Technology, Vol. 80, Smart and Interactive Textiles, pp.118-122.
87. P. K. Patra, P. D. Calvert and S. B. Warner, *Textile based carbon nanostructured flexible antenna*, National Textile Center Annual Report, project number: M06-MD01, November 2007.
88. P. K. Patra, P. D. Calvert, S. B. Warner, D. Kasilingam, P. M. Ajayan and B. Notaros, *Textile based cabon nanostructure flexible antenna*, National Textile Center Annual Report, project number: M06-MD01, November 2008.
89. Y. Li, R. Torah, S. Beeby and J. Tudor, *Inkjet printed flexible antenna on textile for wearable applications*, 2012 Textile Institute World Conference, Selangor, Malaysia.
90. F. M. Lopez, A. V. Quitero, G. Mattana, D. Briand, N. F. de Rooij, *All-additive inkjet printed humidity and temperature sensors fabricated and encapsulated at foil level*, the 14th International Meeting on Chemical Sensors, pp. 1122-1125.
91. M. Hwang, H. Lee, Y. Jang, J. Cho, S. Lee, D. Kim, K. Cho, *Effect of curing conditions of a poly(4-vinylphenol) gate dielectric on performance of a Pentacene-based thin film transistor*, Macromolecular Research, volume 17, No. 6, 2009, pp.436-440.
92. C. Sriprachuabwong, C. Srichan, T. Lomas, A. Tuantranont, *Simple RC low pass filter circuit fabricated by unmodified desktop inkjet printer*, Electrical Engineering and Electronics Computer Telecommunications and Information Technology (ECTI-CON), 2010.
93. J. Lim, J. Kim, Y. J. Yoon, H. Kim, H. G. Yoon, S. Lee, J. Kim, *All-inkjet-printed metal-insulator-metal (MIM) capacitor*, Current Applied Physics, 2011, article in press.
94. J. Lim, J.Kim, Y. J. Yoon, H. Kim, H. G. Yoon, S. Lee, J. Kim, *All-inkjet toprinted metal-insulator-metal (MIM) capacitor*, Current Applied Physics, 2011, doi:10.1016, j.cap.2011.04.035.
95. Y. Li, R. Torah, S. Beeby and J. Tudor, *An all-inkjet printed flexible capacitor for wearable applications*, Symposium on Design, Test, Integration & Packaging of MEMS/MOEMS, France 2012, pp. 192-195.
96. Y. Li, R. Torah, S. Beeby and J. Tudor, *An all-inkjet printed flexible capacitor on a textile using a new poly(4-vinylphenol) dielectric ink for wearable applications*, IEEE Sensors 2012, Taipei.

97. S. E. Molesa, S. K. Volkman, D. R. Redinger, A. Vornbrock and V. Subramanian, *A high performance all inkjetted organic transistor technology*, Student paper, suggested area: displays, sensors and MEMS, 2004 IEEE conference.
98. A. C. Arias, J. Daniel, S. Sambandan, T. N. Ng, B. Russo, B. Krusor, R. A. Street, *All inkjet printed thin film transistors for flexible electronics*, Organic Field-Effect Transistors VII and Organic Semiconductor in Sensors and Bioslectronics, Proc. of SPIE, volume 7054, 2008, 70540L.
99. B. K. Nelson, D. E. Vogel, M. E. Napierala and T. C. Lee, *All inkjet printed thin film transistor*, Patent application publication, US 2007/0146426 A1, 2007.
100. H. Y. Tseng and V. Subramanian, *All inkjet printed self aligned transistor and circuit applications*, 2009 IEEE, International electron devices meeting 09-391.
101. K. Suziki, K. Yutani, M. Nakashima, A. Onodea, S. Mizukami, M. Kato, T. Tano, H. Tomono, M. Yanagisawa and K. Kameyama, *All printed organic TFT backplanes for flexible electronic paper*, International symposium on electronics paper 2010.
102. S. Chung, J. Jang, J. Cho, C. Lee, S. Kwon and Y. Hong, *All-inkjet-printed organic thin-film transistors with silver gate, source/drain electrodes*, Japanese Journal of Applied Physics, Vol. 50, 2011, 03CB05,
103. L. Sun, S. T. Parker, D. Syoji, X. Wang, J. A. Lewis, D. L. Kaplan, *Direct write assembly of 3D silk/hydroxyapatite scaffolds for bone co-cultures*, Advanced Healthcare Materials, volume 1, 2012, pp. 729-735.
104. B. Y. Ahn, D. J. Lorang, E. B. Duoss, J. A. Lewis, *Direct write assembly of microperiodic planar and spanning ITO microelectrodes*, Chemical Communications, volume 46, 2010, pp. 7118-7120.
105. C. C. Ho, D. Steingart, J. Evans and P. Wright, *Tailoring electrochemical capacitor energy storage using direct write dispenser printing*, ECS Transactions, Vol. 16, Iss. 1, 2008, pp. 35-47.
106. C. C. Ho, J. W. Evans, P. K. Wright, Direct write dispenser printing of a zinc microbattery with an ionic liquid gel electrolyte, Journal of Micromechanics and Microengineering, volume 20, 2010, 104009.
107. D. Madan, A. Chen, P. K. Wright and J. W. Evans, *Dispenser Printed Composite Thermoelectric Thick Films for Thermoelectric Generator Applications*. Journal of Applied Physics, Vol. 108, 2011, 034904.
108. L. M. Miller, A. Chen, P. K. Wright and J. W. Evans, *Resonance Frequency Customization for MEMS Vibration Energy Harvesters Using Dispenser Printed Proof Mass*, Proceedings of PowerMEMS 2010 (Leuven, Belgium, 1-3 December 2010), pp. 411-414.
109. Prof. Jennifer A. Lewis, Lewis Research Group, University of Illinois at Urbana-Champaign, http://colloids.matse.illinois.edu/, access date: 13/10/2013.
110. Berkeley Manufacturing Institute, University of California, Berkeley, http://bmi .berkele y.edu/, access date: 13/10/2013.
111. European Commission Implementing Decision of 8 December 2011, *Amending Decision 2006/771/EC on harmonisation of the radio spectrum for use by short-range devices*, 2011/829/EU, Vol. 329, pp.10-18.
112. *United Kingdom, Frequency Allocation Table*, the National Frequency Planning Group on behalf of the Committee on UK Spectrum Strategy, Iss. 17, 2013, pp.1-280.
113. Rolf H. Weber, *Internet of things – New security and privacy challenges*, Computer Law & Security Review, Vol. 26, 2010, pp. 23-30.
114. Microstrip (Patch) Antenna, *Antenna-Theory*, http://www.antenna-theory.com/antennas /patches/antenna.php, access date: 18/01/2014.

115. T. R. Harris, *The design process of a rectangular microstrip antenna*, North Carolina State University, http://www4.ncsu.edu/~trharris/files/text/Harris-740PatchProj.pdf, access date: 18/01/2014.
116. *Glass slide Corning 75×25 mm microscope slide*, product web page, CORNING. http://catalog2.corning.com/Lifesciences/en-US/Shopping/ProductDetails.aspx?produc tid=2948-75X25(Lifesciences)&categoryname=, access date: 01/10/2013.
117. Kapton HN polyimide film datasheet, DuPont, http://www2.dupont.com/Kapton/en_US /assets/downloads/pdf/HN_datasheet.pdf, access date: 01/10/2013.
118. E. Huerta, A. I. Oliva, F. Aviles, J. Gonzalez-Hernandez and J. E. Corona, *Elastic modulus determination of Al-Cu film alloys prepared by thermal diffusion*, Hindawi Publishing Corporation, Journal of Nanomaterials, Vol. 2012, Article ID 895731, 8 pages.
119. Plastibert, a Cotting-Group Company, http://www.plastibert.be/, access date: 01/10/2013.
120. Klopman Internationa, http://www.klopman.com/, access date: 01/10/2013.
121. Report on Specification of Polyester cotton, Klopman International, unpublished report.
122. Fabink-UV Interface pastes, Smart Fabric Inks, http://www.fabinks.com/, access date: 09/06/2013.
123. Introduction of S-parameter in Vector Network Analyser (VNA), Antenna Theory, http://www.antenna-theory.com/definitions/sparameters.php, access date: 17/09/2013.
124. T. Endo, Y. Sunahara, S. Satoh, T. Katagi, *Resonant frequency and radiation efficiency of meander line antennas*, Electronics and Communications in Japan (Part II: Electronics), volume 83, issue 1, 2000, pp. 52-58.
125. Ward Silver and Mark Wilson, *The ARRL Extra Class License Manual for Ham Radio*, published by American Radio Relay League (ARRL), 9th Edition, ISBN: 10-0872591352.
126. *The dipole antenna theory*, Antenna-Theory, http://www.antenna-theory.com/antennas /dipole.php, access date: 18/01/2014.
127. D. Orban and G. J. K. Moernaut, *The basics of patch antennas*, Orban Microwave Products. http://www.orbanmicrowave.com/The_Basics_Of_Patch_Antennas.pdf, access date: 20/09/2013.
128. Dielectric constant (Relative permittivity) definition, 2013 Encyclopedia Britannica, http://www.britannica.com/EBchecked/topic/162637/dielectric-constant, access date: 13/08/2013.
129. M. Ukena, *UV curable inks: will they work for everyone?*, Printing Environmental Technology, Printers National Environmental Assistance Center (US), http://www.pneac.org/sheets/screen/UVCurableInk.pdf, access date: 23/09/2013.
130. *MicroChem*, http://microchem.com/, access date: 18/09/2013.
131. *PEL Printed Electronics Ltd*, http://www.printedelectronics.co.uk, access date: 01/10/2013.
132. *1-Hexanol datasheet*, National Occeanic and Atmospheric Administration (NOAA), USA Government, http://cameochemicals.noaa.gov/chris/HXN.pdf, access date: 13/08/2013.
133. M. Gonuguntla and A. Sharrma, *Polymer patterns in evaporating droplets on dissolving substrates*, Langmuir, Vol. 20, 2004, pp. 3456-3463.
134. *UV chamber with fitted 365 nm wavelength mercury bulb*, UV Light Technology Ltd. http://www.uv-light.co.uk/, access date: 11/08/2013.
135. *PriElex Jettable Resist Version 005/006 Guideline datasheet*, MicroChem, confidential.
136. H. Klauk, M. Halik, U. Zschieschang, G. Schmid and W. Radlik, *High mobility polymer gate dielectric pentacene thin film transistors*, Journal of Applied Physics, Vol. 92, No. 9, 2002, pp. 5259-5263.
137. *PGMEA Material Safety Data Sheet*, Electronics ppt Chemicals, Kanto Corporation, http://mfc.engr.arizona.edu/safety/MSDS%20FOLDER/PGMEA.pdf, access date: 23/08/2013.

138. S. H. Ko, H. Pan, C. O. Grigoropoulos, C. K. Luscombe, J. M. J. Frechet and D. Poulikakos, *All inkjet printed flexible electronics fabrication on a polymer substrate by low temperature high resolution selective laser sintering of metal nanoparticles*, Nanotechnology, Vol. 18, 345202, 2007, pp. 8.
139. *1-Hexanol Material Safety Data Sheet*, Sigma Adrich - 471402.
140. F. Y. Yang, K. J. Chang, M. Y. Hsu and C. C. Liu, *High performance poly(3-hexylthiophene) transistors with thermally cured and photo-cured PVP gate dielectrics*, Journal of Materials Chemistry, Vol. 18, 2008, pp. 5927-5932.
141. *Methods for Nanopatterning and Lithography*, Material Matters, Sigma Aldrich, Vol. 6, No. 1, pp.1.
142. Sartomer, ARKEMA Group, http://www.sartomer.com/, access date: 16/08/2013.
143. Definition of Initiator, Enclopaedia Britannica, http://www.britannica.com/EBchecked /topic/288336/initiator, access date: 18/09/2013.
144. R. Marcelli, S. Catoni, L. Frenguelli, *Low loss coplanar lines on low resistivity silicon by SU-8 thick negative photoresist*, Semiconductor Conference, 2005, Proceedings, vol. 1, pp. 107-110.
145. H. Johnson, Dielectric loss tangents, High Speed Digital Design Online Newsletter, Vol. 4, Iss. 5, http://www.sigcon.com/Pubs/news/4_5.htm, access date: 07/07/2013.
146. C. C. Ho, *Dispenser printed zinc microbattery with an ionic liquid gel electrolyte*, University of California, Berkeley, PhD thesis.
147. Tech tips of component selection for optimal dispensing of epoxies, Epoxy Technology Inc.,http://www.epotek.com/SSCDocs/techtips/Tech%20Tip%2010%20-%20Dispensing %20of%20Epoxies.pdf, access date: 01/09/2013.
148. S. M. Sze, *Chapter 4 p-n junction*, Semiconductor Devices Physics and Technology, 2nd Edition, Published by Wiley, ISBN: 978-0-471-33372-2.
149. A. V. Shah, H. Schade, M. Vanecek, J. Meier, E. Vallat-Sauvain, N. Wyrsch, U. Kroll, C. Droz, J. Bailat, *Thin film silicon solar cell technology*, Progress in Photovoltaics: Research and Applications, volume 12, 2004, pp. 113-142.
150. Robert Hull, *Chapter 8.3 Electron mobility, diffusion and lifetime in e-Si*, Properties of Crystalline Silicon, Publisher: IET, 1999, ISBN: 0852969333, 9780852969335.
151. M C Hamilton, S. Martin and J. Kanicki, *Field effect mobility of organic polymer thin film transistors*, Chemistry of Materials, Vol. 16, 2004, pp.4699-4704.
152. V. Fauzia, A. A. U. Umar, M. M. Salleh, M. Yahya, Optimizing of the inkjet printing *technique parameters for fabrication of bulk heterojunction organic solar cells*, IEEE ICSE Proc. 2010, Melaka, Malaysia.
153. *The printable Electronics Technology Centre (PETEC)*, a business unit of The Centre for Process Innovation (CPI), http://www.uk-cpi.com/printable-electronics/, access date: 09/09/2013.
154. *Materials information of Poly (2,5-bis (3-hexadecyllthiophen-2-yl) thieno [3,2-b] thiophene) (PBTTT)*, Ossila, Enabling Organic Electronics, http://www.ossila.com /oled_opv_ofet_catalogue3/PCDTBT_P3HT_PCBM_PEDOT_PSS_for_organic_photov oltaics/M141-PBTTT.php, access date: 29/09/2013.
155. *Nanofabrication Centre*, Electronics and Computer Science, University of Southampton, http://www.southampton-nanofab.com/, access date: 05/09/2013.
156. Kirk-Othmer Encyclopedia of Chemical Technology, 3rd Edition, New York, NY: John Wiley and Sons, Vol. 15, 1981, pp.703.
157. *Fabrication of Poly(triaryl-amine) Field-effect Transistors*, Sigma Aldrich, http://ww w.sigmaaldrich.com/technical-documents/protocols/materials-science/fabrication-of-poly.html, access date: 01/10/2013.

158. *Supporting document in the topic of Calculating capacitance*, Ossila, Enabling Organic Electronics, http://www.ossila.com/downloads/Calculating_Capacitance.pdf, access date: 25/09/2013.
159. A. Yadav, S. Yadav, S. Singh and N. Tripathi, *analysis and parameter extraction of organic transistor at PTAA with different organic materials*, Internation Journal of Scientific & Technology Research, 2002, Vol. 1 Iss. 10, ISSN: 2277-8616.
160. *Poly[bis(4-phenyl)(2,4,6-trimethylphenyl)amine] (PTAA) Technical Bulletin*, Sigma Aldrich, catalogue number 702471, Technical Bulletin AL-254.
161. Table of principle IR absorptions for certain functional groups, Welleslaye College, http://academics.wellesley.edu/Chemistry/chem211lab/Orgo_Lab_Manual/Appendix/Instruments/InfraredSpec/Chem211%20IR%20Lit%20Value%20Table.pdf, access date: 10/09/2013.
162. Fingerprint region, Illustrated glossary of organic chemistry, Chemistry and Biology Department, UCLA http://www.chem.ucla.edu/harding/IGOC/F/fingerprint_region.html, access date: 10/09/2013.
163. The fingerprint region of an infra-red spectrum, Chemguide, Helping you to understand chemistry, http://www.chemguide.co.uk/analysis/ir/fingerprint.html, access date: 10/09/2013.
164. Digital creative tools for digital printing of smart fabrics, CREATIF, Project number 610414, Call (part) identifier FP&-ICT-2013-10, EU Framework 7 Project, http://www.creatif.ecs.soton.ac.uk/, access date: 11/10/2013.